Development of Mesoporous Carbon/Silica Composites for Precious Metal Recovery

Konstantina Sotiriou

PhD

University of York

Department of Chemistry

September 2020

Abstract

Concerns over the future availability of precious metals, such as gold, have resulted in the inevitable development of efficient technologies for recovery of precious metals from industrially contaminated water streams securing accessibility of these metals to current and future generations. One of the most promising approaches to concentrate precious metals from aqueous solutions is adsorption. Many porous materials, such as activated carbons, silica gels, specific mesoporous materials, have been applied during the last few decades; however, with most waste streams containing a range of metals, the need for specific metal selectivity remains a crucial goal.

Herein, different series of mesoporous carbon/silica composites (CSCs), including nitrogen-doped CSCs (N-CSCs) are prepared to investigate as potential adsorbents for the removal of gold from aqueous media. The materials are synthesised via the wet impregnation of bio-oil from the pyrolysis of waste office paper into a silica framework, and where needed (N-CSCs) the presence of urea as the nitrogen source, at a range of temperatures. The resulting materials exhibit outstanding selectivity towards gold with high loading capacities and gold removal.

Varying the carbonisation temperature between 300˚C and 800˚C allows for tuneable textural and structural properties, surface functionalities and maximum surface coverage yielding a range of different materials; from polymerised bio-oil CSCs at 300 ˚C to graphitic-like CSCs at 800˚C. In all series (A, B and C) of CSCs produced, the best performing materials reproduced at 500˚C, at which temperature they possess the optimal combination of textural properties and chemical functionalities, leading to high adsorption capacities (up to 320 mg g^{-1}) and quantitative gold selectivity and removal (up to 99%), outperforming conventional activated carbons and other porous materials. The novel N-CSCs perform in a similar exceptional manner yet owing to the surface presence of nitrogen functionalities at all synthesis temperatures, loading capacities and gold removal show less variation at the different carbonisation temperatures. The best N-CSC is, nonetheless, obtained at 500˚C with an adsorption capacity of 360 mg g^{-1} and up to 98% gold removal.

The detailed mechanism of adsorption is investigated, including discussion of the role of the factors which influence competition between chemisorption and physisorption processes.

Table of Contents

PART II. CARBON/SILICA COMPOSITES: SERIES B VS SERIES C

PART III. NITROGEN-DOPED CARBON/SILICA COMPOSITES: SERIES N

List of Figures

List of Tables

Acknowledgements

Firstly, massive and special thanks go to all my supervisors, current and previous, Dr Duncan Macquarrie, Dr Vitaliy Budarin and Dr Andrew Hunt, for all their guidance, support and patience throughout my PhD. I can never really thank you enough for what you have taught me, helped me through and all the opportunities you gave me believing in my work. People also deserving special thanks for sharing ideas and setting the grounds for my work, are previous members of GCCE and colleagues Dr Tengyao Jiang and Dr Andrea Munoz Garcia. Everyone's help was invaluable!

A huge thank you goes to Paul, Hannah, Maria and all the technicians' team for providing all the necessary support and training in the lab. Special thanks to all the people running services that were crucial for this project; Dr Meg Stark (Biology Department, University of York), Dr Graeme McAllister (Chemistry Department, University of York), Dr Lorna Eades (School of Chemistry, University of Edinburgh) and Dr David Morgan (School of Catalysis, University of Cardiff). Many thanks go to Dr Nontipa Supanchaiyamat for accommodating and welcoming me to work with her group at the Khon Kaen University in Thailand; it was a unique experience and one I will never forget.

Deepest thanks go to all the people in the GCCE family for making this journey pleasant and truly memorable. I have learnt so much from each and every one of you and I am so happy that our paths have crossed in this chapter of my life; it is really hard to accept that I have to say goodbye. You have been like a family to me and made York feel like a second home. Andrea, Fergal, Jenny, Jonny, Yann, Ben, Tom, Roxana, Tabitha, Joe, Javier and Anna thank you for becoming such a big part of my life and thank you for all the memories we have created!

Finally, my most heartfelt gratitude goes to my family; my loving parents, Ourania and Christakis, and my siblings, Andreas, Chrysanthos and Despianna, for all their love, encouragement and support, especially when I felt like giving up. Thank you for believing in me and motivating me to go through one of the most important journeys of my life. Many thanks go to beloved friends and my special people too, Antonis,

Maria E., Styliana, Joanna, Chrisitiana, Elena and Maria I. for bearing with me during this journey. Whether we were close together or far apart, you were there throughout all good times and bad times, making my days happier and brighter. I love each and every one of you and it would have been unbearable without you. Thank you!

This PhD is dedicated to my heroes; my mother, my father and my dear departed grandfather Dinos.

Declaration

Some of the results presented in this thesis were obtained through collaboration with others, details as follows:

- Chapter 3 – Research for sections of this chapter was carried out by Dr Tengyao Jiang and Dr Andrea Munoz Garcia, fully acknowledged in the text.
- SEM images were obtained with the assistance of Dr Meg Stark (Biology Department, University of York).
- SEM-FIB and SEM-EDX data were obtained with the assistance of Dr Andrew Hunt (Materials Chemistry Research Centre, Khon Kaen University, Thailand).
- XPS analysis was carried out by Dr Joseph Morgan (School of Catalysis, University of Cardiff).
- ICP-MS analysis was carried out by Dr Lorna Eades (School of Chemistry, University of Edinburgh).

All other results are original work of the author. All sources are acknowledged as References.

Part of the work disclosed herein has been published in the following article:

- Synthesis and application of tuneable carbon–silica composites from the microwave pyrolysis of waste paper for selective recovery of gold from acidic solutions

  K. Sotiriou, N. Supanchaiyamat, T. Jiang, I. Janekarn, A. Muñoz García, V.L. Budarin, D.J. MacQuarrie, A.J. Hunt, RSC Advances, 2020, 10, 25228–25238

The work presented in this thesis has not been previously submitted for a degree at this or any other university.

Chapter 1.

Introduction

Chapter 1.

Introduction

1.1 Scope of Thesis

The aim of this thesis is to provide a detailed study into the synthesis of Carbon/Silica Composites derived from waste office paper and their application as adsorbent materials for the selective recovery of gold from aqueous waste streams.

The work focuses on full evaluation of the bio-derived materials to prove their suitability and efficacy as adsorbents, highlighting their unique characteristics and properties which favour gold capture.

Overall, the project addresses all issues and consequences of waste, be it wastewater or municipal solid waste, yet simultaneously acknowledging all opportunities residing with it; while resources are running out, waste holds the potential in recovering valuable chemicals for their re-use or conversion into value-added products.

1.2 Green Chemistry

Green Chemistry is a relatively new emerging field that strives to achieve sustainability at a molecular level. The concept was formulated at the beginning of 1990s, nearly 30 years ago, and has since then gained a lot of attention across the globe.[1] It is defined as the "design of chemical products and process to reduce or eliminate the use and generation of hazardous substances". [2,3] Green Chemistry has had a large impact because it goes beyond just research in a laboratory, as it has influenced education, industry, society, economy and the environment.[4] It is an innovative and economically driven approach toward sustainability, as it challenges research to design and use energy and matter in ways that increase performance and value, while simultaneously protecting the environment and human health.[5]

Sustainability encompasses that the needs of the present generation do not compromise the ability of future generations to meet their own needs.[6] Taking into consideration the concept of sustainability and the prospects of Green Chemistry in

that area, 12 principles have been established.[3] They are principles that chemists should be taking into account while conducting their research, as scientific progress should not be achieved at the expense of causing environmental and socio-economic problems.

The 12 principles of Green Chemistry are:

1. Prevention

It is better to prevent waste than to treat or clean up waste after it has been created.

2. Atom Economy

Synthetic methods should be designed to maximise the incorporation of all materials used in the process into the final product.

3. Less Hazardous Chemical Synthesis

Wherever practicable, synthetic methods should be designed to use and generate substances that possess little or no toxicity to people or the environment.

4. Designing Safer Chemicals

Chemical products should be designed to effect their desired function while minimising their toxicity.

5. Safer Solvents and Auxiliaries

The use of auxiliary substances (e.g. solvents or separation agents) should be made unnecessary whenever possible and innocuous when used.

6. Design for Energy Efficiency

Energy requirements of chemical processes should be recognised for their environmental and economic impacts and should be minimised. If possible, synthetic methods should be conducted at ambient temperature and pressure.

7. Use of Renewable Feedstocks

A raw material or feedstock should be renewable rather than depleting whenever technically and economically practicable.

8. Reduce Derivatives

Unnecessary derivatisation (use of blocking groups, protection/ de-protection, and temporary modification of physical / chemical processes) should be minimised or avoided if possible, because such steps require additional reagents and can generate waste.

9. Catalysis

Catalytic reagents (as selective as possible) are superior to stoichiometric reagents.

10. Design for Degradation

Chemical products should be designed so that at the end of their function they break down into innocuous degradation products and do not persist in the environment.

11. Real-time Analysis for Pollution Prevention

Analytical methodologies need to be further developed to allow for real-time, in-process monitoring and control prior to the formation of hazardous substances.

12. Inherently Safer Chemistry for Accident Prevention

Substances and the form of a substance used in a chemical process should be chosen to minimise the potential for chemical accidents, including releases, explosions, and fires.

The synthesis of bio-derived carbonaceous materials, like the composite materials produced and presented in this thesis, as well as their application for metal adsorption and recovery, both comply with several of the criteria set out by the Green Chemistry Principles.

The carbon source used for the synthesis of materials described in this project is obtained from waste office paper, which is well in agreement with the principles of

Prevention of Waste and Use of Renewable Feedstocks; it prevents waste disposal of any kind, but rather utilises the recycled waste office paper at its end-of-life as feedstock for the production of, perhaps, the most significant starting material in the whole synthetic process. Furthermore, the synthetic processes described avoid the use of templates, hazardous chemicals or harsh conditions, thus enhancing the atom economy and securing safety of the production system throughout all stages. Even though obtaining the carbon source essential to the development of materials requires the utilisation of high carbonisation temperatures, microwave-assisted pyrolysis is used which is much more efficient and has less environmental impact compared to conventional pyrolysis that could have been used. The production system involves several steps such as pressing milled waste office paper into blocks, microwave-assisted pyrolysis of the paper blocks to obtain the bio-oil, mixing of the bio-oil with a silica framework and a doping agent where necessary, as well carbonisation at different temperatures to obtain the final composite materials, but nonetheless avoids the use of any additional/excess reagents or steps and thus minimises the generation of waste streams.

1.3 Sustainability of Precious Metals

1.3.1 The issue of elemental sustainability

Climate change and oil crises have become major issues and hold concerns over the future of elemental sustainability for a number of elements, and in specific various metals.[6] As a result of attempts to be carbon neutral, “low-carbon” technologies have been put to practise and shift technology to a green direction, yet most of those technologies, such as wind turbines, electric cars, fuel cells and catalytic converters, require the acquisition and utilisation of metals for their manufacture and subsequent use.[7,8] So as we shift to greener technologies, a new challenge is born by creating a resource deficit of rare and precious metals. [9]

Such valuable metals, in particular precious metals and platinum-group metals, possess a variety of chemical and physical properties which render them ideal for such purposes.[10] As a result of their constant demand and supply, their conventional and known reserves are running out (Fig.1) and there exist no bio-derived substitutes for

them. They are very finite and unique elements that are being scattered throughout the environment at a very fast rate, making their recovery extremely difficult and very cost-intensive.[11] Major concerns relating to the future availability of these metals are their abundance and the ease of accessing them.

Obtaining the vast majority of metals required for industrial purposes and applications requires the use of environmentally destructive practises .[11] Techniques for removing and recovering metals from soil and water include precipitation,[12] ion exchange.[13] chemical leaching,[14] soil washing,[15] excavation, mining and off-site disposal.[16] Such mechanical processes lead to high levels and fast rates of distribution of the metals and their mining waste in the surrounding water and soil streams.[17] Consequently, the extent of contamination throughout the environment is not controlled and cannot be fully measured, creating the need for assessment of the various potential health and environmental risks posed (i.e. bioaccumulation and toxicity of dispersed metals),[18] as well as the development of 'green' strategies for the recapture and re-use of these elements.[13,19]

The concept of elemental sustainability encompasses issues such as the availability of elements in terms of their abundance and ease of accessibility.[20] For any element to be sustainable, its use by the current generation should not prevent future generations from accessing and using it for their own purposes.[7] Elemental sustainability coincides with various principles of green chemistry, and therefore one needs to seek alternative ways of obtaining and recovering such metals.[7] Suggested pathways should involve the use of clean technologies and acquisition practices, but in addition, should take into consideration economic and social factors (i.e. cost-effectiveness of methods, public acceptance, habitat landscape, etc). [6,21]

Figure 1 Remaining years until depletion of known reserves of elements. Reproduced from Ref.22

1.3.2 Precious metals

Precious metals are naturally occurring metals that are relatively rare and difficult to find, and hold higher economic values compared to others, as they are used in currency, investment commodities and jewellery.[12,22] They are not as reactive as other metals, and in addition to being rare, their higher luster and ductility lead to an increase in their price of acquisition. The most widely known precious metals are gold, silver, platinum and palladium (PGMs).[10,23]

Precious metals are also extensively used in the electronics industry (Table 1) for the manufacture of components in electrical devices, in commercial chemistry as catalysts and in medicine as devices for treating various health conditions.[11,23–25] This increasing demand and the existing limited resources of the metals resulting in insecure supply,[23,26] led to the encouragement of recycling or recovering them and re-using them from secondary metal-containing sources; municipal and industrial waste, electronic and electrical waste landfill sites and aqueous wastewaters.[14,27,28]

Table 1 The average weight of precious metals in typical WEEE. Reproduced from Ref.27

PM (mg/ unit)	Mobile phone		PC		Flat screen/ TV monitor		Laptop	
	Range	AC	Range	AC	Range	AC	Range	AC
Ag	232-319	261	1348-11.408	6378	450-575	515	249-437	343
Au	24.1-29	26.1	-	92.7	110-200	161	104.5-219.8	160.8
Pd	8.7-14.5	11.6	-	39.9	40-44	42	-	40.2

***AC:** average contents; **PM:** precious metal*

As the traditional recovery methods include hydrometallurgical techniques,[29,30] like electrodeposition,[31] solvent extraction and chemical leaching, they end up being very costly and highly energy and labour intensive.[11]

1.3.2.1 Gold

Continuous technological achievements of the 21st century world imply continuous and growing demand on the use of precious metals, like gold, in a wide range industries and applications.[29] Gold holds various uses as a result of its chemical and physical properties, which keep fuelling the need for more gold.[30,32] Due to its very high luster, malleability and tarnish resistance it is highly valued and used in and as jewellery.[33] Another big sector that benefits from the utilisation of gold is the electronics' industry. Gold, being a metal, has good conductivity and general resistance to oxidation and corrosion, which make it ideal to use in electronics connectors in devices such as computers, cell phones and cables.[34,35] Furthermore, gold is a good reflector of electromagnetic radiation (Infrared and Visible light) and it is used as protective coating of artificial satellites and astronauts' helmets. Being non-toxic and very inert, gold is used for medical and medicinal purposes as well, such as in restorative dentistry and to treat arthritis.[36,37] Gold is also used in chemical processes as a catalyst, with most of the reactions being oxidations (i.e. oxidation of CO, oxidation of glucose to gluconic acid, oxidative removal of mercury, etc.).[25,38]

As a result of gold's uses, coupled with a growing demand, low accessibility and substitutability of the metal, fears over the security of supply are increasing (Fig.2). Gold Demand Trends (Gold World Council) published a document for 2016 which represented the 5-year average supply of gold at 1123.4 tonnes, with the year-on-year demand increasing by 15%, however highlighting that the current rates of production fall short of this demand.[39]

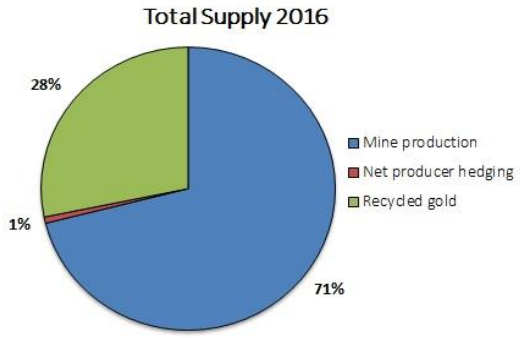

Figure 1 Supply of gold per sector in 2016 (Gold World Council)

One can see why it is crucial to recover gold from the unavoidably increasing waste streams, instead of drying out its existing depleting resources. Many efforts focus on

recycling and re-using gold after recovering the metal from waste products. Depending on the waste stream, route of recovery may differ, with a variety of techniques available to aid the cause. Such techniques include mechanical separation, pyrometallurgical processes, hydrometallurgical processes, and leaching processes, with a further possibility of recovery from leachants.[30]

Pyrometallurgical processing is a conventional method used to recover gold from ores and secondary spent materials, and includes incineration, smelting in a furnace at extremely high temperatures.[30] Hydrometallurgical processing, which is more preferred, involves leaching the gold several times and then subjecting the solution to separation and purification procedures.[40] Such separation and purification procedures include solvent extraction, ion-exchange, electro-wining and cementation. Even though these methods can be exact, predictable and allow for control, they are all very costly, time-consuming and generate considerable amounts of new streams of waste. It is thus, important to replace them with technologies that have lower cost and are more environmentally friendly.[41] One such technology is adsorption, a promising and efficient technology discussed in latter section, that has been gaining more and more interest when it comes to gold recovery.[42]

1.4 Waste: From Land to Lab

Waste is a complex societal problem resulting from increasing population densities, a booming economy, rapid urbanisation and the industrialisation of society.[43,44] Developed and developing countries generate different quantities and quality of waste, yet on a global level the overall impact of pollution can be devastating.[44,45] Waste in any form, be it solid waste, wastewater or emissions, and the subsequent contamination it causes are major problems on environmental, economic and social levels (triple bottom line).[46] It can lead to the pollution of air, soil and water and it is essentially a result of anthropogenic influence, whether on a domestic domain, agricultural, commercial or an industrial one.[47] As a result, the cost of waste can be vast considering its origin and its end-of life (Fig. 3). It is generally difficult to assess the overall cost expressed in terms of the triple bottom line, nonetheless the effects waste can have can result in damage of the economy and human and wildlife populations.[48]

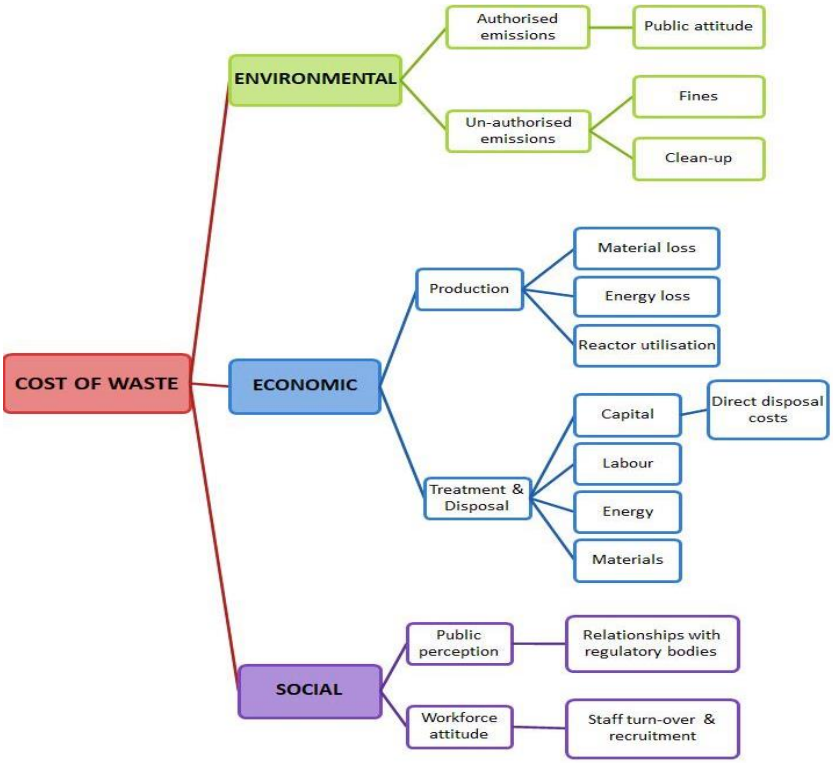

Figure 2 Cost of waste in terms of the triple bottom line

Thinking about waste as an issue, one may also see the potential within it. It is generated in huge amounts worldwide and contains a variety of valuable materials (i.e. metals, plastic, etc.) that can essentially be recycled or recovered.[49] A spectrum of waste management and treatment technologies is put to effect to limit direct discarding of products as waste, but instead extract and convert all valuable components for further use.[50] All waste minimisation and management strategies work hand-in-hand with the waste hierarchy (Fig.4), aiming to protect the environment and improve the quality of life for both current and future generations.[50,51]

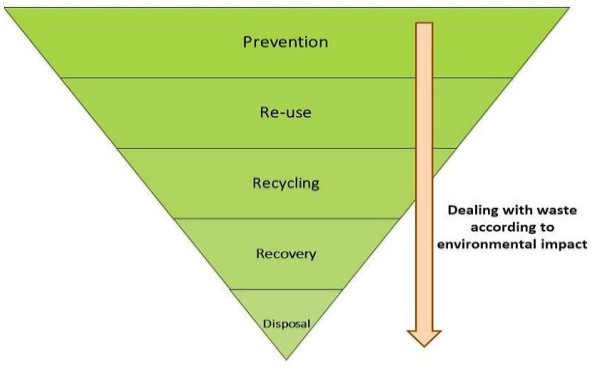

Figure 3 Waste hierarchy (EU Waste Framework Directive 2008/98/EC)

1.4.1 Municipal Solid Waste

Municipal solid waste (MSW) is the waste discarded in urban and rural areas including households, local businesses and governments, and it contains significant amounts of paper, plastic, food, glass, textile and metals. [52,53] Composition of MSW is heterogeneous and depends on the socio-economic level of the area it is generated. The volume of MSW arising varies according to population growth and industrialisation of the area, resulting in goods becoming intrinsically less valuable and global willingness to 'make-do and mend' shifting to a 'throw-away' culture.[43,54] As a result, MSW has become a target for treatment and management, to minimise the negative environmental impacts its rising generation and disposal cause (Table 2).

Table 1 Main environmental impacts of MSW management according to activity. Reproduced from Ref. 44

Activity	Water	Air	Soil	Landscape	Climate
Landfill	Leachate (heavy metals, synthetic organic compounds)	CO_2, CH_4, VOCs, odour, noise	Heavy metals, synthetic organic compounds	Visual effect, vermin	Worst option for GHG emissions [a]
Incineration	Fall-out of atmospheric pollutants	SO_2, NO_x, N_2O, HCl, HF, CO, CO_2, dioxins, furans, PAHs, VOCs, odour, noise	Fly ash, slags	Visual effect	Large GHG emissions [a]
Composting	Leachate	CO_2, CH_4, VOCs, dust, odour, bio-aerosols	Minor impact	Some visual effect	Small GHG emissions [a]
Land-spreading	Bacteria, viruses, heavy metals	Dust, odour, bio-aerosols	Bacteria, viruses, heavy metals, PAHs, PCBs	Vermin, insects	Small GHG emissions [a]
Recycling	Wastewater	Dust, noise	Landfilling of residues	None	Minor emissions
Waste Transportation	Spills	CO_2, SO_2, NO_x, dust, noise	Spills	None	Significant contribution of CO_2

GHG: *Greenhouse gases;* ***PAHs:*** *Polycyclic aromatic hydrocarbons;* ***PCBs:*** *Polychlorinated biphenyls;* ***VOCs:*** *Volatile organic compounds; [a] Assuming no energy recovery*

Precise figures of the amount of MSW globally generated are difficult to acquire due to different metrics, insufficient data and different methods of waste collection (formal or informal) in the different regions.[55] Data from the World Bank (2012), estimated that 44% of total amount of MSW produced is within countries of the Organisation for Economic Co-operation and Development (OECD), followed by 21% within the East Asia and Pacific region (EPA), as shown in Fig.5.[45] Other regions produce considerably less amount of solid waste, yet the overall MSW production levels are on the rise. [52,56] Being rich in various materials and chemicals that are conventionally considered contaminants posing negative environmental effects (Table 2), MSW holds the potential as an alternative biomass resource to produce new materials and supply energy (i.e. paper mill sludge treatment to produce carbon adsorbents[57]).

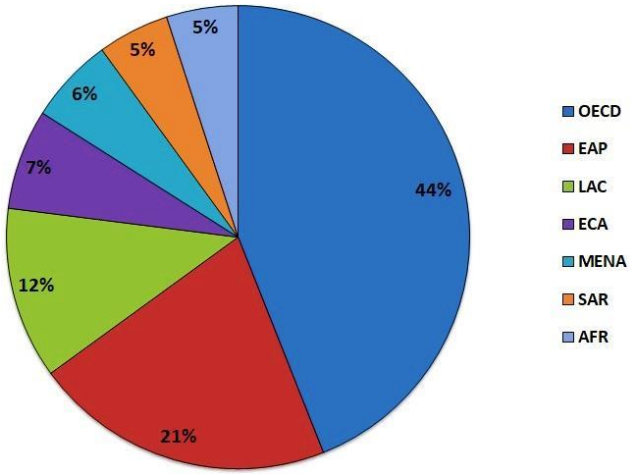

Figure 4 MSW generation by region (World Bank, 2012)

***AFR:** sub-Saharan Africa; **EAP:** East Asia and Pacific; **ECA:** Europe and Central Asia; **LAC:** Latin America and Caribbean; **MENA:** Middle East and North Africa; **OECD:** Organisation for Economic Co-operation and Development; **SAR:** South Asia.*

1.4.1.1 Waste Office Paper

Paper is perhaps the most prominent material in MSW at its end of life, and is a result of the increasing global population consuming paper at an accelerated rate in various fields.[58,59] This cellulosic waste biomass possesses one of the most-established recycling schemes, resulting in approximately 72% of its volume being recycled and re-used in Europe (CEPI 2015), and a corresponding 58% on a global level.[60,61]

It consists of mainly mechanical pulp and a fraction of chemical pulp, with the main chemical components being cellulose, hemicellulose and lignin.[62] Cellulose is the primary component and it is made of polymers of anhydro-D-glucose units aligned by hydrogen bonds, which give it a highly ordered crystalline structure.[63] Hemicellulose and lignin exist in smaller amounts, hemicellulose being the more useful one as it contains sugars and has little strength.[64] Lignin is not involved in the paper-making process due to its hydrophobic nature. Apart from its organic nature, paper consists of inorganic species too, like calcium carbonate, clay and titanium oxide which are used as filling and loading agents.[65]

The use of paper is quite extensive in everyday human life and this essentially creates issues at its end-of-life. Waste paper disposal involves landfill, incineration and recycling.[62] The first two disposal options hold a negative environmental impact, as they generate secondary pollution on land and in the atmosphere.[59] Recycling is the green way to go, as it reduces GHG emissions and allows for re-use of the product, but the process cannot go on indefinitely. Theoretically, waste paper can be recycled up to six times and after that the fibres become very short with reduced tensile strength, preventing re-processing to make new sheets of paper or cardboard.[51,66] This limits further use and cycles back to incineration or off-site disposal of waste paper.

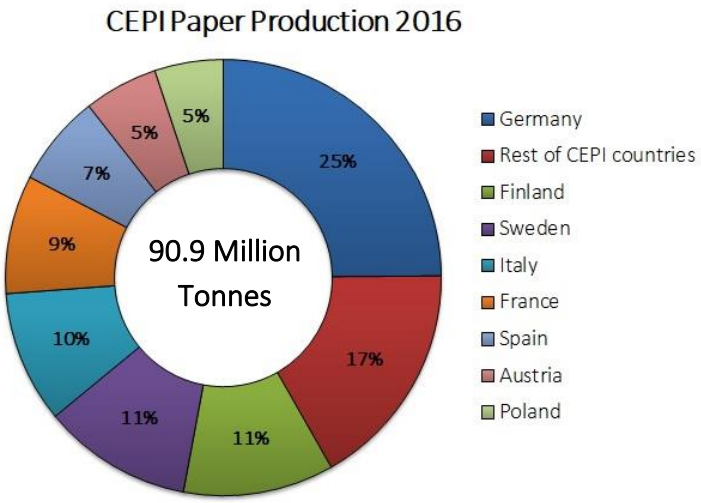

Figure 5 CEPI paper production by country for 2016

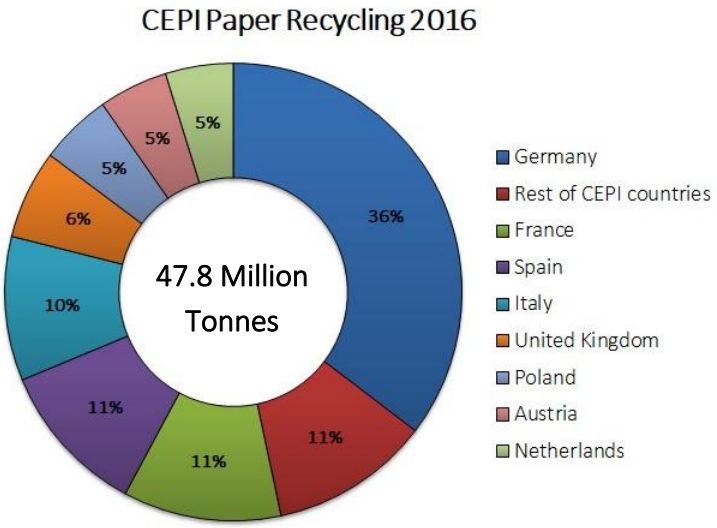

Figure 6 CEPI paper recycling by country for 2016

Societal progression and development created the need for data protection and strictness over confidentiality of written or printed information; documents are now shredded or milled, restricting the potential of recycling as the resulting fibres are too short.[67] If recycling is not an option in such cases, then a significant volume of paper winds up for disposal, either landfill or incineration, causing the loss of valuable cellulosic raw material and environmental pollution.[57,66]

Research work demonstrated that milled waste paper can be used as a source of high value chemicals, such as bio-fuels and sugar derivatives (i.e. lactic acid and gluconic acid), from biochemical conversion.[68] Biochemical conversion though, requires enzymatic hydrolysis, and it results in low degradation rates of lignocellulosic materials due to the resistant crystalline structure of cellulose.[69] Alternatively, waste paper can be pyrolysed to convert into value-added products via its anaerobic thermal decomposition into bio-oil, bio-gas and bio-char.[70] Pyrolysis recovers both the energy and chemical values of the waste biomass, to generate fuels, chemicals and materials.[71]

1.4.2 Waste Electrical and Electronic Equipment

Waste electrical and electronic equipment (WEEE) is a heterogeneous and complex mixture of materials and components and is defined by the WEEE Directive (2002/96/EC) as equipment that is dependent on electric current or electromagnetic

fields to function, and equipment for the generation, transfer or measurement of such currents and fields; the voltage rating to which that applies ranges from 0-1000 V for alternating current (AC) and 0-1500 V for direct current (DC).[72]

WEEE is a growing waste stream and segment of MSW due to the increasing demand of electrical and electronic equipment (EEE) in emerging economies with rapid technological progress.[73] Production of EEE is very resource intensive and can use up to 60% of elements on the periodic table, resulting in waste with high contents of valuable metals that are often mixed in a way that they cannot be readily physically separated.[74,75] In addition to being a source of valuable metals (Table 3) like gold, silver, lithium, nickel, copper, etc., WEEE is also characterised by its partly hazardous nature as a source of heavy metals, polychlorinated biphenyls and brominated flame retardants.[76,77]

Table 2 Main uses of several metals in EEE. Reproduced from Ref.27

Critical Metals	Main uses in EEE
Pd	Multilayer capacitors, connectors, printed wiring board plating
Pt	Hard disks, resistors, conductive plasma display panels
Au	Connecting wires, switch and relay contacts, soldered joints
Ag	Contacts, switches, lead-free solders, conductors, multilayer capacitors
REE	Permanent magnets, battery alloys, phosphors
Co	Rechargeable batteries
Li	Rechargeable batteries
In	Liquid-crystal display glasses, lead-free solders, semiconductors

Material composition of WEEE is difficult to accurately determine because of the extended range of materials found in the waste and the age of discarded equipment, but it can be generalised to the following categories:[76,78]

- Ferrous metals: Iron and steel; account for almost half of the total weight of WEEE.
- Non- ferrous metals: Include precious and critical metals; account for approximately 13% of the total weight; Copper alone accounts for 7%.
- Glass: Accounts for approximately 6% of total weight.
- Plastics: Include polyethylene, polypropylene, polyesters and polycarbonates; account for almost 21% of the total weight.
- Others: Include wood, ceramics, rubber and printed circuit boards; account for the remainder of the total weight.

Composition of WEEE by weight is dominated by metals, implying that there is a high demand of such elements, which might be deficient in the Earth's crust or existing in few, remote locations.[20] As a result, security and supply of elements is at risk, making WEEE an ideal candidate for their recycling and re-capture.[14,72] In developed countries there are advanced technologies for recycling, nonetheless, the collection rate is low leading to lower metal recycling efficiency.[74] In developing countries, the greater volume of WEEE is handled by informal recycling systems and treated by crude processes, leading to metal loss and serious environmental problems, like water and soil pollution (Table 4).[79]

WEEE does not account for much in solid waste, yet the chemical varieties and contents of the abovementioned metals in it are far more than in any other forms of waste; improper handling and disposal can lead to serious pollution, jeopardising the quality of life.[80] As a result, implementation of successful recycling (Fig.6) can 'close' the loop and lead to the recovery of materials and re-use (i.e. recovery of indium from LCDs).[41]

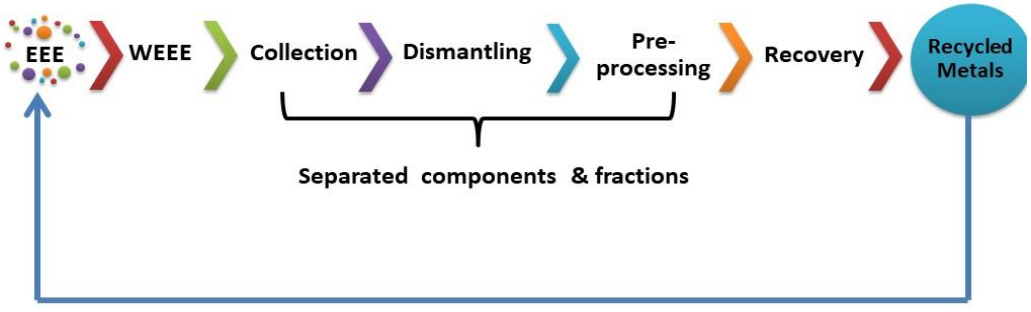

Figure 7 Potential recycling process chain of WEEE

Table 3 Chemical classification of WEEE components and sources and routes of exposure. Adapted from Ref.63

	Component of WEEE	Ecological source of exposure	Route of exposure
Persistent organic pollutants			
Brominated flame retardants, Polybrominated biphenyl ethers	Fire retardants for EEE	Air, dust, water, soil, food	Ingestion, inhalation, transplacental
Polychlorinated biphenyls	Dielectric fluids, lubricants and coolants in generators, capacitors and transformers, fluorescent lighting, ceiling fans, dishwashers, electric motors	Air, dust, food (bio-accumulative in fish and seafood)	Ingestion, inhalation or skin contact, transplacental
Dioxins			
Polychlorinated dibenzodioxins and dibenzofurans	Released as combustion by-product	Air, vapour, dust, water, soil, food	Ingestion, inhalation, skin contact, transplacental
Dioxin-like polychlorinated biphenyls	Dielectric fluids, lubricants and coolants in generators, fluorescent lighting, ceiling fans, dishwashers, electric motors	Released as combustion by-product, air, dust, soil, food (bio-accumulative in fish and seafood)	Ingestion, inhalation, skin contact
Perfluoroalkyls	Fluoropolymers in electronics	Air, dust, water, soil, food	Ingestion, inhalation, skin contact, transplacental

Elements			
Lead	Printed circuit boards, cathode ray tubes, light bulbs, TVs, batteries	Air, dust, water, soil	Ingestion, inhalation, skin contact
Chromium/ hexavalent chromium	Anti-corrosion coatings, data tapes, floppy disks	Air, dust, water, soil	Ingestion, inhalation
Cadmium	Switches, springs, connectors, printed circuit boards, batteries, infrared detectors, semi-conductor chips, ink or toner photocopying machines, cathode ray tubes, mobile phones	Air dust, water, soil, food (especially rice and vegetables)	Ingestion, inhalation
Mercury	Thermostats, sensors, monitors, cells, printed circuit boards, cold cathode fluorescent lamps	Air, vapour, water, soil, food (bio-accumulative in fish and seafood)	Ingestion, inhalation, skin contact
Zinc	Cathode ray tubes, metal coatings	Air, water, soil	Ingestion, inhalation
Nickel	Batteries	Air, water, soil, food (plants)	Ingestion, inhalation, skin contact, transplacental
Lithium	Batteries	Air, water, soil, food (plants)	Ingestion, inhalation, skin contact
Barium	Cathode ray tubes, fluorescent lamps	Air, water, soil, food	Ingestion, inhalation, skin contact
Beryllium	Power supply boxes, computers, X-ray machines, ceramic components	Air, water, food	Ingestion, inhalation, skin contact

1.4.3 Wastewater

One of the major issues faced by humanity in the 21st century is related to water quantity and water quality.[81] Water demand and consumption are dramatically increasing due to population growth and the expansion of industrial processes, yet, its availability decreases at a similar rate since the supply sources remain constant.[82] Supply and availability concerns are becoming more aggravated with constant climate change and pollution of water bodies as a result of human activities.[83,84]

Major concerns arise when waste ends up polluting water streams, as controlling the extent of pollution and applying environmentally friendly techniques to treat it, are very difficult, along with the existing sources running out. [85] There is a vast range of natural and synthetic contaminants that are present in water which may have toxic effects even at the nanogram to microgram per litre level.[81] The number and structural variety of pollutants and contaminants, make it very difficult to assess the extent of contamination and the adverse effects on human and aquatic life they may come with.

1.4.3.1 Potential Contaminants

Sources of water pollution are domestic, agricultural and industrial.[85–87] Without any definite control of what ends up in water streams, a wide variety of contaminants is released and can be separated in the following categories:

i. Chemical

Metals (heavy metals), volatile organic compounds from industrial solvents, chlorinated solvents, dyes, detergents, pesticides, insecticides, fertilisers, petroleum hydrocarbons. Compounds may be present at low concentrations, but can still cause problems due to their toxicity and persistence. [88,89]

ii. Biological

Pathogens (bacteria and micro-organisms like *Salmonella*, *Giardia intestinalis, Cryptosporidium parvum, Schistosoma parasitic worms*). The presence of pathogens

in water leads to waterborne diseases, which, if not diagnosed and treated early, can be deadly. [89,90]

iii. Thermal

Thermal pollution results in the fluctuation of the normal temperature of water and can result in the change of physical properties of water, as well as its quality. Elevated water temperature can result in the decrease of oxygen levels and the subsequent alteration of the food chain composition and reduce the biodiversity of species.[90]

1.4.3.2 Gold Contamination

Gold contamination is a result of anthropogenic practices that aim to extract the metal from its known reserves.[91] The most common practice is mining which may be carried out either by excavation or leaching of gold from its ore.[30,92] Mining involves intensive operations that leave a big environmental footprint, even after the land is cleared.

The most commonly known gold leaching technique is the gold cyanidation process.[30,93] Because of its high affinity for metals like gold (and silver), cyanide proceeds by selectively dissolving and leaching the metals from ores.[94,95] While the purpose of the leaching process is to extract the gold, it is difficult to have absolute control over where the leachate will end up. Several gold mining accidents have occurred which had an immense negative impact on the environment:

- Overflow of process solution containing sodium cyanide occurred within the processing plant site at Newmont Ghana's open pit Ahafo Mine. *(2009, Ahafo Gold Mine, Ghana)*
- Mount Polley mine disaster: A tailing pond breach at Imperial Metals Corp's open pit mine resulted in 10m cubic meters of water and 4.5 cubic meters of toxic slurry being spilled. *(2014, Mount Polley Mine, British Columbia, Canada)*
- 1,072 cubic meters of cyanide solution reached the Potrerillos River due to a valve failure. *(2015, Veladero Mine, San Juan province, Argentina)*

Serious environmental risks are associated with the release of mining waste, either in the solid or liquid forms, as they contain potentially toxic elements like cadmium, lead,

chromium, arsenic, etc.[96] Solubilisation of such contaminants, including gold, results in mine tailings polluting surrounding areas and ending up in acidic water draining from the mine sites.[92]

1.4.3.3 Treatment Methodologies

Metals end up in water streams as a result of mining practices,[91,92] the disposal of electronic waste[35,97] and emissions from chemical processes.[98] Metal ions leach from waste and releases and form secondary aqueous water streams. This causes pollution and sustainability issues, since the metal contaminants are persistent and the currently implemented methods for removal and recovery have poor efficiency,[99] high cost and energy requirements associated with them. [97]

Such conventional treatment methods are mainly mechanical (Fig.7) and include techniques such as electrodeposition, ion exchange, solvent extraction and chemical precipitation.[100,101] These physical techniques have been extensively investigated due to their adaptability and relative ease of execution, yet are not fully nor at all complying with the principles of green chemistry. They might involve pre-treatment steps, the use of auxiliaries and hence generate a whole new stream of tertiary waste, until metals have been successfully removed and treated before re-using.

An alternative method for decontamination gaining more interest over the last decades is adsorption.[102] It employs the use of solid adsorbent materials to bind and concentrate metal ions, and in other cases organic molecules, to their surface. Adsorption has become a more attractive means of treatment, as it is fairly simple, in terms of execution, and can respond rapidly to varying conditions, especially in waste streams (i.e. change of pH or temperature).[103] It is a physical technique proven to be more effective, faster and with lower operation costs than the previously mentioned techniques.[98] A range of different adsorbents are available for metal removal and recovery, and will be discussed in a latter section, specifically for gold.

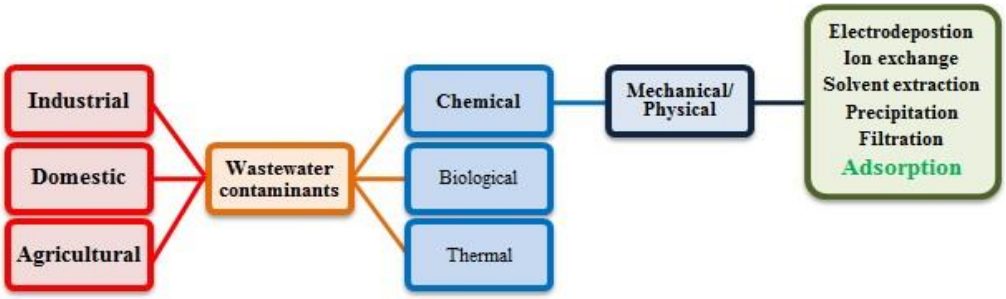

Figure 8 Schematic showing contamination of wastewater from source to treatment

1.5 Adsorption

Adsorption is a surface phenomenon involving phase transfer.[46] The process of adsorption leads to an increase in particle concentration occurring in a thin layer/ film adjacent to the liquid/solid interface. In order for adsorption to take place, the system must consist of an adsorbent and an adsorbate. An adsorbent is the material that will provide its surface/ interface for the process to take place,[104] given it has the right porosity and surface chemistry, whereas the adsorbate consists of the particles that will create the layer on the surface of the adsorbent.[105]

Adsorption is a consequence of surface energy.[106] On the surface of an adsorbent, atoms are not entirely surrounded by other surrounding adsorbent atoms, and hence sites are available to attract adsorbate species.[107] Solid surfaces are characterised by active and energy rich sites that are available to interact with solutes in the adjacent aqueous phase because of their specific electronic properties.[108] The solid material (adsorbent) will provide the surface to enable interactions between itself and the species adsorbed (adsorbate). When the solid particles are immersed in an aqueous medium, solid- liquid interactions take place and cause the formation of the adsorption layer on their surface.[109]

The exact nature of adsorption depends on the species involved, but it can be explained either as physisorption or chemisorption. Physisorption is a result of weak van der Waals' interactions,[110] whereas chemisorption involves electrostatic attractions or covalent bonding (it is accompanied by a chemical reaction).[111]

The adsorption mechanism is assumed to take place by the progression of four consecutive steps:[112]

- Bulk- solution transport

Adsorbate species move from the bulk liquid phase to the hydrodynamic boundary layer around the adsorbent particles.[107]

- Film diffusion transport

Adsorbate species diffuse through the boundary layer of the film to the external surface (the openings of the adsorbent channels or pores) of the adsorbent.[106]

- Intraparticle diffusion transport

Adsorbate species migrate through and into the interior (channels or pores) of the adsorbent by pore diffusion, and/ or by diffusing in the adsorbed state along the internal surface of the adsorbent (surface diffusion).[113]

- Mass action

Energetic interactions between the adsorbate species and the available active sites of the adsorbent to form a layer (monolayer or multilayers).[106]

1.5.1 Porous Adsorbents

Porous materials have the ability to interact with atoms, ions and molecules not only on their surfaces, but also throughout their bulk.[114] As a result, they are suitable to use in applications such as ion-exchange, catalysis, membranes and adsorption.[115–117] The pores of these solids are categorised according to their pore size as follows:

- Macropores: > 50nm (e.g. porous glasses)[118]
- Mesopores: 2- 50 nm (e.g. modified/ templated silica gels like SBA-15, SBA-16)[119,120]
- Micropores: <2 nm (e.g. zeolites, activated carbons)[115,121]

The distribution of sizes, shapes and volumes of the pores in the materials directly relate to their ability to perform as adsorbents.[122]

1.5.1.1 Silica Gels

Silica gels (modified or templated) have been studied and used as adsorbents due to their uniform pore structure (better efficiency in mass transfer) and good mechanical stability. However, they have some disadvantages that potentially limit their use as adsorbents.[123,124] They have relatively low adsorption capacities, high costs associated with their production and are not very selective to metal adsorbates.[125] Furthermore, they have limited resistance to alkaline media, and can only be effective in an acidic environment. Depending on their pore size (between microporous and mesoporous range), they are unsuccessful adsorbents when used to remove or recover large molecules (i.e. dyes).[126]

Mesoporous silicas of the M41S family and SBA series have played an important role in surface chemistry, including adosprtion.[115,127] The mesoporous M41S family of silicate/aluminosilicate mesoporous molecular sieves was first discovered by researchers at Mobil Corporation in 1992. Their synthesis involves sol-gel and templating techniques in alkaline media and three different mesophases have been identified; lamellar MCM-50, hexagonal MCM-41 and cubic MCM-48. The hexagonal MCM-41 with diameters in the range of 1.5-10 nm, owing to its highly regular arrays of uniform-sized channels and its thermal stability, has been regularly applied in adsorption media and advanced composite materials.[128] The mesoporous SBA series was produced in 1998, with the first material being the hexagonal SBA-15 synthesises under acidic conditions. SBA-15 showed larger diameters in the range of 4.6-30 nm, in addition to thermal, mechanical and chemical resistance properties, making it a strong rival to the MCM-41.[128]

Since, the early and late 1990s that marked the birth of MCM-41 and SBA-15, these mesoporous materials have been widely studied and used adsorbents for metal recovery, with recent work exhibiting that they can be enhanced when functionalised and modified.[124,129,130]

1.5.1.2 Activated Carbons

Activated carbons are the most popular adsorbent materials and have been extensively used over the years.[108,131] Activated carbons are constituted primarily by carbon atoms, which form aromatic sheets that cross-link, and other heteroatoms like oxygen, nitrogen, sulfur, etc.[132] Activated carbons can be obtained from a variety of raw materials, including lignocellulosic material, tars, coals, via carbonisation in an inert atmosphere.[133]

Reasons behind their appeal as adsorbents include high specific surface area, well-developed porous structure and large pore volumes, microporosity, good mechanical stability, high adsorption capacities and cost effectiveness.[99,134] However, due to their microporosity they are rendered less effective in the adsorption of large hydrophilic molecules, like dyes, vitamins, dextrins, etc., and as a result the presence of pores in the mesopore range is preferred and considerable interest has been shown in synthesising mesoporous carbons.[115,134]

With the discovery of ordered mesoporous materials (OMM), a novel generation of silica templates was generated that allowed for the synthesis of mesoporous carbons, as well. *Ryoo et al* were the first to synthesise the CMK series of ordered mesoporous carbons (OMC), with CMK-1 being the first OMC.[134,135] CMK-1 was produced in the channels of mesostructured silicates/aluminosilicates like the MCM-48, with specific surface area in the range of 1000-2000 $m^2 g^{-1}$ while maintaining pores in the mesopore range.

Since then, increasing interest in synthesising mesoporous carbon materials has been observed. Advances in the preparation methods of these materials have been made, with mesoporous bio-derived materials being the focus as adsorbents for metal recovery.

1.5.1.3 Other Non-Conventional, Low -Cost Adsorbents

Except activated carbons and silica gels, modified or not, other adsorbents are gaining interest as they have lower costs associated with them. Such adsorbents are usually by-products or waste that may pose various disposal issues due to their bulk volume

and physical nature.[131,136] Potential sources included agricultural and household waste, as well as industrial waste, sea materials, soil, etc.[137] Such adsorbents are considered low cost, as opposed to the commercially available and commonly used ones, since they usually require little processing and they are abundant on Earth (either abundant in nature or in quantitative amounts in waste streams).[90,138]

Examples of non-conventional low cost-adsorbents are included in Table 5.

Table 4 Other non-conventional low cost adsorbents for wastewater treatment[19,136]

Material	Pollutant	Maximum adsorption capacity / mg g^{-1}
Apricot shell	Methylene blue	1.33
Almond shell	Methylene blue	4.11
Alfalfa	Au(III)	293
Banana peel	Pb(II)	2.18
Barley straw (raw)	Cu(II)	4.64
Buckwheat hulls	Au(III)	297.00
Cashew nut shell (raw)	Ni(II)	18.86
Chitosan	Cr(VI)	7.94
Corncob	Acid blue	1060.00
Cystoseira baccata (Algae)	Hg(II)	329.00
Garden grass (raw)	Pb(II)	58.34
Grapefruit peel	U(VI)	140.79
Lentil shell	Cu(II)	9.59
Mango peel	Zn(II)	45.29
Native garlic peel	Pb(II)	51.73
Olive stone (raw)	Cd(II)	3.25
Orange peel	Basic violet 10 dye	20.50

Pomegranate peel carbon	Fe(II)	18.52
Pomelo peel	Cu(II)	19.70
Rice husk	Au(III)	106.50

1.6 Carbon/Silica Composites

Keeping in mind both the advantages and disadvantages of silica gels and activated carbons, alternative materials are sought that combine the virtues of both to be efficient and effective adsorbents. Cost-effective substitutes are composite materials derived from waste biomass and low-cost amorphous silicas, such as K60. Recent work demonstrated the viable synthesis of mesoporous CSCs via the wet impregnation of pyrolysis oil into a SBA-15 silica framework.[124,139] The incorporation of carbon onto the walls of silica leads to mechanically and chemically enhanced carbonaceous materials, which retain the pore characteristics of the parent silica material.[140–142] This clean and economical synthesis of CSCs enables particular control over both the porosity and the graphitic content or functionality of the carbon surface. As a result, these alternative porous composite materials offer great prospect with relation to adsorption, since they combine great mechanical stability, high adsorption capacities resembling those of activated carbons and porosity that allows them to be used as adsorbents for a range of species, small or large.[143,144]

Carbon-silica composites are, in general, chemical coatings that cover the surface of silica supports, which are in turn converted to carbonaceous layers via thermochemical conversion or acid treatment.[145] They have been used in a range of applications including catalysis,[146,147] drug delivery systems[148], energy storage and adsorption.[144,149] To date, the use of such materials in adsorption applications has focused on the removal of heavy metals and also gaseous pollutants like ammonia and carbon dioxide.

PART I

CARBON/SILICA COMPOSITES:

SERIES A

Chapter 2.

Carbon Silica/Composites Series A:

Synthesis and Characterisation

Aspects of the work presented in this chapter have appeared in:

Oral presentation at 3rd EuCheMS Congress on Green and Sustainable Chemistry (EuGSC), York, UK, September 2017

Oral presentation at Critical Elements Day: Solutions to the Challenges of Matching Increasing Demand with Declining Mineral Resources, York, UK, November 2017

Oral presentation at the 8th IUPAC International Conference on Green Chemistry, Bangkok, Thailand, September 2018

Poster presentation at the 9th World Convention on Recycling and Waste Management, Osaka, Japan, October 2018 (1st poster prize awarded)

Synthesis and application of tuneable carbon–silica composites from the microwave pyrolysis of waste paper for selective recovery of gold from acidic solutions

K. Sotiriou, N. Supanchaiyamat, T. Jiang, I. Janekarn, A. Muñoz García, V.L. Budarin, D.J. MacQuarrie, A.J. Hunt, RSC Advances, 2020, 10, 25228–25238

Chapter 2.

Carbon/Silica Composites Series A: Synthesis and Characterisation

2.1 Introduction

Recent work demonstrated the viable synthesis of mesoporous CSCs via the wet impregnation of pyrolysis oil into a SBA-15 silica framework.[124,139] The incorporation of carbon onto the walls of silica leads to mechanically, chemically and thermally enhanced carbonaceous materials, which retain the pore characteristics of the parent silica material.[140–142] This clean and economical synthesis of CSCs enables particular control over both the porosity and the graphitic content or functionality of the carbon surface. As a result, these alternative porous composite materials offer great prospect with relation to adsorption, since they combine great mechanical stability, high adsorption capacities resembling those of activated carbons and porosity that allows them to be used as adsorbents for a range of species, small or large.[143,144]

Carbon-silica composites have been used in a range of applications including catalysis,[146,147] drug delivery systems[148], energy storage and adsorption.[144,149] To date, the use of such materials in adsorption applications has focused on the removal of heavy metals and also gaseous pollutants like ammonia and carbon dioxide, but not much in the removal of gold.

2.2 Aims

The overall objective of this chapter is to provide a full assessment on the development of the Series A CSCs by Dr Tengyao Jiang.

The aim of the work presented herein:

- To investigate the influence of carbonisation temperature on the physiochemical properties of Series A CSCs.

2.3 Results and Discussion

2.3.1 Preparation of Series A CSCs

The three types of carbon/silica composites synthesised for this work, are described in Table 6, along with the abbreviated name that will be used throughout this thesis.

Table 5 Material description and abbreviation

Starting Material	Carbonisation Temperature (K and ˚C)	Abbreviation
Pyrolysis oil BO-A and Silica K60	573 / 300	CSC-A3
Pyrolysis oil BO-A and Silica K60	773 / 500	CSC-A5
Pyrolysis oil BO-A and Silica K60	1073 / 800	CSC-A8

The typical method of preparation consists of four main stages:

1. Milled waste office paper pressed into blocks
2. Microwave-assisted pyrolysis of blocks to collect bio-oil
3. Wet impregnation of bio-oil into silica framework (ratio 1:1)
4. Carbonisation at different temperatures (300˚C, 500˚C, 800˚C) under nitrogen atmosphere.

Amorphous silica gel K60 with reported average particle size of 0.040 – 0.063 mm is used for the material synthesis. Unlike ordered mesoporous silicas, such as the SBA or MCM series which possess a regular pore arrangement,[150] silica gel K60 is amorphous silica with a more random pore distribution and is commonly used in column chromatography.

The synthetic route followed for the preparation of materials is described in Section 8.1.2.3 (Chapter 8). Series A CSCs were produced by Dr T. Jang as part of his research, while characterisation and application of materials in gold adsorption is performed by the author.

2.3.2. Physical Properties of Series A CSCs

Nitrogen adsorption/desorption porosimetry is used to provide analysis of the textural properties of Series A CSCs. Characterisation of the isotherms obtained illustrates type IV isotherm profiles with H2 hysteresis loop classification for all Series A CSCs (Fig.10). The similar hysteresis loop between the CSCs and silica K60 indicates that the introduction of organic matter into silica pores does not affect the pore structure significantly. The typical type-IV isotherm plot with a gradual rise in adsorption branch during capillary condensation for silica K60 and the CSC materials, is indicative of mesoporosity.[150] This demonstrates that these CSC materials possess a broad pore size range and distribution.[151]

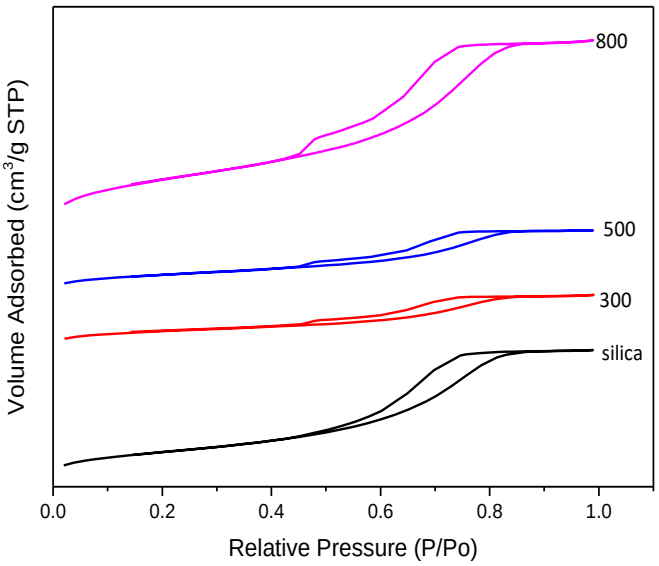

Figure 9 Overlapped nitrogen adsorption isotherms for CSC-A3, CSC-A5, CSC-A8 and silica K60

A summary of material properties is given in Table 7. BET surface area, pore volume and pore diameter of materials produced at 300 ˚C and 500 ˚C are lower than the parent silica due to the introduction of a carbonaceous layer into the silica pores, consistent with previous synthesis of CSCs.[152] As adsorption isotherms and hysteresis loops are similar, it can be deduced that that the introduction of organic matter into the silica pores does not affect mesoporosity significantly.

Table 6 Textural properties of silica K60 and Series A CSCs from porosimetry

Material	BET surface area ($m^2\ g^{-1}$)	Pore volume ($cm^3\ g^{-1}$)	Pore diameter (nm)	Carbon layer thickness (nm)
Silica K60	467	0.80	6.7	-
CSC-A3	321	0.32	4.4	1.15
CSC-A5	380	0.39	4.5	1.10
CSC-A8	1056	1.22	4.8	0.95

A significant reduction in pore volume from 0.8 $cm^3\ g^{-1}$ in silica gel K60 to 0.32 $cm^3\ g^{-1}$ in CSC-A3 reveals that a proportion of the pores are blocked by the polymerised bio-oil. As the carbonisation temperature increases to 500 ˚C, BET surface area, pore volume and diameter marginally increase. CSC-A8 exhibits a much larger surface area and pore volume when compared to the parent silica and the rest Series A CSCs. These changes are likely due to the loss of some carbon from within the pores and the subsequent formation of a more porous carbonaceous layer on the silica surface. This is associated with the rapid release of gases (i.e. CO_2, CO and H_2O) upon heating, and further carbonisation or decomposition of the bio-oil that occurs with an increase from 500˚C to 800˚C. This bio-oil decomposition results in a very high specific surface area (1056 $m^2\ g^{-1}$) for CSC-A8, related to the formation of highly porous aromatic composite material. The estimated thickness of the polymer film decreases relative to the carbonisation temperature, corresponding to a loss of small organic molecules, water and CO_2, and leading to the formation of an aromatic carbonaceous layer within the silica framework. This is in good agreement with XPS data (Fig. 15) which demonstrate the development of a highly aromatic structure at 800˚C, and nitrogen adsorption data that present an increase in pore volume and diameter (Table 17).

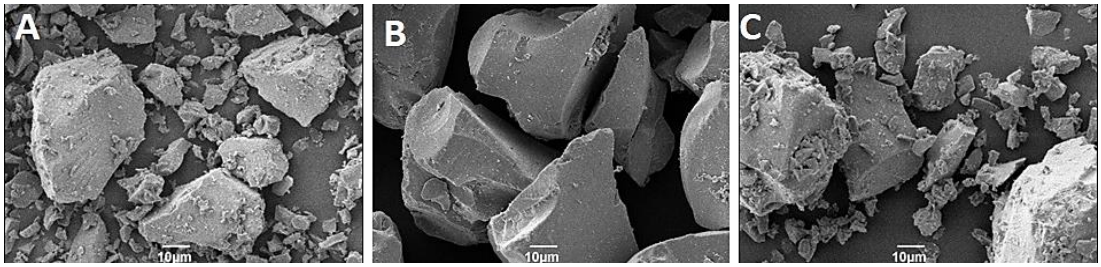

Figure 10 SEM images for A) CSS-A3, B) CSC-A5, C) CSC-A8

Scanning electron microscopy (SEM) images (Fig. 11) illustrate a pattern as carbonisation temperature increases for Series A CSCs. All materials appear to have a variation in size and shape distribution of particles present. Even though CSC-A3 consists of a combination of larger and smaller particles, CSC-A5 appears to only contain the larger pieces and, surprisingly, the smaller particles re-occur in the CSC-A8. The pattern creates the postulation of a mechanism (Fig. 12) which agrees with the porosimetry data.

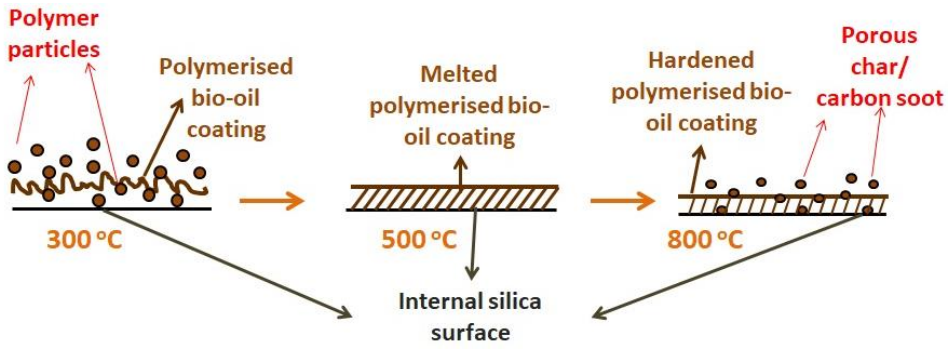

Figure 11 Suggested synthesis mechanism during carbonisation of Series A CSCs

At the lower carbonisation temperature (300 ˚C) the oxygenated compounds in the bio-oil and silanol groups of the silica interact within the pores and on the surface of the template. This leads to the formation of small polymer particles that potentially cause pore-blockage, resulting in reduced BET surface area and pore volume for CSC-A3. As the temperature is increased to 500 °C, the polymerised system is speculated to undergo a softening process or melt, during which the polymerised organic matter spreads to cover the surface uniformly, eliminating the presence of smaller polymer particles. The highest temperature material CSC-A8, then, potentially undergoes further decomposition, during which the production and rapid release of gases, including CO_2 and CO are observed. The theory is supported by TG-IR data which demonstrate a clear release of CO_2 at 550˚C (Fig. 13). It is suspected that the carbon particles at this temperature are a result of porous char or soot production, resulting from the release of gases from a rapidly hardening material. The rapid release of gases leads to the significant additional porosity throughout the composite material, hence the very high BET surface area of CSC-A8.

Another plausible explanation for the difference in size of particles in Series A CSCs, can be the effect of mechanical grinding during the first stages of their synthesis.

While the bio-oil is added to the silica K60, magnetic stirring is used to ensure mixing of both material precursors. The abrasive forces generated between the magnetic stirrer and the round bottom flask, may lead to fracturing of silica particles in CSC-A3 and CSC-A8, and thus the appearance of smaller particles in their SEM images (Fig.11). CSC-A5, which does not follow this pattern, may be assumed of having superior mechanical properties when compared to the other two CSCs of Series A.

2.3.3 Chemical Properties of Series A CSCs

The TG-IR spectrum of the uncarbonised mixture used to produce Series A CSCs is illustrated below (Fig. 13).

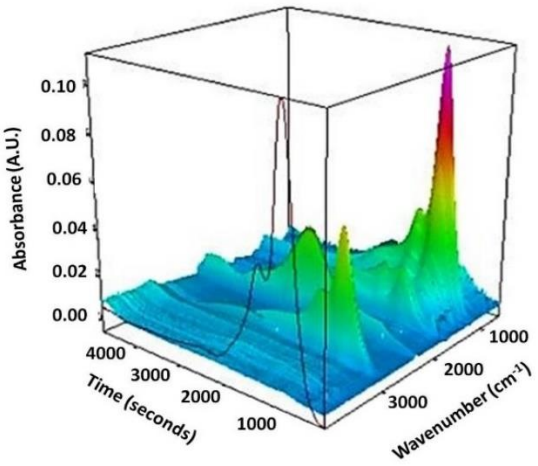

Figure 12 3D TG-IR spectrum of the off-gases from the thermal treatment of the uncarbonised sample used for Series A

The spectrum clearly shows a significant peak located at 1082 cm^{-1}, which is ascribed to C-O-C groups, possibly due to the presence of a decomposition product from saccharides. Another characteristic peak at 2979 cm^{-1} can be assigned to -CH stretching vibrations, indicating the presence of –CH, $–CH_2$ or $–CH_3$ groups. Although the intensities of these peaks are decreasing from 160°C onwards, they can be detected until 400°C, indicating the sample still contains these components before 400°C. A peak at 1807 cm^{-1} can be attributed to the carbonyl group associated with anhydrides, suggesting that these groups are released at this temperature. The fact that there is second band close to the peak at 1807 cm^{-1} is further evidence of the presence of anhydrides. A sharp peak at 877 cm^{-1} can be ascribed to the bending vibration of methylene groups.[152] The minor peak at 2350 cm^{-1} is attributed to the vibrations of CO_2, compared to the standard IR spectrum of carbon dioxide.

In terms of mass loss relevant to temperature, the following are observed for the uncarbonised material Series A:

- Around 100 ˚C, most of the moisture content present from the bio-oil and parent silica is lost.
- Between 180 ˚C and 230 ˚C , the system undergoes elimination reactions and saccharide decomposition, leading to the removal of volatile acids.
- Between 300 ˚C and 450 ˚C, most of the oxygenated compounds and aliphatic chains undergo decomposition.
- Above 550 ˚C, condensation of the silanol groups of the parent silica begins and the decomposition of aliphatic chains is complete, allowing for a degree of aromaticity at higher temperatures. Within this temperature range, CO_2 and CO are given off, too, further establishing the additional porosity of the materials indicated by porosimetry results.

DRIFT spectra of Series A CSCs (Fig. 14), illustrate that increasing the carbonisation temperature results in the decomposition of organic matter and a change in the functional groups present, shifting from an aliphatic and polar oxygenated coated surface to a more aromatic carbon layer. The carbonisation temperature-dependence of CSCs holds great potential for the development of tuneable properties as it enables the continuum surface functionality of the material from hydroxyl and carbonyl rich surfaces at 300 ˚C to carbonaceous aromatic surfaces at 800 ˚C.[152] Aliphatic C-H stretching observed at 2900 cm^{-1} and C=O stretching at 1650 cm^{-1} are due to the presence of oxygenated compounds like carboxylic acids, ketones, aldehydes and esters, originating from the original components of the bio-oil.[152,153] These peaks, as well as the O-H stretch at 3500 cm^{-1}, are evident in the spectrum of CSC-A3 as expected, but weaken and disappear as temperature increases to 500 ˚C and 800 ˚C. Above 500˚C, the hydroxyl group is significantly reduced due to the crosslinking effect of silanols in the material. Spectra for all CSCs show stretching bands around 1060 cm^{-1} and 800 cm^{-1} corresponding to Si-O-Si bonds, confirming the

presence of the silica substrate in the composite materials and the changes on the carbonaceous part of the structure.[152]

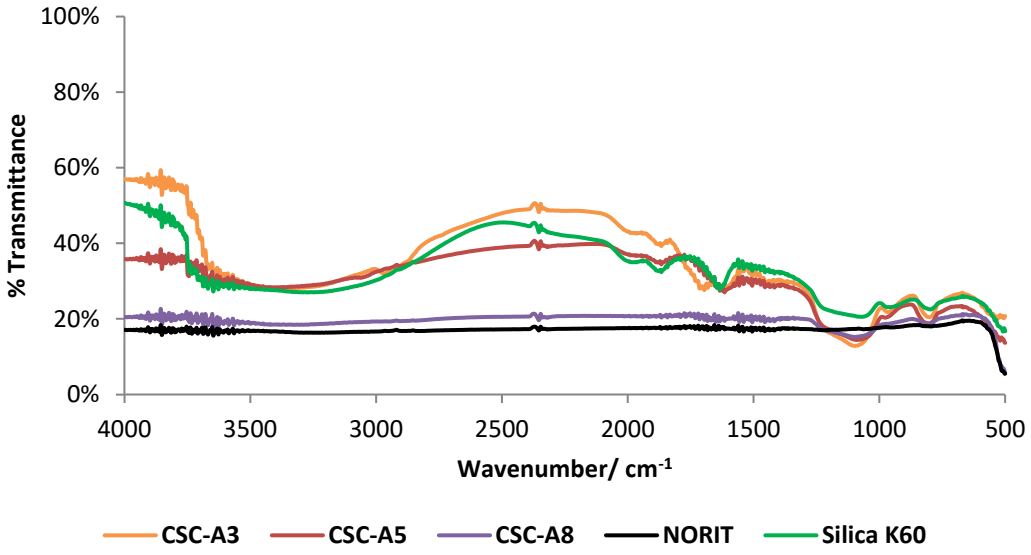

Figure 13 Overlapped DRIFT spectra of CSC-A3, CSC-A5, CSC-A8, NORIT activated carbon and Silica K60

The carbonisation temperature dependence of the materials produced has an immense potential for the development of tuneable properties, as it enables the continuum surface functionality of the materials; from hydroxyl and carbonyl rich surfaces at 300 ˚C to aromatic surfaces at 800 ˚C .[152,154]

Table 7 % Atomic content deduced from Carbon XPS spectra of C1s for Series A CSCs

	% Atomic Content		
	C	Si	O
CSC-A3	51.0	15.6	33.4
CSC-A5	55.1	14.1	30.8
CSC-A8	59.7	12.2	28.1
	C/O ratio	C/Si ratio	
CSC-A3	1.53	3.27	
CSC-A5	1.79	3.99	
CSC-A8	2.12	4.89	

The C, O and Si elemental content of Series A CSCs is measured by XPS. XPS data show that with increasing carbonisation the % C content on the surface increases, whereas % O and % Si contents decrease. The C/O and C/Si ratios increase as well, indicating

that the surface is losing oxygenated functionalities as the carbonisation temperature increases, and that carbon coverage is successful. (Table 8). These results are in good correlation with DRIFT data of the materials (Fig.14), as a significant loss in the proportion of hydrophilic compounds containing oxygen is observed upon heating to higher temperatures. Oxygen is still present on the surface of all Series A CSCs, as it facilitates the interaction between the polymerised bio-oil and the silanol groups in silica to give rise to the anticipated C-O-Si bonds as observed.

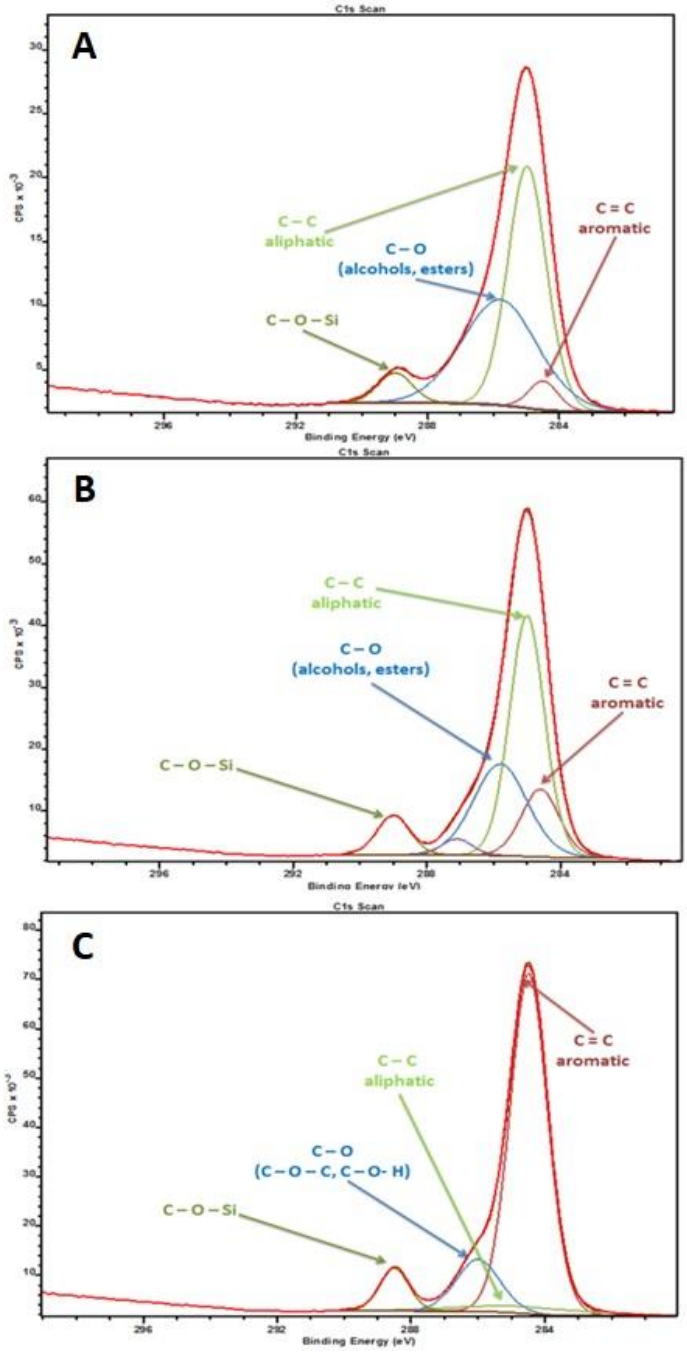

Figure 14 Carbon XPS Spectra of C1s (A) CSC-A3, (B) CSC-A5, (C) CSC-A8

Based on C1s spectra deconvolution for Series A materials (Fig.15), oxygenated carbon functionalities decompose with increasing temperature, showing an increase in aromatic character and a significant loss of hydrophilic and aliphatic compounds containing oxygen. Oxygen is still substantially present at all temperatures, along with silicon, confirming the presence of the parent silica. The presence of oxygen enables the interaction between the polymerised bio-oil and the silanol groups in the parent silica, giving rise to the observed C-O-Si bond (Fig.15).[154]

Every type of bond appears at a specific binding energy which allows for identification of different functional groups through deconvolution of the main peaks. C1s peaks of the spectra are deconvoluted and assigned, giving rise to four contributions due to: C=C groups (aromatic), C–C groups (aliphatic), C –O groups (C–O–C or C–O–H) and C–O–Si group at 284.4 eV, 284.6 eV, 285.8 eV and 288.9 eV binding energies, respectively.[116,155,156] XPS and DRIFT data are in good agreement, confirming the shift from aliphatic and polar hydroxyl character, which predominated in CSC-A3 , to aromatic character observed in CSC-A8.

Comparing % C with CHN analysis (Table 9), an opposite pattern in composition is observed; w/w% C decreases with increasing carbonisation temperature. This can simply corroborate with the hypothesis made previously, that as temperature increases some of the carbon is being removed from the surface due to the release of CO_2 and CO. Based on CHN analysis, decrease in w/w% O or w/w% Si contents cannot be measured quantitatively, as they are not differentiated and are both accounted for in the rest bulk content value.

Table 8 % Elemental composition of Series A CSCs

	w/w % Elemental composition			
	C	H	N	Rest
CSC-A3	45.3	6.2	-	48.4
CSC-A5	40.3	5.6	-	53.8
CSC-A8	39.6	4.3	-	56.1

2.4 Conclusion

A novel series of mesoporous carbon/silica composites (Series A) have been successfully prepared from bio-oil, obtained from the microwave-assisted pyrolysis of waste office paper, and commercially available silica K60 gel. The composite materials possess tuneable surface chemistry and textural properties and are obtained by increasing the carbonisation temperature during their synthesis.

At low temperatures the materials are rich in oxygen functionalities (CSC-A3), and as the temperature increases the materials begin to lose their aliphatic and polar character becoming more aromatic (CSC-A8). During the carbonisation process and as the temperature is increase from 300 ˚C to 800 ˚C , the materials retain their porosity, with difference though in BET specific surface area and pore volume. The most interesting results are presented in CSC-A8, which has a surface area of 1056 m^2 g^{-1}. This observation is assumed to be associated with the formation of porous char at this synthesis temperature, suggesting possible degree of microporosity as well.

The surface functionalities and the carbon film are expected to influence the performance of Series A CSCs when used as adsorbents, yet the tuneability in surface chemistry can provide interesting outcomes with regards to adsorption. The effectiveness of Series A CSCs as adsorbents will be discussed in the following chapter.

Chapter 3.

Carbon Silica/Composites Series A:

Application in Gold Adsorption

Aspects of the work presented in this chapter have appeared in:

Oral presentation at 3rd EuCheMS Congress on Green and Sustainable Chemistry (EuGSC), York, UK, September 2017

Oral presentation at Critical Elements Day: Solutions to the Challenges of Matching Increasing Demand with Declining Mineral Resources, York, UK, November 2017

Oral presentation at the 8th IUPAC International Conference on Green Chemistry, Bangkok, Thailand, September 2018

Poster presentation at the 9th World Convention on Recycling and Waste Management, Osaka, Japan, October 2018 (1st poster prize awarded)

Synthesis and application of tuneable carbon–silica composites from the microwave pyrolysis of waste paper for selective recovery of gold from acidic solutions

K. Sotiriou, N. Supanchaiyamat, T. Jiang, I. Janekarn, A. Muñoz García, V.L. Budarin, D.J. MacQuarrie, A.J. Hunt, RSC Advances, 2020, 10, 25228–25238

Chapter 3.

Carbon/Silica Composites Series A: Application in Gold Adsorption

3.1 Introduction

Precious metals like gold are used in many applications, ranging from electronics to catalysis, in addition to jewellery and medical treatments. [34,37] This exponential demand as a result of the plethora of uses and the existing limited resources of gold resulting, encourage a 'recycle and re-use' approach to recover the metal.[157]

Efforts are currently focused on secondary metal sources, such mine tailings.[96] Mine tailings contain various metals (e.g. Cu, Zn, Pt, Pd), including gold and they are an interesting stream of waste, as they can also become a source of the metal. Implemented and conventional removal techniques include chemical precipitation, electrodeposition, and many other mechanical methods, but have high cost and high energy requirements associated with them. [97] An attractive alternative for treating wastewater, like mine tailings, is adsorption.[102]

Several activated carbons and templated mesoporous materials have been used to recover gold, but newer and greener materials are always necessary. While, the materials that have been commonly used for gold recovery may be effective, they lack selectivity.[104] Adsorbents like 'hybrid' materials, such as carbon/silica composites, combine adsorption qualities of carbonaceous and siliceous materials and have great potential in removing and recovering gold from solution.[158,159]

3.2 Aims

The overall objective of this chapter is to provide a full assessment on the performance of the Series A composite materials as adsorbents for the removal of gold from acidic solutions.

The aims of the work presented herein:

- To investigate the influence that the physiochemical properties of the Series A composite materials have on adsorption.
- To propose the possible adsorption mechanism on the surface of the Series A composite materials using isotherm models and adsorption kinetics.

3.3 Results and Discussion

3.3.1 Gold Selectivity

Selectivity is important in the field of metal separation and recovery, especially for waste containing various co-existing metal ions. It is therefore vital to prove that materials cannot only recover gold from solution, but also 'select' during the process.

Initial batch adsorption experiments demonstrate that Series A CSCs exhibit significant selectivity toward gold from an acidic solution (pH 3) containing precious and base metals including nickel, copper, zinc, palladium, platinum and gold in similar concentrations. The choice of metals is made based on the following factors: 1) metal composition of mine tailing samples from North American Palladium, Lac des Iles mine in Ontario, Canada and 2) significant concentrations in WEEE after extensive use in commercial electronics. [14,41]

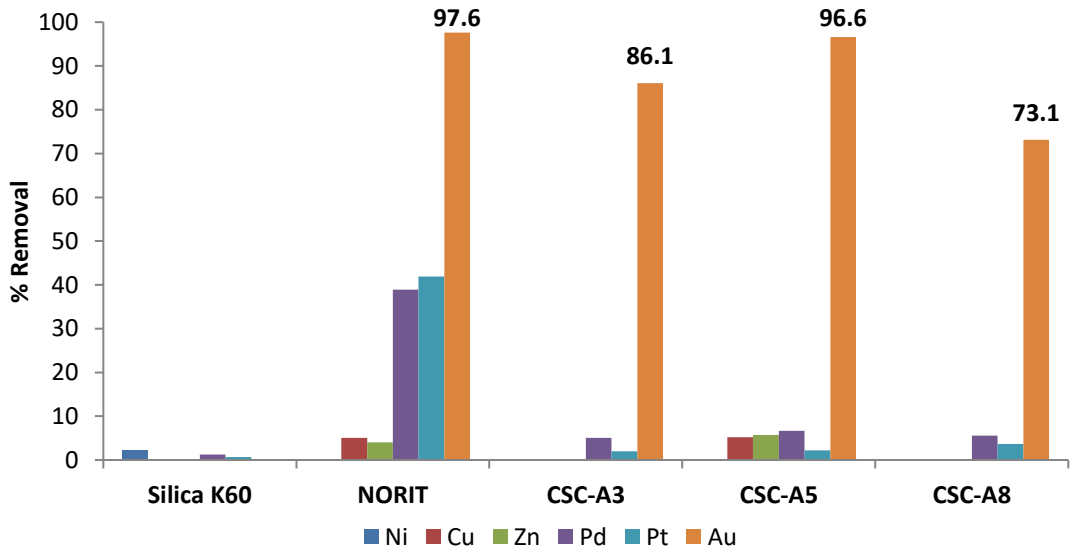

Figure 15 % Removal after multi-metal adsorption using Series C CSCs, silica K60 and NORIT activated carbon

Data illustrated in Figure 16, confirm the successful selective adsorption of gold from the multi-metal mixture. Silica gel K60 demonstrates poor adsorption of all elements and the activated carbon NORIT shows a significant adsorption of all metals, yet poor selectivity as it performs well in removing most of the metals. In contrast, Series A CSCs demonstrate a balance between strong adsorption and high selectivity towards gold. The adsorption of gold in the case of Series A CSCs is predominately affected by surface functionality and the porosity of materials. All three materials show exceptional gold removal (Fig.16), with the highest of them being for the CSC-A5, resembling that of activated carbon NORIT. CSC-A5 appears to be the best composite material as the adsorbent, at which temperature the material is assumed to have the optimum balance between surface functionality and porosity, thus introducing the notion of enhanced adsorption capacity and gold removal if the 'right' surface functionality and porosity are achieved. CSC-A5 accomplishes 96.6% removal of gold during the multi-metal adsorption experiment, competing extremely well with activated carbon NORIT.

3.3.2 Mechanism of Gold Adsorption

As will be expanded below, the mechanism of gold adsorption involves two processes: 1) an irreversible process involving a chemical reaction, proposed chemisorption, during which Au^{+3} ions are reduced mainly to elemental gold when interacting with the adsorbent surface, and 2) the traditional reversible physisorption during which electrostatic interactions are dominant.[42,108,160] In gold (III) chloride solutions, gold occurs as the $[AuCl_4]^{-1}$ anion complex. The high affinity of the carbonaceous surface of CSCs for Au(III) is due to the high reduction potential, E^o ($[AuCl_4]^{-1}$/ Au= 1.00V), of the metal halide to reduce to the metallic Au(0) and the similarly high reduction potential, E^o ($[AuCl_4]^{-1}$/ $[AuCl_2]^{-1}$= 0.93V) for the reduction to Au(I) via this reduction-adsorption mechanism.[28,107,161] The mechanism allows for the creation of vacancies on the surface of the material as the reduced species deposit, which leads to higher uptake of the metal from solution and increased adsorption capacity of the adsorbate surface, consistent with previous studies with activated carbon.[162]

Simultaneously, the system undergoes physisorption as well, which involves weak van der Waals' and electrostatic interactions between the aurochlorate anion in solution

and the surface of the CSCs.[154,163] During physisorption a thin film of the adsorbate is created on the surface of the material, after species' diffusion through the layer and into the pores of the materials.[160]

The surface chemistry of materials plays a key role in the mechanism of adsorption. It is anticipated that owing to the materials oxygen-containing functionalities (carbonyl, carboxyl, hydroxyl groups) present on the carbonaceous surface, supported by XPS and IR data, the system will favour chemisorption; reduction of the gold species from Au(III) to Au(0), with simultaneous oxidation of the protonated carbonaceous surface.

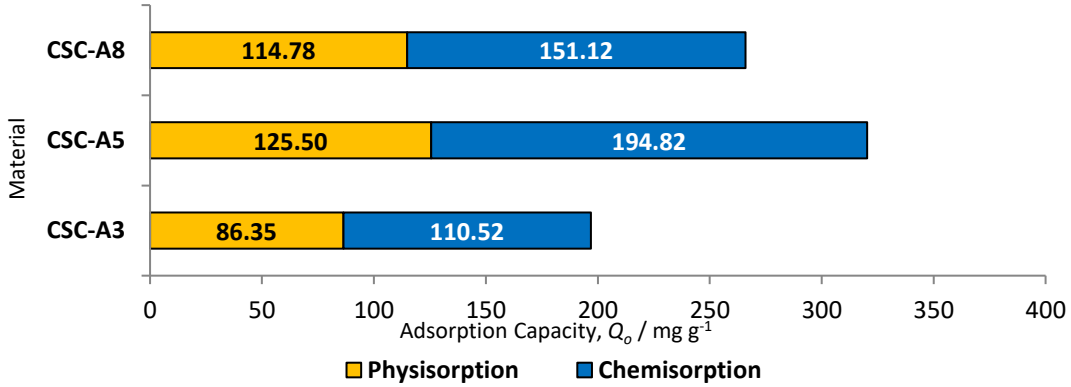

Figure 16 Nature of adsorption for all Series A CSCs

As seen in Figure 17, all three CSCs of Series A mainly undergo chemisorption, or better described as adsorption-reduction, during the process. This suggests that during this irreversible step Au(III) is being reduced to its elemental form. For this to be reasonable though, the surface of materials must oxidise at the same time.

XPS results clearly indicate the presence of reduced gold species on the surface of CSCs after adsorption (Fig.18). Deconvolution of Au4f (7/2, 5/2) spectra present three doublets, in which the two peaks within the doublet are 3.7 eV apart.[28,164] The main doublet is found at 84.6 eV (7/2), which corresponds to metallic Au(0) confirming the reduction of the [$AuCl_4^{-1}$] species. The other two doublets at 86.1 eV and 86.6 eV are related to Au(I) and Au(III), respectively.

This is in good agreement with the reduction-adsorption mechanism proposed, further demonstrating the affinity of the carbonaceous nature of the materials

towards gold. Data from the deconvolution of the Au4f XPS spectra (Fig.18) indicate that the gold is mainly reduced to Au(0), with a small proportion of it reduced to Au(I). This reduction to Au(0) is well in agreement with the TEM images (Fig.19) of Series A which illustrate nanoparticle formation due to gold reduction.

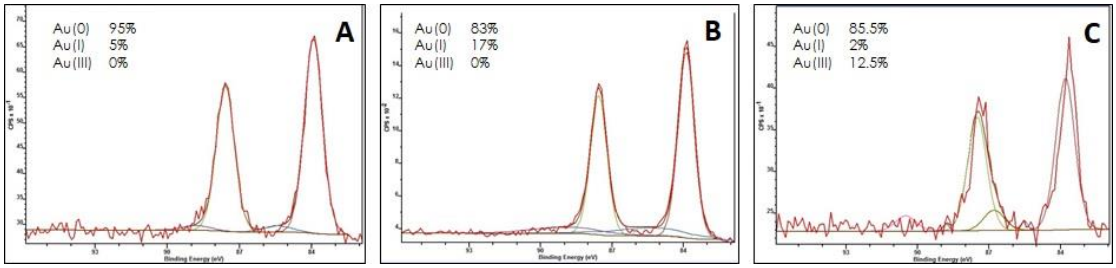

Figure 17 Au4f XPS spectra for (A) CSC-A3, (B) CSC-A5, (C) CSC-A8

The reduction of gold ions is caused by the simultaneous oxidation of the surface of CSCs. There are several functional groups present on the surface of materials, especially those carbonised at 300 ˚C and 500 ˚C, that can oxidise (i.e. hydroxyl and carbonyl groups) when reacting with the gold species. The following hypotheses can be used to explain the redox mechanism occurring during gold adsorption:

- Oxidation of hydroxyl groups to carbonyl groups: Literature describes that during the process the $[AuCl_4]^{-1}$ is initially adsorbed onto the surface by forming a chelating complex with the oxygen atoms of hydroxyl groups. The hydroxyl groups are then oxidised to ketones, leading to a decrease in the concentration of O-H groups and an increase in the concentration of C=O groups.
- Decomposition of the carbon surface: Oxidation of carboxylic groups to produce CO_2, is accompanied by decomposition of the surface, thus inducing an increase in the C/O ratio after adsorption.

Elemental analysis carried out by XPS shows higher C/O ratios (Table 10) after adsorption for all materials of Series A, suggesting that the oxygenated functionalities on the surface are removed as they oxidise, thus confirming the reduction mechanism.

Table 9 Comparison of CSC C/O ratio before and after adsorption of gold

C/O ratio

Material	Before adsorption	After adsorption	Variation
CSC-A3	1.5	1.7	+ 0.2
CSC-A5	1.8	2.0	+ 0.2
CSC-A8	2.1	2.4	+ 0.3

Transmission Electron Microscopy (TEM) images of Series A CSCs (Fig.19) obtained after adsorption clearly illustrate the formation of gold nanoparticles (AuNPs), and are in good correlation with the XPS data, proving the reduction of Au(III) ions to metallic gold Au(0) during the process. Spherical, hexagonal and triangular gold nanoparticles of different sizes are observed. The larger nanoparticles seen, may be the result of agglomeration of smaller nanoparticles around a core molecule, in this case silica.[165,166]

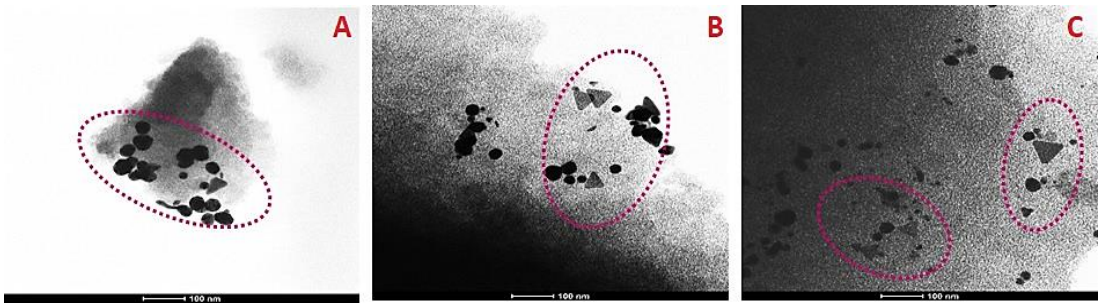

Figure 18 TEM images showing AuNPs formation after adsorption in (A) CSC-A3, (B) CSC-A5, (C) CSC-A8 at 100nm scale

It can be suggested that the recovery of gold from solution occurs in three steps: adsorption, reduction and aggregation. During overall adsorption, both reversible physisorption and irreversible chemisorption occur. During physisorption, the $AuCl_4^-$ species is electrostatically attracted and brought to proximity to the protonated surface of the composite material. Then, the aurochlorate complex appears to be chemically adsorbed to the surface, at which moment it is possible that one of the chloride ligands is replaced by a hydroxyl group on the adsorbent surface. Since, a chemical interaction can be easily assumed to take place, the gold ions are then reduced due to the electron-donor groups on the surface of materials, ultimately causing oxidation of the surface and reduction of Au(III) to mainly Au(0). Finally, the nanoparticles produced are released from the surface and agglomerate to form clusters of AuNPs (or 'free' gold in solution). The release of AuNPs from the surface of materials, leaves more active sites available for further adsorption in the system. This suggested three-part mechanism is, as previously demonstrated, consistent with data obtained from XPS and TEM.

The chloride ions participate as ligands during the adsorption process, yet XPS data show no concentration of said ions on the surface of materials. Further investigation needs to be carried out, to clearly determine what happens to the Cl^- ions; this was out of the scope of this work and is discussed in Further Work Chapter 9, Section 9.2.

3.3.3 Gold Adsorption Isotherms

In order to investigate the mechanism of gold adsorption onto the composite materials, experimental data are applied to three models; the Langmuir model, the Freundlich model and the Dubinin-Radushkevich (D-R) model. Isotherm parameters from equations are calculated using the linear form of the isotherm equations. All parameters and correlation coefficient (R^2) are summarised in Table 11 (plots showing isotherm fitting can be found in Appendix 2).

3.3.3.1 Langmuir Isotherm

The linear form of the model allows for the determination of the monolayer adsorption capacity of the solid,[167] The linear form of the Langmuir equation is:

$$\frac{C_e}{q_e} = \frac{1}{K_L} + \frac{a_L}{K_L} C_e$$

$$Q_o = \frac{K_L}{a_L}$$

Equation 1 Linear forms of Langmuir equation

Where C_e is the metal concentration (mg L^{-1}), q_e is the adsorption capacity at equilibrium and K_L (L g^{-1}) and α_L (L mg^{-1}) are Langmuir equilibrium constants. Q_o (mg g^{-1}) is the monolayer adsorption capacity of the solid.

The model assumes that:[118,168]

- Surface of the adsorbent is uniform (homogeneous) and all adsorption sites are equivalent.
- Adsorbed molecules do not interact with adsorbate molecules on adjacent sites.
- Adsorption throughout the process occurs via the same mechanism.

- At maximum adsorption only monolayer coverage occurs. Adsorbate molecules do not deposit on already adsorbed molecules of adsorbate, but only at the available free active sites of the adsorbent.

3.3.3.2 Freundlich Isotherm

The linear form of the model describes multilayer adsorption on heterogeneous solid surfaces, and is characterised by the heterogeneity factor ***n***. The linear form of the Freundlich equation is:

$$\ln qe = \ln kf + \frac{1}{n} \ln Ce$$

Equation 2 Linear form of Freundlich equation

Where q_e is the adsorption capacity at equilibrium, C_e is the metal concentration (mg L^{-1}), ***kf*** is the Freundlich constant and is associated with the adsorption capacity of the solid. ***n*** is the heterogeneity factor and portrays the intensity of adsorption.[169] If the value of ***n*** is very close or greater than 1, then adsorption of the adsorbate molecules is favourable.

The Freundlich model is related to the Langmuir model, but it suggests adsorption on a non-uniform, heterogeneous surface, where multilayer coverage can take place.[170,171]

3.3.3.3 Dubinin-Radushkevich Isotherm

The linear form of the model describes adsorption onto porous solids. The linear form of the D-R equation is:

$$ln\ qe = ln\ qm - K'\varepsilon^2$$

$$\varepsilon = RT\ ln(1 + \frac{1}{Ce})$$

Equation 3 Linear forms of D-R model

Where q_e is the adsorption capacity at equilibrium, q_m is the monolayer saturation capacity (L g^{-1}), ε is the Polanyl potential and K' is the constant of adsorption energy which gives the mean free energy (E) of adsorption per molecule of adsorbate when transferee to the surface of the solid from solution.[172]

$$E = \frac{1}{\sqrt{2K'}}$$

Equation 4 Relationship between D-R adsorption constant and mean free energy of adsorption

The mean free energy of adsorption *(E)* gives details about the chemical and physical adsorption (chemisorption and physisorption, respectively), where if the value ranges between 8-16 kJ mol^{-1} it suggests physisorption of the adsorbate onto the surface of the solid.[173]

The D-R model assumes heterogeneity of the adsorbent and that adsorption is limited to monolayer coverage.[174]

Model fittings are done for the part of adsorption represented by physisorption, where the system was no longer irreversible. Fitting to all three adsorption models shows that the materials have better correlation to the Langmuir type adsorption with R^2 values over 0.99 for all Series A CSCs (Table 11). The monolayer adsorption capacities represented by Q_0, exhibit deviations when compared to the adsorption capacities calculated experimentally (Table 11). The experimental capacities q_e for all materials are higher than the theoretical Q_o values as per the Langmuir model, with the difference between them accounted for the part of the system mainly favouring chemisorption.

Even though all Series A CSCs have a better fit to the Langmuir model, which assumes monolayer coverage of adsorption sites, some materials illustrate a good fit to the D-

R model, too. For instance, CSC-A3, CSC-A5 and CSC-A8 show a good fit to the D-R model (R^2 values 0.92, 0.95 and 0.93, respectively) which assumes monolayer coverage onto the porous material with surface heterogeinety.[175] The D-R model also assumes that adsorption proceeds via pore filling rather than layer-by-layer coverage.[176,177] Materials fit well with other models than the Langmuir as well, as they are proven to have surface heterogeneity which means that adsorption could be multi-layer or accompanied with pore filling, and not limited to monolayer coverage.

Table 10 Isotherm modelling parameters for all CSCs Series A

Isotherm parameters	CSC-A3	CSC-A5	CSC-A8
q_e (mg g^{-1})	196.97	320.32	265.90
Langmuir			
α_L (L mg^{-1})	0.23	0.24	0.09
K_L (L g^{-1})	39.37	57.80	21.37
Q_o (mg g^{-1})	169.50	242.20	232.60
R^2	0.9988	0.9953	0.9924
Freundlich			
Kf	68.76	124.18	78.12
N	6.11	7.27	5.34
R^2	0.8205	0.7934	0.8607
D-R			
q_m (mol g^{-1})	155.73	237.94	187.24
K' x10^{-8} (mol^2 J^{-2})	6	7	7
E (kJ mol^{-1})	2.89	2.67	2.67
R^2	0.9200	0.9518	0.9273

3.3.4 Effect of Gold Concentration on Adsorption Capacity

ICP-OES analysis is used to determine the adsorption capacity and % gold removal for Series A CSCs at room temperature. Isotherm plots (Fig.21) show an increase in adsorption capacity and over 98% removal of gold (Fig.20) with decreasing gold concentration in the low concentration regions (25 mg L^{-1} to 100 mg L^{-1}), and a decrease/ plateau at the higher concentration regions (150 mg $L^{-1}$to 500 mg L^{-1}) with values dropping to less than 60% removal.

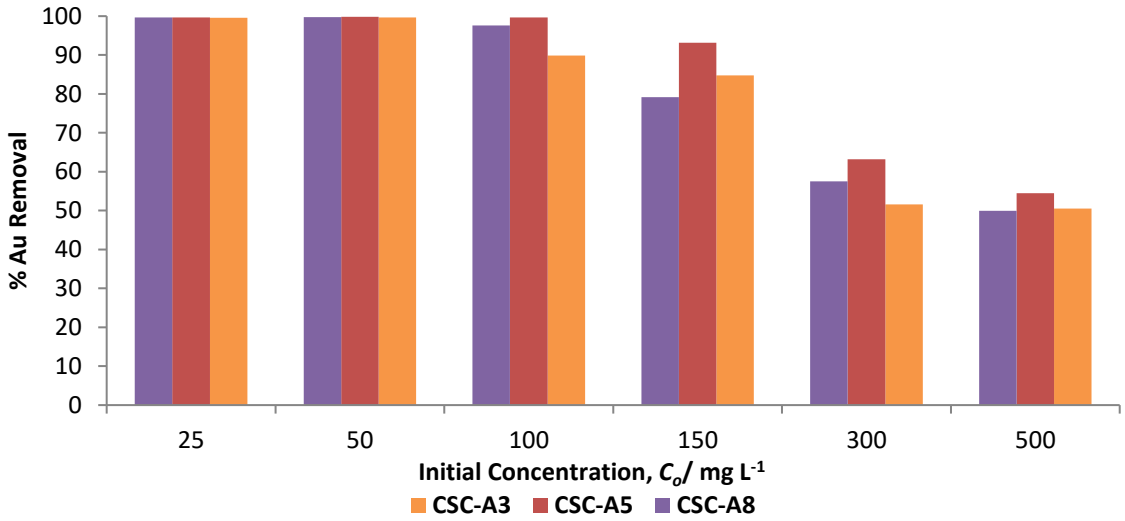

Figure 19 % Gold Removal with Series A CSCs at room temperature

As shown, Series A CSCs have extremely high gold removal at the low region concentrations, with CSC-A5 achieving 99% removal up until 100 mg L^{-1} (Fig.20). As the solution concentration increases, it is evident that CSC-C5 continues to perform well, being the best out of the three materials, as it shows the highest removal of gold at the range of higher concentrations, maintaining gold removal over 50%.

These trends in gold removal demonstrate that adsorption is concentration dependent at constant pH. Initially, at the low region concentrations (20 mg L^{-1} to 100 mg L^{-1}), a significant adsorption is observed. The very high % gold removal observed at those concentrations, along with the XPS data suggest that irreversible chemisorption is taking place as gold is being adsorbed on the active sites of the material via its reduction.[161,178] Adsorption in the higher concentration regions (200 mg L^{-1} to 500 mg L^{-1}) is hence speculated to mainly proceed by reversible physisorption.

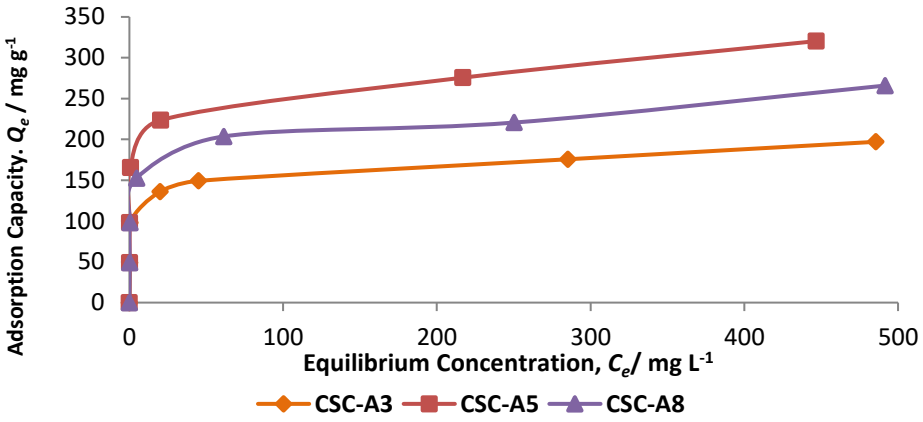

Figure 20 Isotherm plots for Series A CSCs at room temperature

Adsorption plots (Fig.21) illustrate a pattern, further suggesting the two different adsorption mechanisms. Initially, at the low region concentrations, a very strong and high adsorption is observed, resulting in the sharp incline of the adsorption curves. The very high % gold removal values observed can be corroborated with the irreversible chemisorption taking place. Adsorption in the higher concentration regions follows a different mechanism (reversible physisorption) as the isotherm plots show a much less pronounced adsorption and removal of gold from solution.

Removal of gold from solution is shown to be directly associated with the total adsorption capacity, q_e, of materials. Maximum adsorption capacity values, q_e, (Table 11) demonstrate that the best adsorbent material of this series is the one carbonised at 500°C with an adsorption capacity of 320 mg g^{-1}. It appears, that at this temperature the carbon layer has a unique surface structure facilitating a greater extent of adsorption, mainly due to greater reduction ability.[154]

The adsorption capacities of the materials can be associated with the reduction-adsorption mechanism (chemisorption) occurring at the low region concentrations. The high values can be attributed to the balance between surface functionalities of the material and the significant porosity retained by the parent silica framework.[116] CSC-A5 appeared to have the highest relative chemisorption out of the three materials (Fig. 17), suggesting that the carbon layer has a unique surface structure allowing for greater reduction ability of the material. Whereas, CSC-A3 and CSC-A8 perform with a greater extent of physisorption rather than chemisorption, again, speculating that the reducing ability of the material is less as surface functionalities amongst the three materials differ, and hence their subsequent lower maximum adsorption capacity

values. In general, chemisorption is prominent at the low concentrations of gold, whereas reversible physisorption describes the process better at higher concentrations (good correlation with the good fits to the Langmuir model). Enhanced chemisorption at the lower concentrations, when physisorption is always observed, allows for increased loading capacities at the range of concentrations tested, as observed.

3.3.5 Effect of Time on Gold Adsorption

Plots of % gold removal against time indicate similar, slow adsorption for the three CSCs, as opposed to the very rapid adsorption observed for activated carbon NORIT (Fig, 22). As expected, adsorption onto activated carbon NORIT happens very fast, reaching equilibrium after 6 hours. The shape of the plot suggests that adsorption is taking place in two steps; initially rapid adsorption, where the bulk solution of $AuCl_3$ is adsorbed, followed by slower adsorption until equilibrium is reached.[179]

Due to the larger pore size of the CSCs (mesoporous) in comparison to the microporous activated carbon NORIT, the rate of adsorption onto the CSCs is anticipated to be faster, assumingly due to faster diffusion; yet studies indicate that the adsorption occurs slowly, without reaching equilibrium. As a result, all correlations and calculations presented by the kinetic models applied will only be indicative of what could potentially be happening in equilibrium systems. Further investigation needs to be done to assess and determine adsorption rates by kinetic models (i.e. further increase in contact time). Nonetheless, plots show good correlation with % removal values illustrated in Fig. 20.

Mass transfer mechanisms from the solution to the adsorption sites within the adsorbent particles can be constrained by mass transfer resistances that determine the time required to reach equilibrium.[106] The rate of adsorption is commonly limited by diffusion processes toward the external surface and within the pores of materials; yet, it could also be possible that that in the case of Series A CSCs, the reason behind the slow adsorption observed is that the gold species moves slowly from the bulk liquid phase to the boundary layer of the materials' surface.[174] As a result, adsorption is slower than expected due to the limited adsorbate diffusion into the pore network

or interactions of the adsorbate species with the active sites of the materials during the 24-hour period.

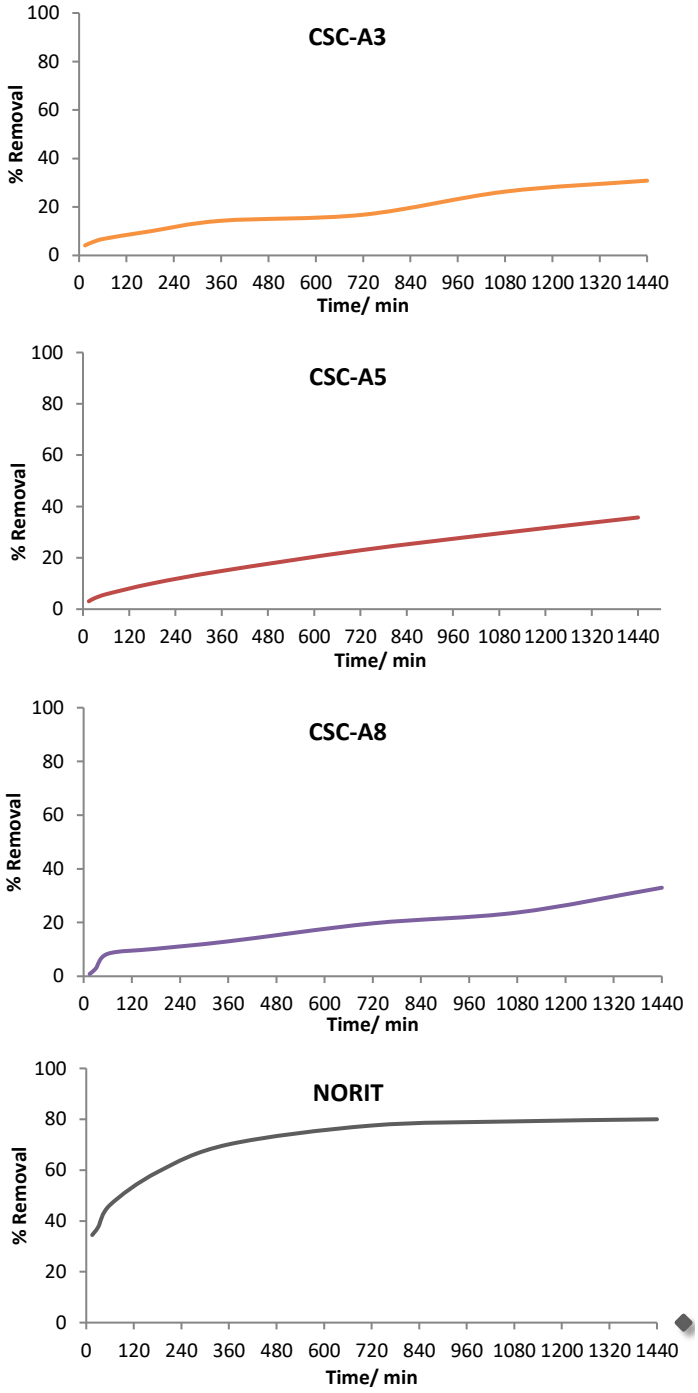

Figure 21 Rate of uptake of gold with all CSCs Series A and activated carbon NORIT at room temperature

3.3.5.1 Rate of Adsorption: Kinetic Models

In the case of porous adsorbents, adsorption equilibria are not established instantaneously. Mass transfer from the solution to the adsorption sites within the particles of the adsorbent is sometimes restricted by mass transfer resistances in the system, that determine the time needed to reach equilibrium.[180] Rate of adsorption is most commonly limited by a diffusion process towards the external surface of the adsorbent and within the porous adsorbent particles. [181] Adsorption kinetics are used to determine the rate of reaction and the rate-limiting mass transfer mechanisms of the system.[111]

To further understand and describe the rate of gold adsorption various kinetic models have been applied and their validity was based on R^2 and q_e values; the pseudo-first-order (PFO) model, the pseudo-second-order (PS0) model and the Elovich model, as well as the intraparticle-diffusion-transport model and the film-diffusion-transport model. All kinetic parameters are summarised in Table 12 (graphs showing isotherm fitting can be found in Appendix 2).

3.3.5.1.1 Pseudo-First Order Model

The linear equation for the model is:

$$log(qe - qt) = -\frac{k1}{2.303}.t + log\ qe$$

Equation 5 Linear expression for pseudo-first-order kinetic model

Where, q_e is the total amount adsorbed at presumed equilibrium (mg g^{-1}), q_t is the amount adsorbed (mg g^{-1}) at given time t (min) and k_1 is the pseudo-first-order rate constant of adsorption (min^{-1}). [168,182]

3.3.5.1.2 Pseudo-Second Order Model

The linear equation for the model is:

$$\frac{t}{qt} = \frac{1}{k2\ qe^2} + \frac{1}{qe}.t$$

Equation 6 Linear expression for pseudo-second-order kinetic model

Where, q_e is the total amount adsorbed at presumed equilibrium (mg g^{-1}), q_t is the amount adsorbed (mg g^{-1}) at given time t (min) and k_2 is the pseudo-second-order rate constant of adsorption (g mg^{-1} min^{-1}). [183,184]

The initial rate of adsorption, h (mg g^{-1} min^{-1}), can be calculated from q_e and k_2 using the following expression:

$$h = qe^2 \,.\, k_2$$

Equation 7 Expression to fine initial rate of adsorption for pseudo-second-order kinetics

3.3.5.1.3 Elovich Model

The linear equation for the model is:

$$q_t = \frac{ln\, a_e b_e}{b_e} + \frac{1}{b_e} ln\, t$$

Equation 8 Linear expression for Elovich kinetic model

Where, q_t is the amount adsorbed (mg g^{-1}) at given time t (min), α_e is the initial adsorption rate (mg g^{-1} min^{-1}) and b_e is the constant related to the activation energy of the adsorption and the extent of surface coverage (g mg^{-1}). [185,186]

3.3.5.2 Rate of Adsorption: Diffusion Models

The progress of adsorption is characterised by four successive steps (bulk- solution transport, film diffusion transport, intraparticle diffusion transport and mass action), yet only two of the steps are fast enough to determine the rate of adsorption.[169] Rate of adsorption can be determined either by film diffusion transport or intraparticle diffusion transport. Since both act in series, the slower process will define the total adsorption rate.[106]

The most common assumptions of kinetic diffusion models are:[126]

- Temperature is constant.
- Stirring velocity is constant.
- Bulk solution is completely and thoroughly mixed.

- Mass transfer into and within the adsorbent are diffusion processes.
- Interaction and attachment of the adsorbate onto the surface of adsorbent is much faster than the diffusion processes.
- Adsorbent is spherical and isotropic.

3.3.5.2.1 Film-Diffusion Transport Model

The model assumes that the rate of adsorption is equal to the rate at which the adsorbate species movies across the boundary layer of the liquid film. [187,188]

$$\ln(1 - \frac{qt}{qe}) = -R'.t$$

Equation 9 Expression for film diffusion transport kinetic model

Where, q_e is the total amount adsorbed at presumed equilibrium (mg g^{-1}), q_t is the amount adsorbed (mg g^{-1}) at given time t (min) and R' is the liquid film diffusion constant (min^{-1}).

3.3.5.2.2 Intraparticle-Diffusion Transport Model

The model assumes that the amount of adsorbate species that diffused through and/or along the surface of adsorbent is proportional to the square root of time.[113,189]

$$qt = k_{int} . \sqrt{t}$$

Equation 10 Expression for film diffusion transport kinetic model

Where, q_t is the amount adsorbed (mg g^{-1}) at given time t (min) and k_{int} is the intraparticle diffusion constant.

Table 11 Kinetic models for gold adsorption on all CSCs Series A and activated carbon NORIT (for comparison) at room temperature

Parameters	CSC-A3	CSC-A5	CSC-A8	NORIT
Pseudo- first order model				
$q_{e\ CALCULATED}$ *(mg g^{-1})*	89.16	107.80	94.58	135.86
$q_{e\ EXPERIMENTAL}$ *(mg g$^{-1)}$*	98.39	113.98	105.18	255.19
$k_1\ 10^{\wedge 3}$ *(min^{-1})*	1.38	1.38	1.15	3.45
R^2	0.9163	0.9898	0.9738	0.9904
Pseudo- second order model				
$q_{e\ CALCULATED}$ *(mg g^{-1})*	104.17	131.58	125.00	263.16
$q_{e\ EXPERIMENTAL}$ *(mg g$^{-1)}$*	98.37	113.98	105.18	255.19
$k_2\ 10^{\wedge 5}$ *(g mg^{-1}min^{-1})*	3.19	1.87	1.53	8.34
h *(mg g^{-1}min^{-1})*	0.35	0.32	0.24	5.77
R^2	0.8728	0.9053	0.8708	0.9992
Elovich model				
b_e *(g mg^{-1})*	0.06	0.05	0.05	0.03
α_e *(mg g^{-1}min^{-1})*	1.28	1.15	1.01	44.35
RE	0.17	0.19	0.18	$8.83 \times 10^{\wedge 5}$
R^2	0.8491	0.8799	0.8878	0.9867

Film diffusion transport model				
R'	0.0016	0.0016	0.0012	0.0046
R^2	0.8972	0.9845	0.9339	0.8966
Intraparticle diffusion transport model				
k_{int}	2.45	2.83	2.49	8.66
R^2	0.9683	0.9869	0.9615	-0.29

Comparison of the R^2 values for the pseudo-first order and pseudo-second order equations show that the pseudo-first order model is a better fit for the data for all CSCs with R^2 ranging from 0.92 to 0.99, while activated carbon NORIT exhibits the best fit to the pseudo-second order model with R^2 value of 0.9992 (Table 12). Calculated values of q_e show less discrepancy to the experimental values of q_e for Series A CSCs in the pseudo-first order data when compared to the pseudo-second order data, which is in good correlation given their better fit to the first model.

Usually, PFO kinetics demonstrate the rate dependence of adsorption of a liquid/ solid system on the solids adsorption capacity, as well as the concentration of the adsorbate in the bulk solution, and they tend to be a good fit only for the first 30 minutes of adsorption.[169,190] After that, data show a better fit to the PSO kinetics. In the case of Series A CSCs, where adsorption is overall very slow (Fig.22) and a high bulk-liquid concentration is used (favouring slow rates of adsorption), the PFO model is expected to show a better fit. Yet, since the adsorption mechanism involves the reduction of the gold species (mainly Au^{3+} to Au^0), it is suspected that determining the rate-determining step might be a little more complex than fitting data to just one model.

Applying the Elovich model to calculate RE (approaching equilibrium parameter) for gold adsorption onto Series ACSCs, demonstrates a *Zone II* adsorption; meaning that adsorption is expressed through a mild rising curve to reach equilibrium, as shown in Figure 22. Determining RE values can further support, whether adsorption to reach equilibrium occurs slowly or rapidly. RE>0.3 indicates a slow rising curve (*Zone I*

adsorption), 0.3>RE>0.1 indicates a mild rising curve (*Zone II* adsorption), 0.1>RE>0.02 indicates a rapid rising curve (*Zone III* adsorption) and RE<0.02 indicates instantly approaching equilibrium (*Zone IV* adsorption).[185] RE value for activated carbon NORIT is, too, in good correlation with a *Zone IV* adsorption, as it reached equilibrium extremely quickly.

PSO offers an excellent fit to activated carbon NORIT, indicating that the rate-controlling step is a chemical reaction involving valence forces through sharing or exchanging electrons between adsorbate and adsorbent. This model is consistent with the reduction-adsorption adsorption mechanism occurring on aromatic / graphitic surfaces.[191] For the adsorption of gold onto activated carbon, the rate is controlled by the availability of active sites on its surface to facilitate chemisorption via the reduction of Au^{3+} to elemental Au.

Since, gold reduction is not the rate-controlling step for any of the CSCs, mass transfer/ diffusion models are applied to determine it.[106,113,187] All Series A CSCs show better fits to the intraparticle diffusion model, even though CSC-A5 has a very good fit to the film-diffusion model as well. Based on the intraparticle diffusion transport model, the adsorbate species (Au^{3+} or Au^{0}) diffuse in the pores or along the internal surface of the CSCs, before any energetic interactions occur. Fits of the model for Series A CSCs did not pass through the origin, indicating that intraparticle diffusion was not the only rate-limiting step. Due to the nature of adsorption, or the anticipated adsorption system, it makes sense that there might be more steps dictating the rate.[168]

As shown by XPS analysis post-adsorption, gold was reduced from Au(III) to Au(0), establishing that chemisorption is part of the adsorption mechanism.[161] If, none of the CSCs follow PSO kinetics that state that chemisorption is the slow or the rate-limiting step, it can be assumed that chemisorption occurs very rapidly, either before or after mass transfer. Chemisorption can be potentially occurring at the very initial step of adsorption, where the adsorbate moves towards the boundary layer around the adsorbent material and electrostatic forces of attraction act (protonated surface of CSCs due to chemical functionalities present) to facilitate the reduction of gold. The alternative is that chemisorption takes place rapidly, as soon as the adsorbate diffuses

through the pores and the internal surface of the CSCs and energetic interactions facilitate electron transfer for the reduction of gold.

In summary, kinetic data for the Series A CSCs fit well to the PFO and intraparticle diffusion transport models, suggesting the possibility of more than one rate-determining steps, and that a more complex adsorption mechanism is involved.

3.4 Conclusion

The adsorption data are successfully modelled using the Langmuir, Freundlich and D-R isotherms. The Langmuir model gives the best fit for all three materials, with R^2 very close to unity. Yet, the unusual shape of the isotherm plots indicates that aside traditional physisorption taking place, a very rapid chemisorption occurs at the lower-concentration regions. Series A composite materials exhibit unusually high % removal of gold at low concentration (>98%), rather than at higher concentrations, making them ideal for water treatment of metal contaminants and mine tailings which are usually found in trace amounts. Even though all three materials are extremely selective towards gold, with high maximum surface coverage, CSC-A5 is the best with an adsorption capacity of 320 mg g^{-1} and 99% removal, attributed to the unique system of chemisorption taking place. The mechanism of adsorption involves the reduction of the Au(III)to its metallic form leading to the formation of AuNPs. To allow for the reduction of Au(III), the surface chemistry of the materials is affected by oxidation of certain functional groups (i.e. hydroxyl, carbonyl and carboxyl groups). Adsorption presumably leads to monolayer coverage of the surface, as suggested by Langmuir, yet rates of adsorption are rather difficult to determine by a single kinetic model, due to the complexity of the adsorption system to reach equilibrium.

The key information about Series A carbon/silica composites materials from the work carried out for Part I of this thesis, is that they hold tuneable properties (porosity, BET surface area, chemical functionalities) that exclusively depend on the carbonisation temperature. These properties are held responsible for the selective behaviour of the materials towards gold adsorption and the mechanism via which the process will proceed.

PART II

CARBON/SILICA COMPOSITES:

SERIES B VS SERIES C

Chapter 4.

Carbon Silica/Composites

Series B and Series C:

Synthesis and Characterisation

Aspects of the work presented in this chapter have appeared in:

Oral presentation at the 8th IUPAC International Conference on Green Chemistry, Bangkok, Thailand, September 2018

Poster presentation at the 9th World Convention on Recycling and Waste Management, Osaka, Japan, October 2018 (1st poster prize awarded)

Chapter 4.

Carbon Silica/Composites Series B and Series C: Synthesis and Characterisation

4.1 Introduction

After the promising results obtained from both the characterisation and application of Series A CSCs, the experimental procedure is repeated to produce a second series of materials to re-examine and validate their success as novel adsorbents for the removal of gold. Primary observations and characterisation of Series B CSCs have shown considerable differences when comparing to Series A materials. As a result, a sequence of questions emerges. What is the cause of these deviations, if the synthetic route and conditions have not been altered? Can, theoretically, very similar but not identical feedstock produce different pyrolysis oils and, hence, adsorbents? What is the effect, if any, on the loading capacities and mechanisms during the process of adsorption? A case is now built to resolve all queries by producing a third series of materials, Series C CSCs, to delve further into all differences and similarities among virtually alike materials.

4.1.1 Microwave - Assisted Pyrolysis

Microwave pyrolysis is a thermochemical conversion process which involves the thermal decomposition of organic molecules in the absence of air.[192] It is caused by molecular motion via migration of ionic species or the rotation of dipolar species caused by microwave adsorption to generate heat due to friction among the molecules.[193] Microwave pyrolysis is usually preferred over the conventional pyrolysis methods (e.g. incineration, gasification, liquefaction, etc.) for a range of reasons. While traditional methods can have slow heating rates, require high heating temperatures and can essentially only heat the surface of materials before conducting heat to the inside, microwave pyrolysis is an attractive alternative due to advantages like:[194–196]

- Non- contact, volumetric heating.
- Energy transfer rather than heat transfer.
- Rapid heating leading to reduced processing time and high 'reaction' rates.
- Controlled, targeted and uniform heating. The energy generated penetrates the surface of materials and reaches through to their core, resulting in high efficiency and more even heating profiles.
- Better safety as surroundings are cooler than the material itself, leading to immediate cooling on switching off microwave
- Simple operation and handling. Higher level of automation and safety.

The products of microwave pyrolysis are bio-oil, bio-gas and bio-char .[197] The solid residue (bio-char) is commonly used as a fuel alternative to charcoal.[198] The bio-gas released consists of the volatile species. During the process, volatiles condense into two fractions; one aqueous fraction mostly consisting of the volatile acids and water, [199] and one organic fraction (bio-oil). The bio-oil produced is the fraction of interest due to the large number of compounds it contains.[200]

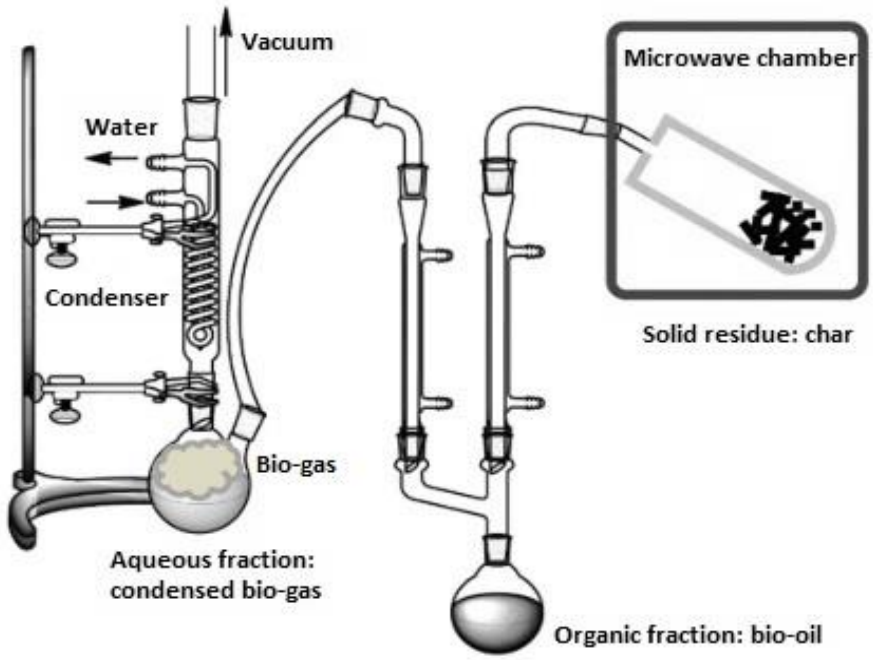

Figure 22 Example of experimental set-up for microwave assisted pyrolysis for wastepaper. Reproduced from Ref. 200

4.1.2 Pyrolysis Oil

Pyrolysis oil, commonly referred to as bio-oil when it comes from biomass, is perhaps the most valuable product of microwave pyrolysis due to the huge variety of chemical components it contains, depending on the biomass it originated from. It is a dark brown, free-flowing liquid with a distinctive smoky odour, and it holds a variety of physical properties depending on its chemical composition.[65] Its yield typically ranges between 35% - 60%, essentially depending on the composition of biomass feedstock, and pyrolysis parameters such as temperature, pressure, heating rate and residence time.[201] It is usually a complex mixture of several hundreds of organic compounds (mainly acids, alcohols, aldehydes, esters, ketones, phenols, sugars, furans and lignin derived oligomers) issued from the depolymerisation of cellulose, lignin and hemicellulose..[65,202] Aside from its organic composition, bio-oil may also contain mineral/ inorganic matter (i.e. potassium, magnesium, phosphorus) as well as a degree of water content, again, depending on the original biomass.[71,203] Generally, the majority of inorganic components remain in the char, but for bio-masses like waste paper, which is richer in inorganics than most biomass, a proportion of them may end up in the bio-oil too.[204]

As a result of its nature it holds some generally undesired properties, which usually include:[205]

- High viscosity.
- High ash content.
- High oxygen content, leading to low heating value.
- High corrosiveness; it has an acidic pH of around 2-3.

Depending on the pyrolysis method the water content in bio-oil varies. For instance, during conventional pyrolysis the aqueous layer does not separate so the bio-oil can have high water content. During microwave assisted pyrolysis, and depending on the experimental setup and method parameters, there is separation between the aqueous fraction and the organic fraction (bio-oil) and as a result water content in the bio-oil is fairly low.[206,207]

Nonetheless, the fact that pyrolysis oil is bio-derived and it contains such a big range of organic functionalities, bio-oil can be employed in the industrial sector as:[207–209]

- Combustion fuel for heat generation and power generation.
- Transportation fuel after upgrading.
- Production of chemicals and resins.

4.2 Aims

The overall objective of this chapter is to provide a full assessment on the development of two new series of materials, CSCs Series B and Series C, for qualitative and quantitative comparison of the resulting materials.

The aims of the work presented herein:

- To investigate the differences between the pyrolysis oils utilised to produce the two different series of CSCs, by characterising the feedstock (waste office paper) and product (pyrolysis oils).
- To investigate the influence of carbonisation temperature on the physicochemical properties of the two different series of CSCs.

4.3 Results and Discussion

4.3.1 Preparation of Series B and Series C

The bio-oils used for the synthesis of the composite materials are obtained from the microwave-assisted pyrolysis of waste office paper. Bio-oil B (BO-B) is used to produce Series B CSCs, and similarly bio-oil C (BO-C) is used to produce Series C CSCs.

The typical method of preparation consists of four main stages:

1. Milled waste office paper pressed into blocks
2. Microwave-assisted pyrolysis of blocks to collect bio-oil
3. Wet impregnation of bio-oil into silica framework
4. Carbonisation at different temperatures (300˚C, 500˚C, 800˚C) under nitrogen atmosphere.

The synthetic routes followed for the preparation of pyrolysis oils and the materials are described in detail in Section 8.1.2.3 (Chapter 8).

4.3.2 Physical and Chemical Properties of the Pyrolysis Oils

It is essential to characterise the carbon precursor in all morphs (waste office paper → paper blocks → pyrolysis oil) to be able to understand and communicate how and why the final adsorbent materials will behave the way they do during adsorption. Various characterisation techniques are used to provide insights to the physical and chemical nature of the carbon source utilised to independently develop Series B and Series C adsorbents.

The pyrolysis oils are obtained by heating the reactor vessel to 40 ˚C / 800W for 4 minutes and then to 200 ˚C / 1200W for 8 minutes, under vacuum. The pyrolysis oil (organic fraction) separates and collects in a round bottom flask, as illustrated in Section 8.1.2.2 (Chapter 8).

4.3.2.1 Elemental and Proximate Analysis

The parameters determined by proximate analysis include moisture content, volatile matter content, fixed carbon content and ash content, and they are determined by a TG characterization of each sample in both air and nitrogen atmosphere, as appropriate. For elemental analysis, the carbon, hydrogen, nitrogen and oxygen content of each sample are quantitatively determined. Results by proximate and elemental analysis for the milled office paper and the paper blocks show little variation between them (Table 13). The variation results from the fact that milled paper is used as provided, whereas paper blocks are produced by mixing with de-ionised water, pressing the mixture into blocks and drying in an oven. The drying step in the block-making process removes any absorbed water existent in the original milled paper and as a result, the bulk moisture content of paper blocks is less than that of the feedstock.

Considerable differences in content between the resulting bio-oils and the paper blocks used are noted (Table 13). Moisture and fixed carbon content increase, with volatile matter and ash content simultaneously decreasing. The significant increase in moisture content from 4.5 w/w% to 19.9 w/w% and 16.9 w/w%, in BO-B and BO-C

respectively, suggests that during pyrolysis enough of the water generated, mainly due to dehydration reactions, is trapped in the organic fraction, the bio-oil, instead of condensing and separating for collection in the aqueous fraction. [210] The parallel decrease in volatile matter content observed in both bio-oils suggests that most of the light volatile compounds evaporated and collected in the aqueous fraction during the process, likely due to secondary reactions such as thermal cracking of the volatile compounds.[206] Hence, bulk volatile matter is reduced from 73.9 w/w% in the paper blocks to 59.4 w/w% in BO-B and 58.8 w/w% in BO-C.

Table 12. Elemental and proximate analysis of waste office paper, paper blocks and bio-oils

	Waste office paper	Paper blocks	BO-B	BO-C
		Proximate Analysis (w/w %)		
Moisture	7.2	4.5	19.9	16.9
Volatile matter	71.8	73.9	59.4	58.8
Fixed carbon	12.0	11.7	18.8	23.8
Ash	8.9	10.0	1.9	0.5
		Elemental Analysis (w/w %)		
C	37.1	37.4	25.9	36.5
H	5.1	5.1	8.6	6.8
N	N.D[a]	N.D[a]	N.D[a]	N.D[a]
O[b]	57.8	57.5	65.5	56.7

[a] N.D.: not detected; [b] Calculated by difference

Elemental analysis results show major differences between BO-B and BO-C. During microwave assisted pyrolysis, the organic fractions appear to separate differently, resulting in bio-oils with different carbon, hydrogen and oxygen composition. BO-C has evidently more carbon (36.5 w/w%) than BO-B (25.9 w/w%), which is anticipated to influence the adsorption behaviour of materials. The amount and functionality of carbon that will result in the adsorbents, can change surface properties that will in turn affect diffusional resistance and accessibility, as well as the mechanism of adsorption.[211]

Comparing elemental composition of all three bio-oils used in this research (Fig.24), the following observations are made:

a. BO-A has the highest carbon content (48.9 w/w%) and lowest oxygen content (43.6 w/w%) of the three.
b. BO-B has the lowest carbon content (25.9 w/w%) and highest oxygen content (65.5 w/w%) of the three.
c. Hydrogen content is maintained within reasonable range (6.8 – 8.6 w/w%) in all three bio-oils.

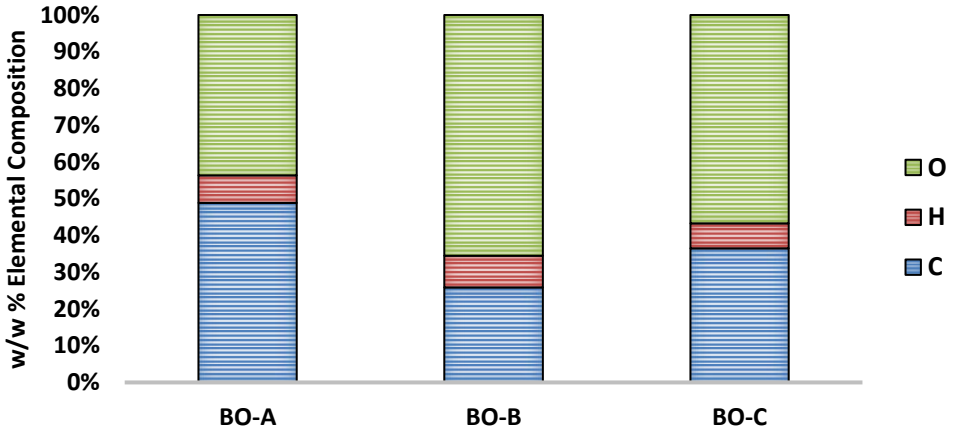

Figure 23 Elemental Composition of BO-A, BO-B and BO-C

Seeing as how the silica plays no part during phase transfer, one can easily hypothesise that the amount of carbon and oxygen that will end up on the surface of materials, will have the greatest impact on adsorption. Therefore, the bulk elemental composition of the carbon source can provide quantitative indications of the surface composition of resulting materials.

4.3.2.2 Mineral Content Analysis

The mineral contents of the feedstock and the bio-oils are determined by ICP-MS (described in Section 8.2.6, Chapter 8).

Analysis indicates significant amounts of elements like aluminium, calcium magnesium, sodium, sulfur and silicon (Table 14). Milled waste office paper is richer in these elements in comparison to the paper blocks and the bio-oils, presumably because during the water-mixing and pressing steps of the preparation of paper

blocks, the dissolved minerals are discarded. Mineral contents in both bio-oils are notably lower, proposing that during pyrolysis the elements can end up in all products of the process (organic fraction, condensed gas/ aqueous fraction and char), with the organic fraction containing just a portion of them (i.e. calcium content in paper blocks is 41916.5 ppm, whereas in BO-B it is 366.54 ppm and in BO-C 402.1 ppm).

Table 13 Mineral contents of milled paper, paper blocks and resulting bio-oil

Element (ppm)	Waste Office Paper	Paper Blocks	BO-B	BO-C
Ag	0.10	0.01	< 0.01	< 0.01
Al	111.54	67.92	36.47	4.24
As	4.93	< 0.01	9.67	12.59
Au	1.14	< 0.01	< 0.01	0.62
B	12.68	2.15	11.55	9.62
Ba	83.49	56.56	1.74	1.39
Be	< 0.01	< 0.01	< 0.01	< 0.01
Bi	< 0.01	< 0.01	< 0.01	1.09
Ca	77947.30	41916.50	366.54	402.10
Cd	< 0.01	< 0.01	< 0.01	< 0.01
Co	< 0.01	< 0.01	0.10	< 0.01
Cr	1.84	0.45	0.09	0.33
Cu	44.32	9.19	5.43	4.41
Fe	689.50	114.52	99.93	33.84
Hg	4.34	0.66	1.77	2.27
K	152.49	67.16	9.77	6.67
La	70.05	17.36	0.47	0.39
Li	< 0.01	< 0.01	< 0.01	< 0.01
Mg	705.82	380.89	24.22	26.28
Mn	10.40	4.22	0.96	0.34
Mo	< 0.01	0.14	1.19	0.87
Na	919.72	324.19	58.85	57.30
Ni	1.91	< 0.01	0.10	1.25
P	37.70	16.99	14.47	1.76
Pb	< 0.01	< 0.01	< 0.01	0.64

Pd	4.78	0.02	< 0.01	0.06
Pt	< 0.01	< 0.01	< 0.01	< 0.01
Rb	< 0.01	< 0.01	< 0.01	< 0.01
S	590	292	84	65
Sb	< 0.01	1.10	4.61	6.35
Sc	0.34	0.25	0.19	0.03
Se	< 0.01	< 0.01	21.67	8.80
Si	337.30	190.89	86.54	17.41
Sn	< 0.01	< 0.01	0.94	3.10
Sr	152.04	76.20	6.59	7.89
Te	< 0.01	< 0.01	< 0.01	< 0.01
Ti	18.19	11.07	13.66	0.49
Tl	< 0.01	< 0.01	2.49	2.29
V	0.65	< 0.01	0.41	0.35
W	3.33	0.87	3.54	3.53
Zn	9.25	3.01	1.17	0.96
Zr	4.34	0.18	0.58	0.18

Presence of such elements in the feedstock and pyrolysis oils can be attributed to chemicals used in the paper manufacturing process as follows:[61,201]

- Calcium carbonate is used as filler and in coating.
- Calcium magnesium carbonate is used as filler and in coating.
- Magnesium bisulfite is used in sulfite pulping.
- Sodium bisulfite is used in sulphite pulping.
- Sodium hydrosulfite is used in bleaching.
- Sodium thiosulfate is used in bleaching.
- Kaolinite (aluminosilicate) is used as filler and sizing agent.

4.3.2.3 Infrared Spectroscopy

Fourier transform-infrared spectroscopy in attenuated total reflectance (ATR) mode is used to characterize the chemical composition of feedstock (milled waste office paper and paper blocks) and to examine changes in functionality of both bio-oils after

microwave pyrolysis. The experimental details for ATR-IR characterization are described in Section 8.2.2 (Chapter 8).

ATR-IR spectra of the milled waste office paper, the paper blocks and the resulting bio-oils BO-B and BO-C are shown in Figures 25 & 26. The spectra (Fig.25) for the milled office paper and paper blocks are almost identical, as expected. Both spectra exhibit a broad, yet weak, band between 3600 cm^{-1} and 3200 cm^{-1}, attributed to the O-H stretching vibration resulting from the presence of water and cellulosic matter.[212] Another broad but weak band appears between 2950 cm^{-1} and 2800 cm^{-1}, corresponding to C-H stretching vibrations due to aliphatic or saturated structures in the feedstock. A very broad and strong band is observed between 1520 cm^{-1} and 1220 cm^{-1} and can be attributed to several functionalities: C-H deformation at 1365 cm^{-1}; C-OH stretch at 1322cm^{-1}; C-O-C stretch at 1250 cm^{-1}. C-O-C vibrations were also accounted for at 1165 cm^{-1} and 1095 cm^{-1}. The sharp band observed at 881 cm^{-1} can be attributed to asymmetric carbonate deformation due to the presence of $CaCO_3$ (residue in milled paper and paper blocks after paper manufacturing).[201]

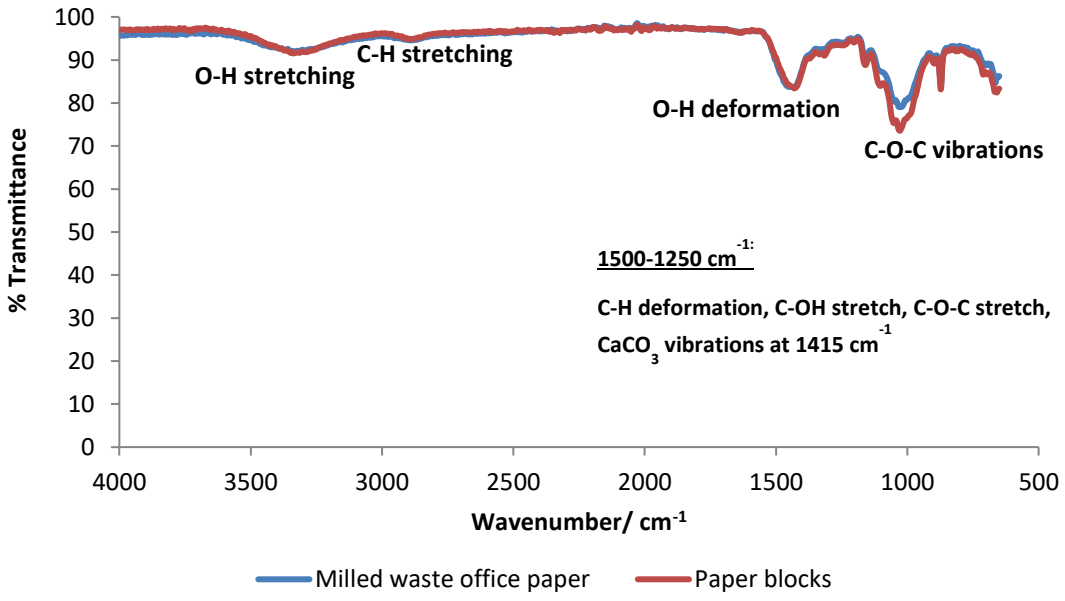

Figure 24 Overlapped ATR-IR spectra of milled waste office paper and paper blocks

The bio-oil spectra (Fig.26) show a change in their chemical nature, comparing them to the similar spectra of both milled paper and paper blocks. The most significant change with respect to the paper feedstock is the appearance of medium intensity

bands centred at 1722 cm^{-1} and 1634 cm^{-1}, corresponding to C=O stretching and C=C stretching vibrations. The C=O stretching vibrations attributed to carbonyl compounds indicated the presence of aldehydes, ketones, esters and carboxylic acids in the bio-oil.[65] The intense, broad O-H stretching vibration band between 3600 cm^{-1} and 3000 cm^{-1} (centered at 3416 cm^{-1}), together with the intense carbonyl stretching vibration band (centered at 1715 cm^{-1}), further confirm the presence of carboxylic acids.[71] The band at 1640 cm^{-1}, suggesting O-H deformations, in addition to the broad O-H stretching band, confirm the presence of water and an increase in hydrogen bonding. The band assigned to C=C stretching indicate the presence of alkene or aromatic compounds. The weak band between 3000 cm^{-1} and 2800 cm^{-1}, corresponding to C-H stretching vibrations, suggest the persistence of aliphatic or saturated structures in the bio-oil, too. The broad and strong band observed between 1520 cm^{-1} and 1220 cm^{-1} for both feedstock materials (milled paper and paper blocks) and the resulting bio-oils can be attributed to the same functionalities suggesting that the bio-oils are rich in oxygenated compounds (carbohydrates, sugars and derivatives): C-H deformation at 1385 cm^{-1}; C-OH stretch at 1345cm^{-1}; C-O-C stretch at 1274 and 1079 cm^{-1}.[213]

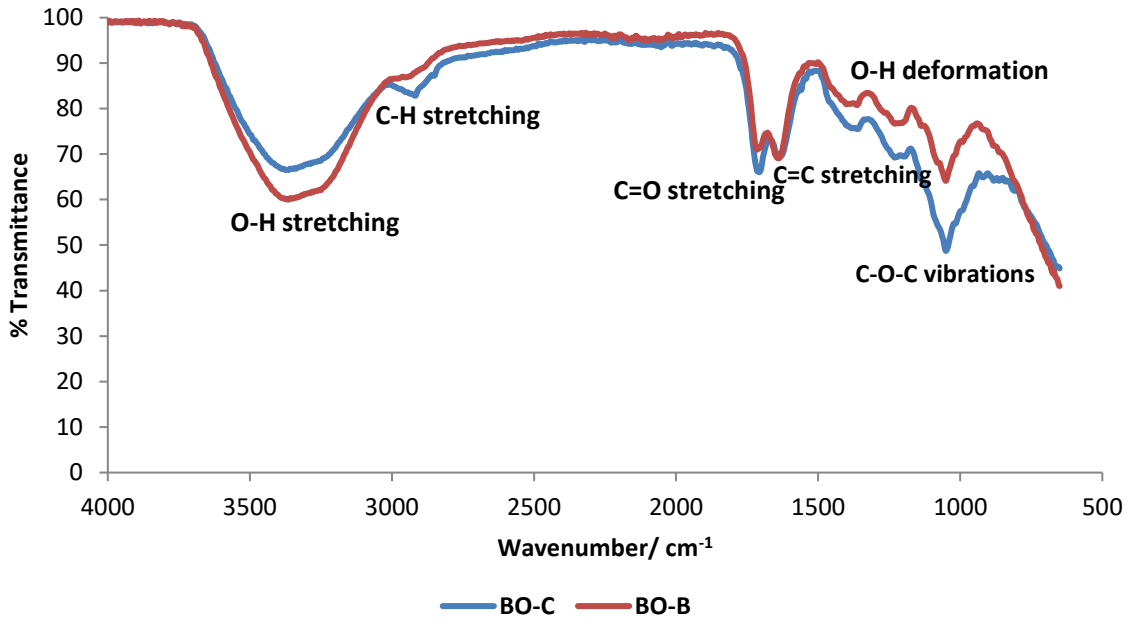

Figure 25 Overlapped ATR-IR spectra of BO-B and BO-C

4.3.2.4 Gas Chromatography and Mass Spectral Analysis

Gas chromatography-mass spectrometry (GC-MS) is used to identify the major compounds present in the bio-oils. The technique can provide quantitative and qualitative analysis of the mixture, yet due to the complexity of the bio-oil and the presence of different types of organics with insufficient volatility under the operational conditions, complete and accurate identification of peaks is very difficult.

Sample preparation and method used for GC-MS analysis are described in Section 8.2.3 (Chapter 8); for identification of chromatographic peaks the NIST 2008 library is used.

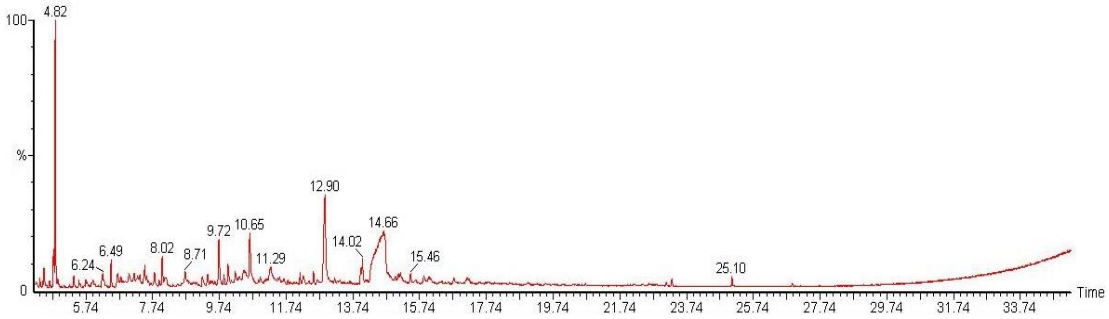

Figure 26 Chromatogram generated for BO-B

Figure 27 illustrates the chromatogram obtained for BO-B by GC analysis, and the major identified compounds according to the NIST database are included in Table 15.

Table 14 Major identified compounds in BO-B according to the NIST database

Retention Time/ min	Compound
3.17	Acetic acid
3.71	2,5-Dimethylfuran
4.23	2,5-Dimethoxytetrahydrofuran
4.67	2(5H)-Furanone
4.82	1,2-Cyclopentanedione
6.01	1-Hydroxy-2-pentanone
6.49	3-Methyl-1,2-cyclopentanedione
7.55	2-Methoxyphenol (Guaiacol)

8.03	Levoglucosenone
9.43	2-Furanmethanol
9.75	1,4:3,6-Dianhydro-α-d-glucopyranose
9.89	1,2-Benzenediol (Catechol)
10.01	5-(Hydroxymethyl)-2-furaldehyde (HMF)
14.65	Levoglucosan

Figure 28 illustrates the chromatogram obtained for BO-B by GC analysis, and the major identified compounds according to the NIST database are included in Table 16.

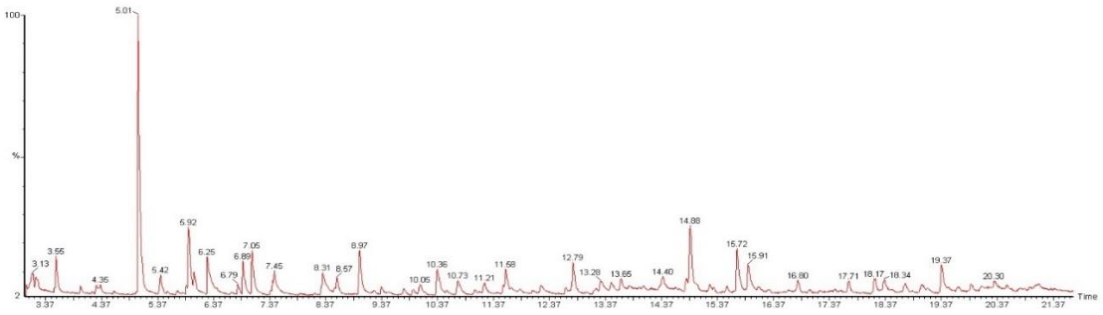

Figure 27 Chromatogram generated for BO-C

Table 15 Major identified compounds in BO-C according to the NIST database

Retention Time/ min	Compound
3.13	Acetic acid
3.65	2,5-Dimethylfuran
4.35	2,5-Dimethoxytetrahydrofuran
5.01	2(5H)-Furanone
5.92	1-Hydroxy-2-pentanone
6.25	3-methyl-1,2-cyclopentanedione
7.0	3-Methyl-1,2-cyclopentanedione
7.45	2-Methoxyphenol (Guaiacol)
8.31	Levoglucosenone
8.97	2-Furanmethanol
10.36	3-methylbenzaldehyde
12.79	5-(Hydroxymethyl)-2-furaldehyde (HMF)
14.88	Levoglucosan
15.72 -31.58	Polyaromatic structures

Usually, components of bio-oils can be divided into four different classes: anhydrosugars, carboxyl compounds, carbonyl compounds and aromatic compounds.[71] However, in many occasions there is overlap among these classes, as compounds may fall under more than one division due to their chemical diversity. Therefore, compounds are assigned to three broader divisions: 1) carbohydrates and their non- furanic derivatives, 2) furanic compounds and 3) phenolic compounds.

Compounds in the division of carbohydrates and their derivatives that were identified in the bio-oil include levoglucosenone, 1,4:3,6-dianhydro-α-d-glucopyranose and levoglucosan. Furans and their derivatives identified in the bio-oil include 2,5-dimethylfuran, 2,5-dimethoxytetrahydrofuran, 2(5H)-furanone and HMF. Phenolic compounds like guaiacol were also found in the bio-oil, along with smaller polar molecules like acetic acid.

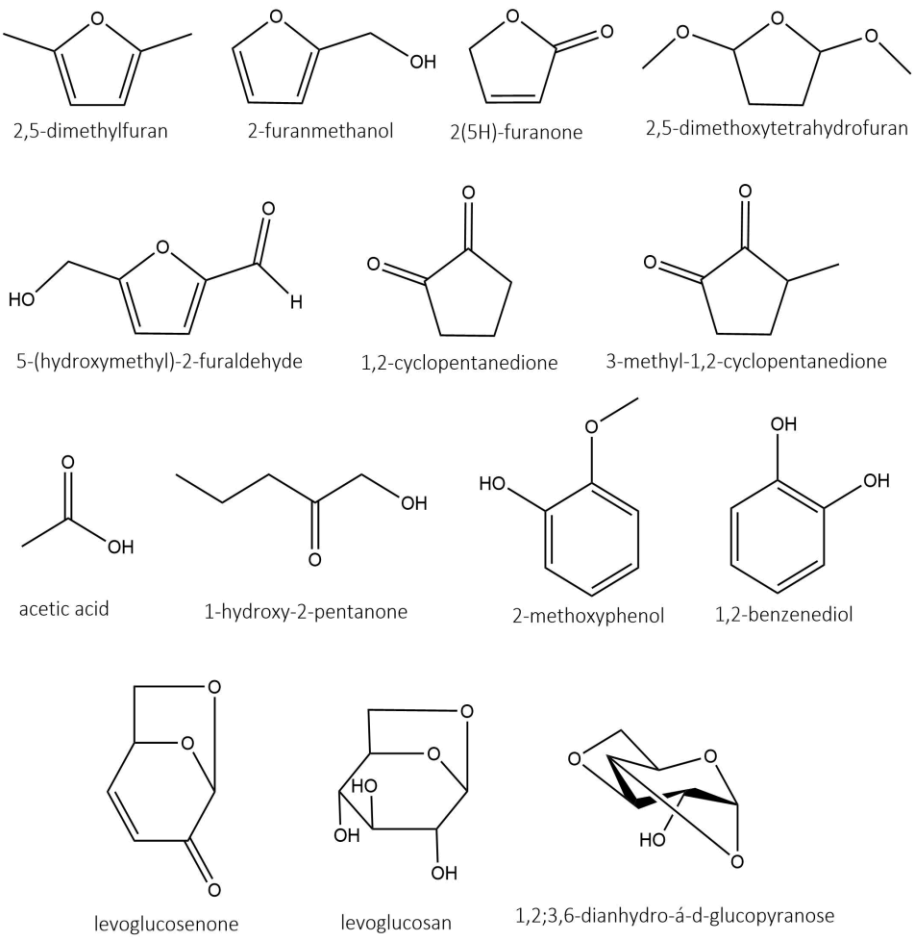

Figure 28 Most commonly identified chemical structures in bio-oils by GC

4.3.3 Physical and Chemical Properties of Series B and Series C CSCs

The synthetic conditions and method to produce Series B and Series C adsorbents are identical to those followed to produce Series A CSCs and are fully described in Section 8.1.2.3 (Chapter 8). The six types of carbon/silica composites synthesised for this work, are described in Table 17, along with the abbreviated name that will be used throughout this thesis.

Table 16 Material description and abbreviation

Starting Material	Carbonisation Temperature (K and ˚C)	Abbreviation
BO-B and Silica K60	573 / 300	CSC-B3
BO-B and Silica K60	773 / 500	CSC-B5
BO-B and Silica K60	1073 / 800	CSC-B8
BO-C and Silica K60	573 / 300	CSC-C3
BO-C and Silica K60	773 / 500	CSC-C5
BO-C and Silica K60	1073 / 800	CSC-C8

Nitrogen adsorption/desorption porosimetry is used to provide quantitative analysis of the textural properties of Series B and Series C CSCs. Characterisation of the isotherms obtained from the analysis illustrates type IV isotherm profiles with H2 hysteresis loop classification for all Series B (Fig.30) and Series C CSCs (Fig.31), as also observed for Series A CSCs.[154] The type IV isotherm profile is indicative of mesoporosity, in which profile the initial part is due to monolayer-multilayer adsorption on the mesopore walls. At this stage, the monolayer is full and multilayer adsorption commences.[214] The observed H2-type hysteresis loop associated with the gradual capillary condensation is further confirmation of the mesoporosity of Series B and Series C materials and reveals that they have a broad pore size distribution or non-uniform pore structures. The H2-type hysteresis loop is commonly affected by the network connecting the pores, and as the pore structure becomes more complex the adsorption branch follows a gradual increase.[214,215] The desorption branch is caused by pore-blocking in the necks of the pores, but since a broader pore size distribution is observed for Series B and Series C CSCs, the decrease in the desorption branch is gradual as the pore necks vary over a wider range.[216]

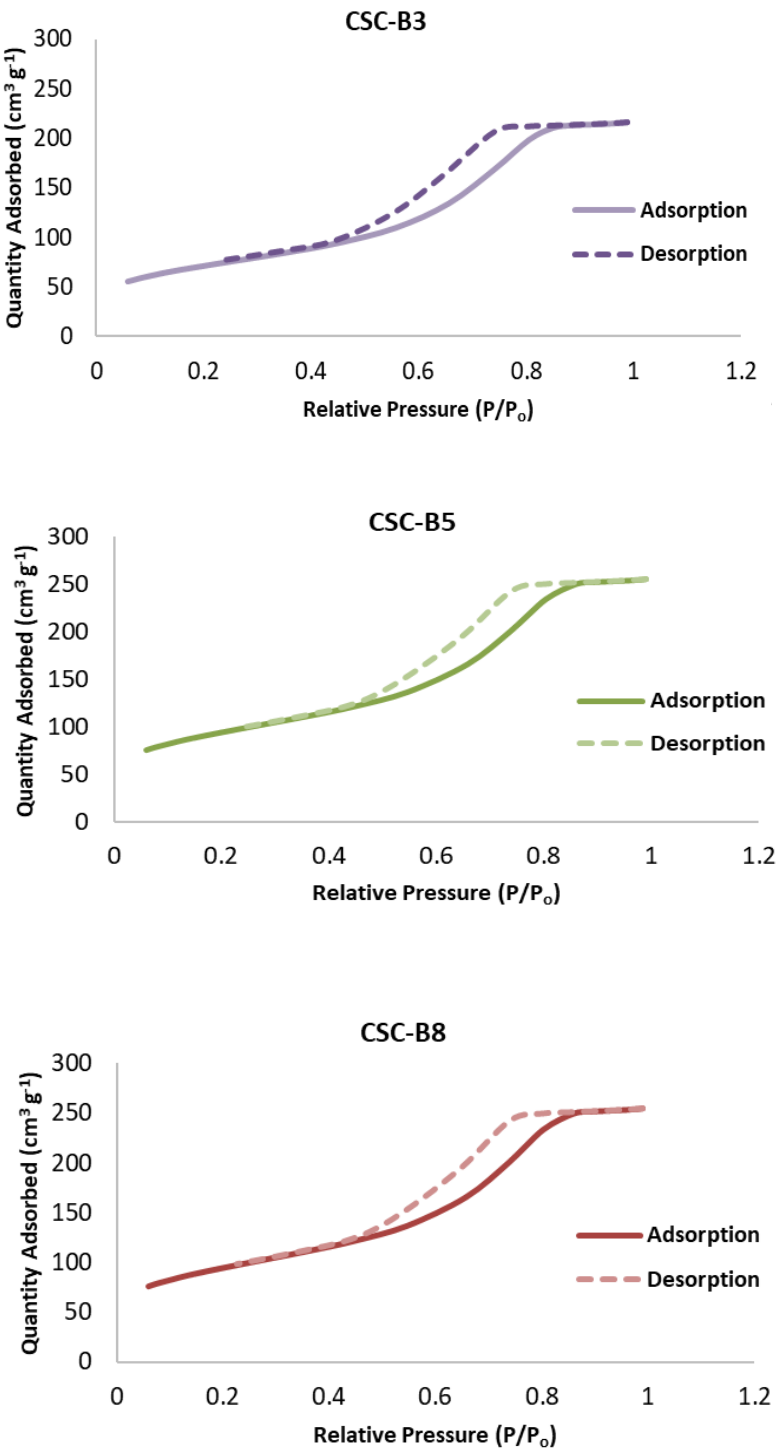

Figure 29 Nitrogen adsorption isotherms for CSC-B3, CSC-B5 and CSC-B8

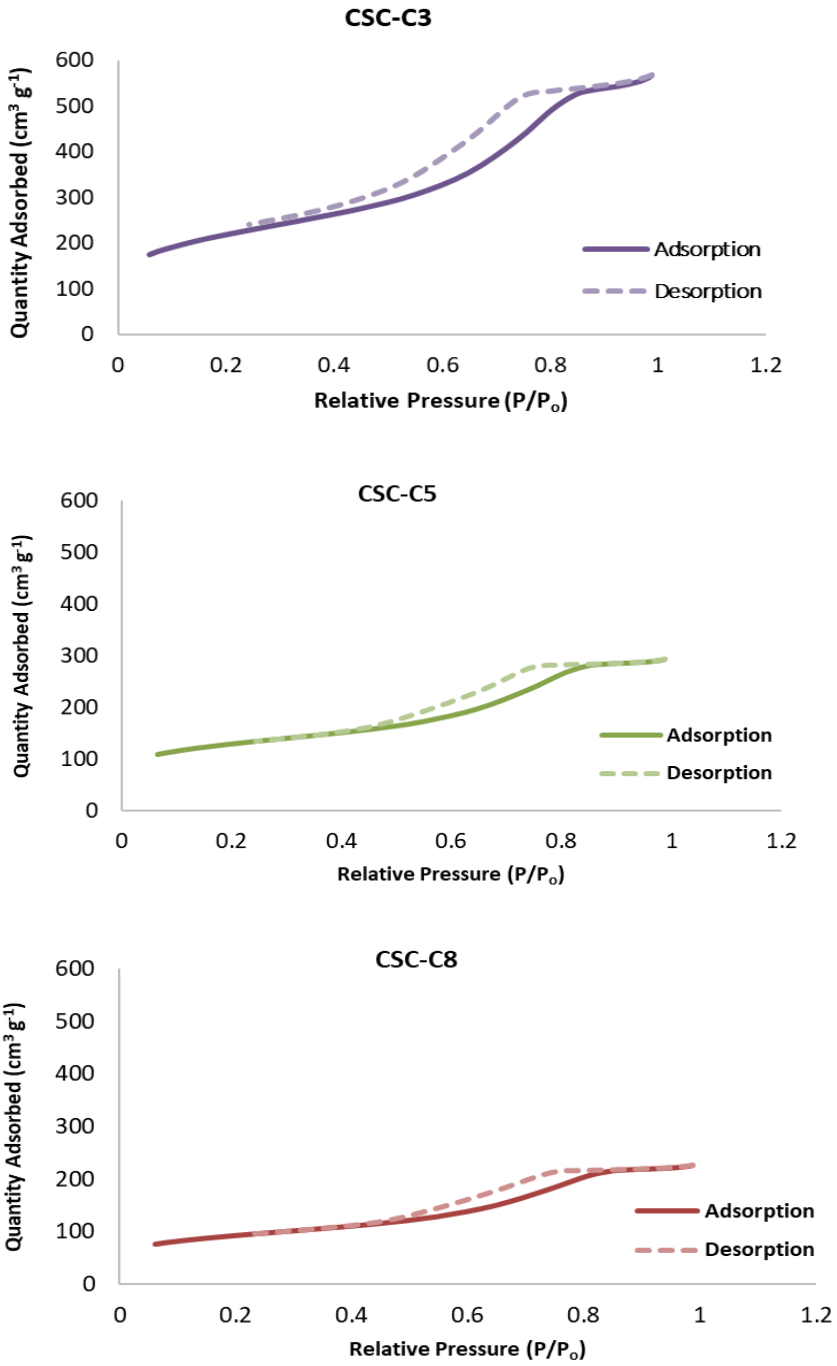

Figure 30 Nitrogen adsorption isotherms for CSC-C3, CSC-C5 and CSC-C8

A summary of material properties is given in Table 18. BET surface area, pore volume and pore diameter of materials produced at 300 ˚C and 500 ˚C are lower than the parent silica due to the introduction of carbon into the silica surface and within the pores. As adsorption isotherms and hysteresis loops are similar, it can be deduced that that the introduction of organic matter into the silica pores does not affect mesoporosity significantly.[154]

Table 17 Textural properties of Silica K60, Series B and Series C materials from porosimetry

Material	BET surface area ($mg^2\ g^{-1}$)	Pore volume ($cm^3\ g^{-1}$)	Pore diameter (nm)	Carbon layer thickness (nm)
Silica K60	467	0.80	6.7	-
CSC-B3	257	0.32	5.3	0.70
CSC-B5	336	0.37	5.1	0.80
CSC-B8	272	0.31	5.9	0.40
CSC-C3	330	0.29	4.2	1.25
CSC-C5	454	0.37	3.9	1.40
CSC-C8	779	0.74	5.3	0.70

At 300 ˚C there is significant reduction in pore volume from 0.80 $cm^3\ g^{-1}$ in Silica K60 to 0.32 $cm^3\ g^{-1}$ and 0.29 $cm^3\ g^{-1}$ in CSC-B3 and CSC-C3, respectively. This reduction demonstrates that the polymerised bio-oil in each case is well distributed within the mesopores. As the carbonisation temperature increases to 500 ˚C , there is a marginal increase in BET surface area, pore volume and diameter, due to the carbon layer shrinking within the pores.[217] Interestingly, at 800 ˚C the materials CSC-B8 and CSC-C8, exhibit the opposite pattern; CSC-B8 shows a decrease in BET surface area and pore volume, whereas CSC-C8 shows an increase in both values. CSC-C8 is much like CSC-A8, with these increases suggesting the loss of some carbon from within the pores and a subsequent formation of a more porous carbon layer on the silica surface. This decomposition of bio-oil in each material is consistent with the rapid release of gases (CO_2, CO and H_2O) that occurs as the carbonisation temperature increases from 500 ˚C to 800 ˚C (Fig.33 & 34) This decomposition leads to the formation of highly aromatic porous carbon on the surface, and as a result surface areas increase to 779 $mg^2\ g^{-1}$ and 1056 $mg^2\ g^{-1}$ for CSC-C8 and CSC-A8, respectively (Table 7 & 18).[152] On the other hand, CSC-B8 shows a decrease in surface area to 272 $mg^2\ g^{-1}$, suggesting that a portion of the larger and less stable mesopores may be shrinking or collapsing.[218]

Thickness of the carbon layer, as calculated by porosimetry data, is evidently decreasing with increasing carbonisation temperature. The only exception being for CSC-B5 and CSC-C5, at which temperature a slight increase is observed. Nonetheless, the decrease in the thickness of the carbon layer relative to carbonisation temperature, is anticipated and is proof of the formation of an aromatic carbonaceous layer on the surface of materials.

Scanning electron microscopy (SEM) images of both Series B and Series C materials (Fig.32) are obtained to help demonstrate the textural properties of materials upon carbonisation and the similarities and differences among them. It is evident in all images that the materials have a variation in size and distribution in particles, the variation being more pronounced in the images obtained for Series C materials (Fig. 32 D-F).

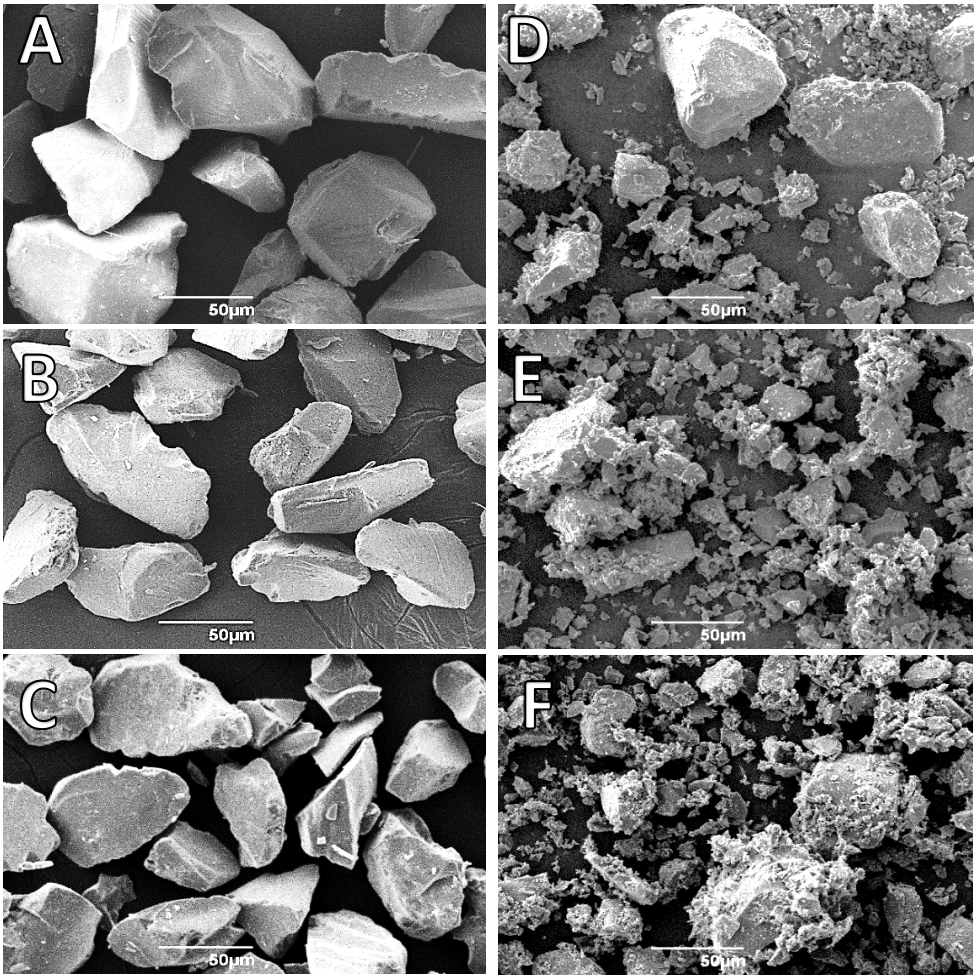

Figure 31 SEM images (A) CSC-B3, (B) CSC-B5, (C) CSC-B8, (D) CSC-C3, (E) CSC-C5 and (F) CSC-C8

SEM images of Series B materials (Fig.32 A-C) show a more uniform coverage of the carbon layer over the Silica K60 framework at all carbonisation temperatures, confirming successful coverage and a constant carbonaceous layer across the surface. Surprisingly enough, Series C materials exhibit a similar pattern to Series A materials; they consist of a combination of smaller and larger particles, with a significant proportion of the smaller particles. As previously proposed for Series A CSCs, one plausible explanation for these observations may be the mechanical grinding of the CSCs.[154] During the preparation of Series C materials, the abrasive forces induced by the magnetic stirrer bar and the round bottom flask may cause fracturing of some silica particles in the materials leading to the formation of smaller particles. Another possible reason may be the formation of porous char as the carbonisation temperature increases from 300 ˚C to 800˚C, due to the rapid release of gases upon increasing carbonisation temperature, as suggested by thermal analysis results (Fig.34). The rapid release of gases may be accompanied with the formation of porous carbon particles on the surface, which may appear as the smaller and rougher particles observed in the SEM images of Series C CSCs.

The TG-IR spectra of the uncarbonised sample of Series B (Fig.33) and the uncarbonised sample of Series C (Fig.34) are illustrated below.

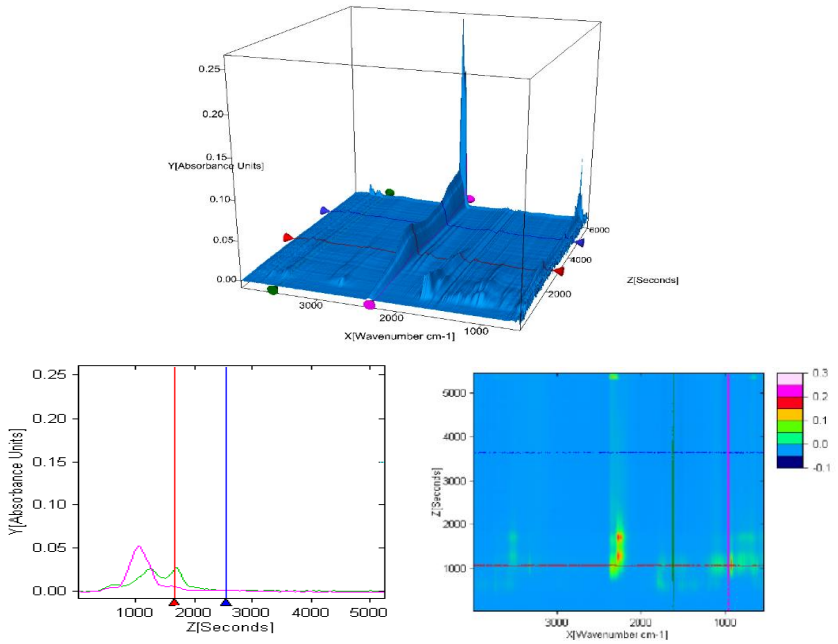

Figure 32 3D TG-IR spectrum of the off-gases from the thermal treatment of the uncarbonised sample used for Series B

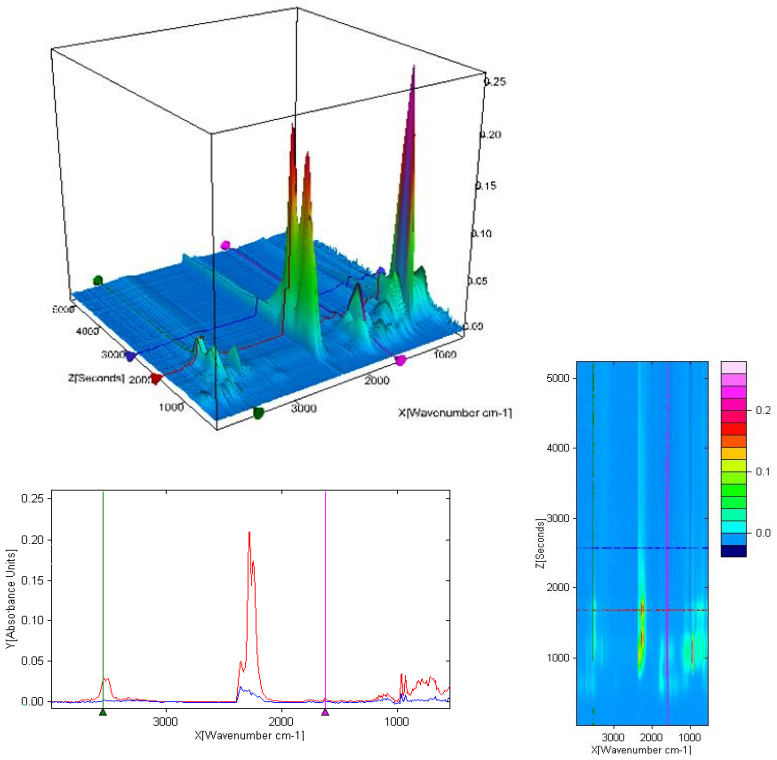

Figure 33 3D TG-IR spectrum of the off-gases from the thermal treatment of the uncarbonised sample used for Series C

The TG-IR spectra (Fig. 33 & 34) of the uncarbonised samples of Series B and Series C, show four major peaks, very similar to those observed for the uncarbonised sample of Series A.

- Peak located at 1066 cm^{-1} for Series B and 1079 cm^{-1} for Series C may be assigned to C-O-C groups, possible due to the decomposition product from saccharides.
- Major peak located at 2387 cm^{-1} for Series B and 2986 cm^{-1} for Series C may be attributed to the vibrations of CO_2, compared to the standard IR spectrum of carbon dioxide.
- Major peak located at 3015 cm^{-1} for Series B and minor peak at 3120 cm^{-1} for Series C may be assigned to -CH stretching vibrations, indicating the presence of –CH, $–CH_2$ or $–CH_3$ groups. Although the intensities of these peaks were decreasing from 180°C onwards, they could be detected until 400 °C, indicating the sample still contained these components before 400 °C.

- Peak at 1811 cm^{-1} for Series B may be attributed to the carbonyl group associated with anhydrides, suggesting that these groups were released at this temperature.

Both spectra taken at the maximum decomposition of uncarbonised material and show a similar evolution of gases including CO_2 and H_2O.[145,154] In terms of mass loss relevant to temperature, the following are observed for the uncarbonised material of both Series B and Series C:

- Around 100 ˚C, most of the moisture content present from the bio-oil and parent silica is lost.
- Between 180 ˚C and 230 ˚C, the system undergoes elimination reactions and saccharide decomposition, leading to the removal of volatile acids.
- Between 300 ˚C and 450 ˚C, most of the oxygenated compounds and aliphatic chains undergo decomposition.
- Above 550 ˚C, condensation of the silanol groups of the parent silica begins and the decomposition of aliphatic chains is complete, allowing for aromatisation at higher temperatures. Within this temperature range, CO_2 and CO are given off, too, further establishing the additional porosity of the materials indicated by porosimetry results.

These observations are proof that the CSCs produces have tuneable structural and textural properties as carbonisation temperature during their synthesis increases.

DRIFT spectra of Series B and Series C CSCs (Fig. 35 & Fig.36) illustrate the same shift in functional character as expected and observed in Series A CSCs (Fig.14); with increasing carbonisation temperature organic matter decomposes changing the functional groups present, shifting from an aliphatic and polar oxygenated coated surface to a more aromatic carbon layer. [154]

Aliphatic C-H stretching observed at 2900 cm^{-1} and C=O stretching at 1650 cm^{-1} are due to the presence of oxygenated compounds like carboxylic acids, ketones, aldehydes and esters, originating from the original components of the bio-oils.[152,153] These peaks, as well as the O-H stretch at 3500 cm^{-1}, are evident in the spectra of CSC-B3 and CSC-C3 as expected, but weaken and disappear as temperature increased to

500˚C and 800˚C. The hydroxyl group is reduced significantly due to the crosslinking effect of silica. Above 500˚C, bands representing C=O, C-H and O-H bands gradually weaken, being indicative of thermal decomposition taking place and reducing the amount of oxygenated compounds on the surface, leaving a more aromatic surface at 800˚C. Spectra for all Series B and Series C CSCs show stretching bands at 1060 cm^{-1} and 800 cm^{-1} corresponding to Si-O-Si bonds, confirming the presence of the silica substrate in the composite materials and the changes on the carbonaceous part of the structure.[152]

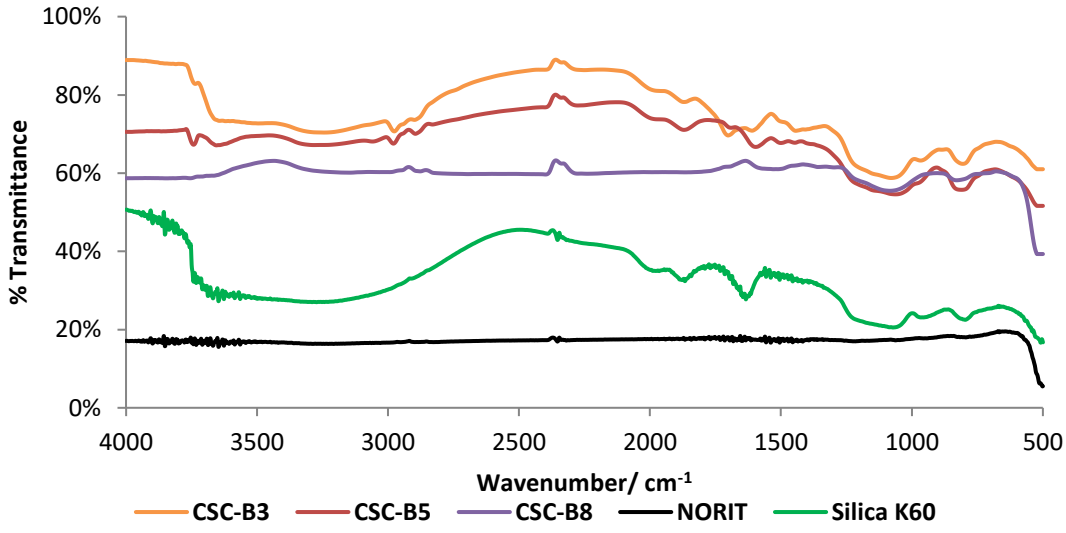

Figure 34 Overlapped DRIFT spectra of CSC-B3, CSC-B5, CSC-B8, NORIT activated carbon and Silica K60

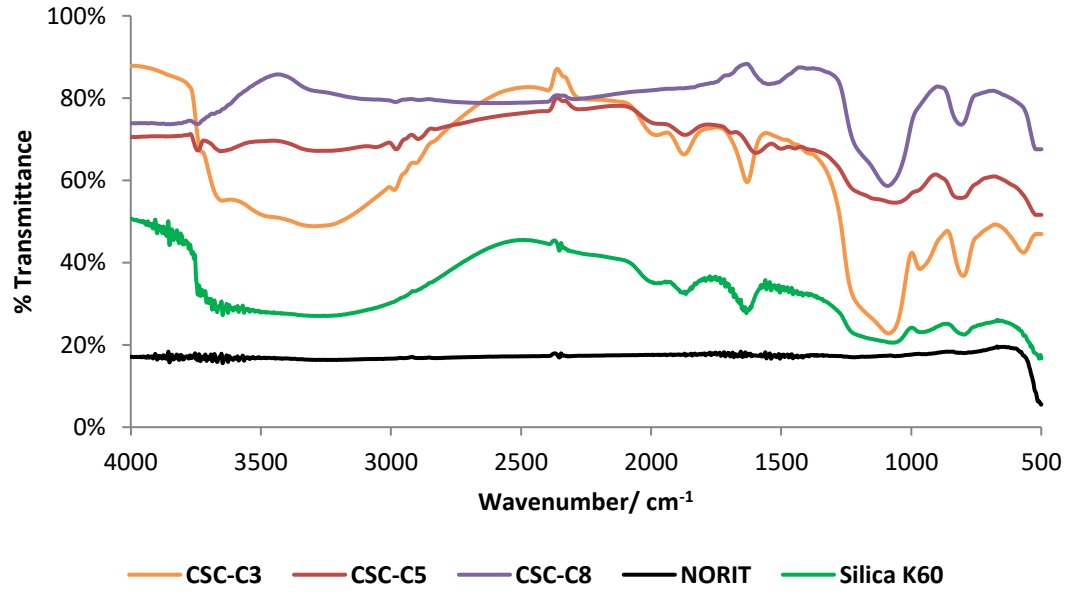

Figure 35 Overlapped DRIFT spectra of CSC-C3, CSC-C5, CSC-C8, NORIT activated carbon and Silica K60

The carbonisation temperature dependence of the materials produced has a great potential for development of tuneable properties, as shown for Series A CSCs, as it enables the continuum surface functionality of the material, from hydroxyl and carbonyl rich surface at 300 ˚C to carbonaceous aromatic surfaces at 800 ˚C .[152,154]

Table 18 % Atomic content deduced from Carbon XPS spectra of C1s for Series A, B and C

	% Atomic Content			
	C	Si	O	N
CSC-A3	51.0	15.6	33.4	-
CSC-A5	55.1	14.1	30.08	-
CSC-A8	59.7	12.2	28.1	-
CSC-B3	13.6	25.0	61.4	-
CSC-B5	10.2	27.1	62.7	-
CSC-B8	9.9	26.7	63.4	-
CSC-C3	22.7	21.7	55.7	-
CSC-C5	12.2	26.0	61.8	-
CSC-C8	9.6	27.1	63.3	-

The C, O and Si elemental surface content of the Series B and Series C CSCs is measured by XPS. XPS data show that with increasing carbonisation temperature, the % C content on the surface decreases, whereas % O and % Si increase (Table 19). These results exhibit an opposite trend to that initially observed for Series A CSCs, which portrays an increase in the % C content and a corresponding decrease in % O and % Si. One may deduce, that with the decrease of C % and increase of % O and % Si contents, the materials are not losing hydrophilic compounds containing oxygen on heating to higher temperatures, and as a result there is little to no shift from aliphatic and polar character to more aromaticity. Combining results from DRIFT data and the deconvolution of the C1s carbon peaks, the shift in functionality is confirmed, even though % atomic content might suggest otherwise.

Based on C1s spectra deconvolution for Series B and Series C materials (Fig.39), oxygenated carbon functionalities decompose with increasing temperature, showing an increase in aromatic character and loss of hydrophilic and aliphatic compounds containing oxygen. Oxygen is still substantially present at all temperatures, along with

silicon, confirming the presence of the parent silica. The presence of oxygen facilitates the interaction between the polymerised bio-oil and the silanol groups in the parent silica, giving rise to the observed C-O-Si bond.[154] The presence of silicon and oxygen may further indicate that parts of the CSC surface are not coated by the carbon film created during carbonisation. These exposed silica sections will very likely affect the adsorption process and overall gold removal discussed in the following chapter, as they will not provide any active sites for adsorption.

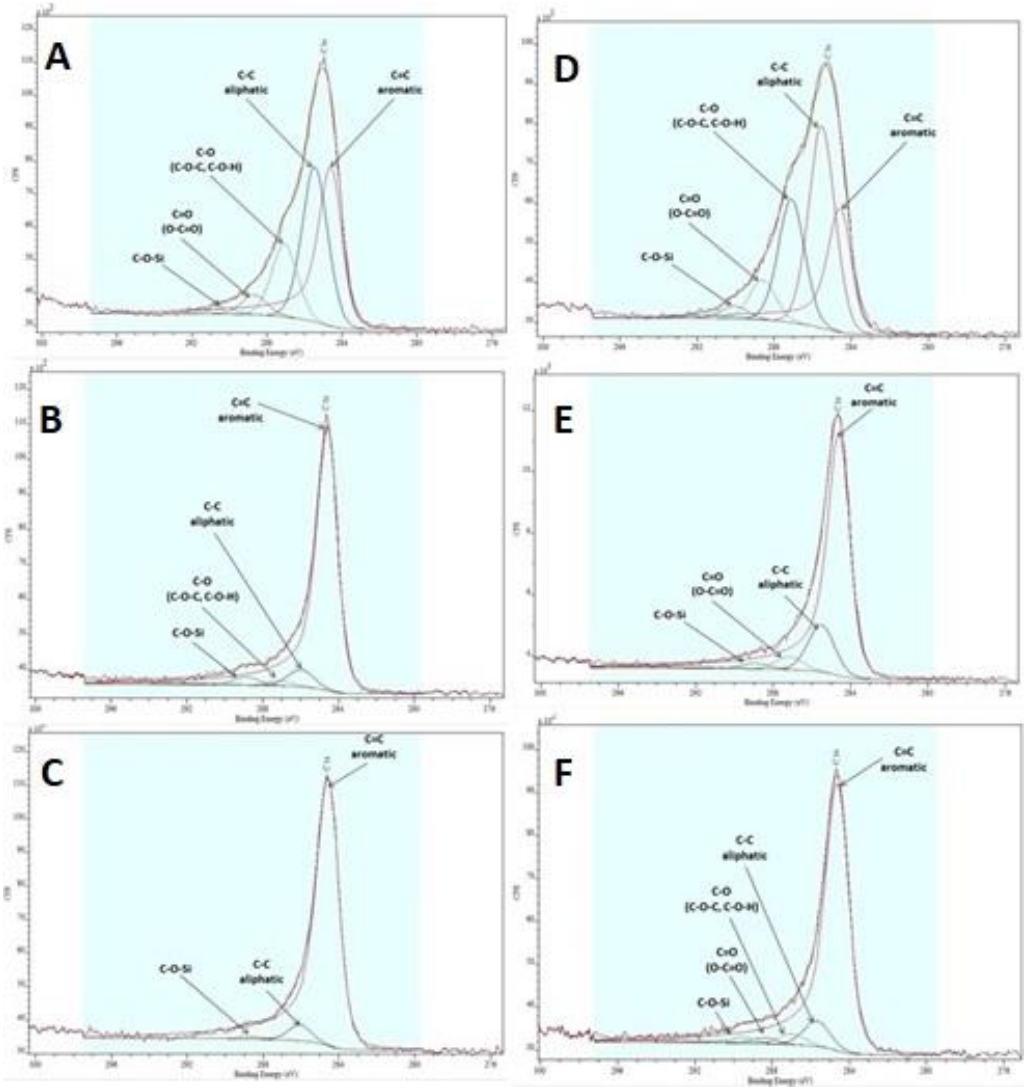

Figure 36 Carbon XPS Spectra of C1s (A) CSC-B3, (B) CSC-B5, (C) CSC-B8, (D) CSC-C3, (E) CSC-C5 and (F) CSC-C8

Every type of bond appears at a specific binding energy which allows for identification of different functional groups through deconvolution of the main peaks. C1s peaks of the spectra are deconvoluted and assigned giving rise to five contributions due to: C=C groups (aromatic), C–C groups (aliphatic), C –O groups (C–O–C or C–O–H), C=O groups

(O-C=O) and C–O–Si group at 284.4 eV, 284.6 eV, 285.8 eV, 287.2 eV and 288.9 eV binding energies, respectively.[116,155,156] XPS and DRIFT data are in fairly good correlation, confirming the shift from aliphatic and polar hydroxyl character at the lower carbonisation temperature to aromatic character observed in the materials produced at 800° C.

Comparing % C with CHN analysis (Table 20), indicates that carbon is concentrated on the surface of materials, with the overall amount throughout the bulk being lower. Based on CHN analysis, decrease in w/w% O or w/w% Si contents cannot be measured quantitatively, as they are not differentiated and are both accounted for in the rest bulk content value.

Table 19 % Elemental composition of Series A, B and C CSCs

	w/w % Elemental composition			
	C	H	N	Rest
CSC-A3	45.3	6.2	-	48.4
CSC-A5	40.3	5.6	-	53.8
CSC-A8	39.6	4.3	-	56.1
CSC-B3	16.4	1.1	-	82.5
CSC-B5	14.9	0.5	-	84.6
CSC-B8	14.6	0.3	-	85.1
CSC-C3	28.3	3.4	-	68.3
CSC-C5	24.8	2.7	-	72.5
CSC-C8	25.2	2.2	-	72.6

Between the different series of CSCs produced, materials carbonised at the same temperature show variations in the amount of carbon on the surface and throughout the bulk. Series A CSCs have the highest amount of bulk carbon, followed by Series C CSCs and Series B CSCs, being the ones with the lowest. This is purely attributed to the original carbon source: the bio-oils used as the carbon precursors to synthesise each series of composite materials. Even though the feedstock (milled waste office paper), in addition to the microwave conditions, parameters and setup used are the same in each instance, different quality bio-oils are obtained. Between the three bio-oils (BO-

A, BO-B & BO-C) the fractions of matter differed, with BO-A having the highest C content at 48.9 w/w%, followed by BO-C at 36.5 w/w% and then BO-B at 25.9 w/w%. As a result, the corresponding series of materials had lower carbon throughout their bulk, as anticipated.

4.4 Conclusion

Two novel series of bio-derived mesoporous carbon/silica composites (Series B and Series C) have been successfully prepared from bio-oil, obtained from the microwave-assisted pyrolysis of waste office paper, and commercially available Silica K60 gel. Although the general properties of the new materials are similar to those of Series A, interesting differences in terms of structure and surface composition are noted. Materials with tuneable surface chemistry and textural properties are obtained by varying the carbonisation temperature during their synthesis. At low temperatures the materials are rich in oxygen functionalities (CSC-B3 and CSC-C3), and as the temperature increases the materials begin to lose their aliphatic and polar character becoming more aromatic (CSC-B8 and CSC-C8); a general trend observed for both Series B and Series C composite materials.

Investigation of the carbon source for each series, i.e. bio-oil BO-B for Series B and bio-oil BO-C for Series C, has shown that during microwave pyrolysis of identical feedstock/ biomass, separation of fractions can occur differently, and thus affect physical and chemical properties of the bio-oil. The major differences observed between bio-oil BO-B and BO-C are in the moisture and carbon contents. Bio-oil BO-B, importantly, contains significantly less carbon than bio-oil BO-C and bio-oil BO-A, and as a result, Series B composite materials have reduced content of carbon on their surface and throughout their bulk.

Seeing as how, the adsorption behaviour of materials is affected by the surface functionalities and the carbon film, the range of materials produced is expected to present interesting and exciting results. Series B and Series C materials produced at the same temperature possess similar surface functionalities, yet a completely different carbon film. Their performance adsorbents will be discussed in the following chapter.

Chapter 5.

Carbon Silica/Composites

Series B and Series C:

Application in Gold Adsorption

Aspects of the work presented in this chapter have appeared in:

Oral presentation at the 8th IUPAC International Conference on Green Chemistry, Bangkok, Thailand, September 2018

Poster presentation at the 9th World Convention on Recycling and Waste Management, Osaka, Japan, October 2018 (1st poster prize awarded)

Chapter 5.

Carbon/Silica Composites Series B and Series C: Application in Gold Adsorption

5.1 Introduction

The development of Series A composite materials and their application in gold adsorption has presented exciting results, creating the need for the development of more and newer series materials that will exhibit a similar outstanding selectivity toward gold and high removal rates.

Findings from Chapter 4 show that the production of similar yet different mesoporous carbon/silica composites (Series B and Series C) is possible and successful. It is crucial now, that the newly prepared Series B and Series C CSCs are tested as adsorbents for gold removal, to prove their performance efficacy. Characterisation results of Series B and Series C materials exhibit interesting physiochemical properties, and thus their application in gold adsorption is anticipated to show equally interesting outcomes.

5.2 Aims

The overall objective of this chapter is to provide a full assessment on the performance of the newly synthesised Series B and Series C composite materials as adsorbents for the removal of gold from acidic solutions.

The aims of the work presented herein:

- To investigate the influence that the physiochemical properties of the Series B and Series C composite materials have on adsorption.
- To propose the possible adsorption mechanism on the surface of the Series B and Series C composite materials using isotherm models.

5.3 Results and Discussion

5.3.1 Gold Selectivity

Initial batch adsorption experiments demonstrate that both new series of CSCs exhibit significant selectivity toward gold from an acidic solution (pH 3) containing precious and base metals like nickel, copper, zinc, palladium, platinum and gold in similar concentrations. (Fig. 38 & 39).

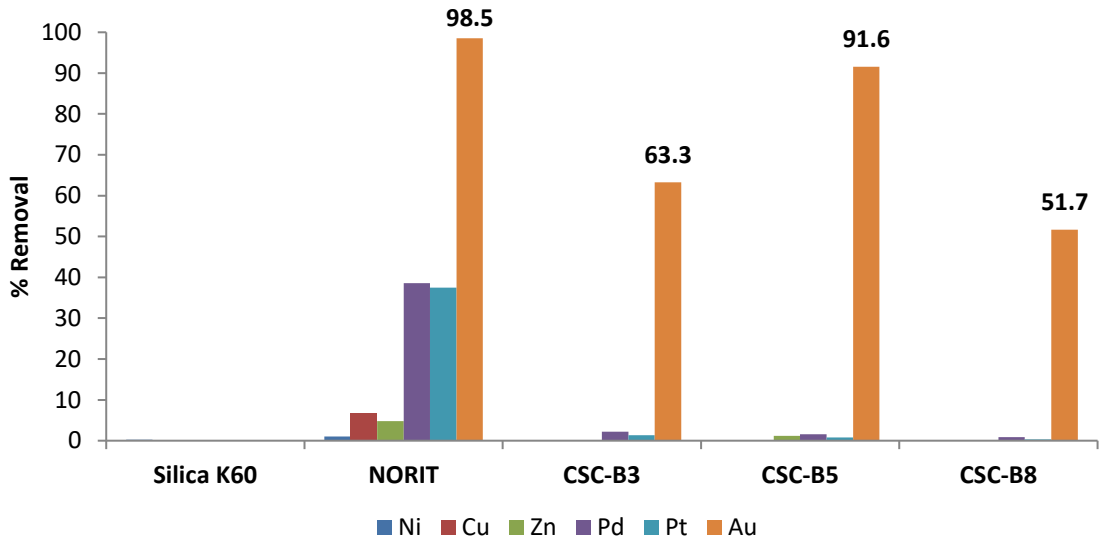

Figure 37 % Removal after multi-metal adsorption using Series B CSCs, silica K60 and NORIT activated carbon

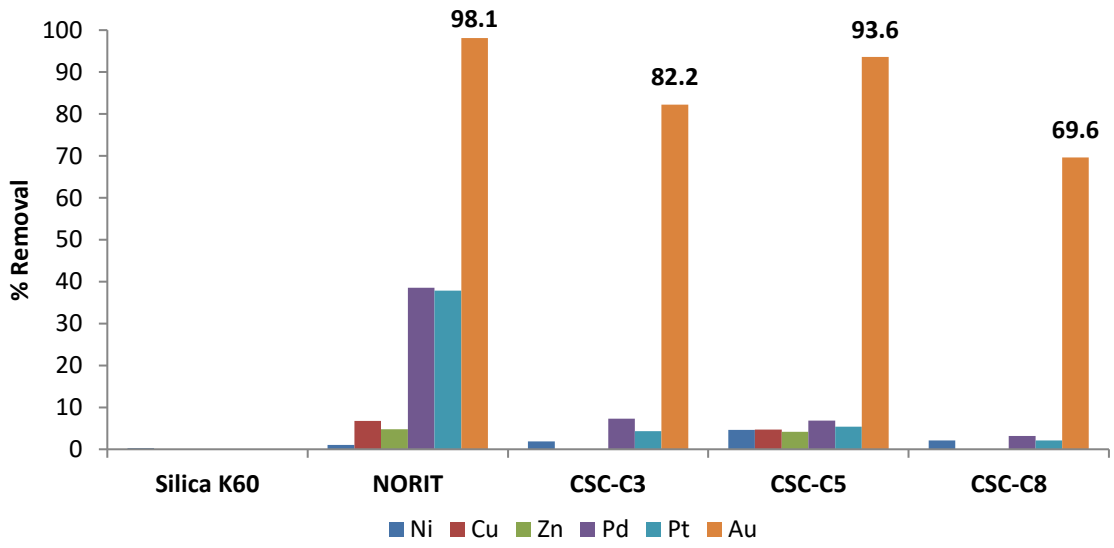

Figure 38 % Removal after multi-metal adsorption using Series C CSCs, silica K60 and NORIT activated carbon

The choice of metals is made based on factors previously mentioned (Chapter 2): 1) metal composition of mine tailing samples from North American Palladium, Lac des Iles mine in Ontario, Canada and 2) significant concentrations in WEEE after extensive use in commercial electronics. [14,41]

As observed for Series A CSCs, materials of Series B and Series C demonstrate a significant preference to those metals with higher reduction potentials, i.e. gold, platinum and palladium.[219] Worth noting is that NORIT activated carbon demonstrates substantial adsorption of all elements in solution, whereas silica K60 demonstrates very little to no adsorption of the elements. While NORIT activated carbon exhibits good adsorption of most elements, it lacks selectivity, as opposed to both Series B and Series C CSCs which show a clear preference in adsorbing gold, similarly observed for Series A CSCs. In the case of all CSCs (Series A, B and C), the adsorption of gold is mostly controlled by surface functionality and the reduction of Au(III) to Au(0) on the surface.[159] Therefore, all CSCs demonstrate a balance between strong adsorption and high selectivity towards gold.

When comparing Series B CSCs to Series C CSCs produced at the same carbonisation temperature, it is evident that Series C materials show a greater selectivity toward gold with higher removal of the metal from solution. Since surface functionality plays a primary role in the adsorption process and as seen via characterisation results of all materials, it is expected that Series C CSCs will perform better than Series B. The best materials for both Series B and Series C are the ones produced at 500 ˚C , at which carbonisation temperature CSCs have the ideal balance between surface functionality and porosity. A similar observation is noticed with Series A CSCs, which first introduced the notion of enhanced adsorption capacity and gold removal if the right balance between surface functionality and porosity is achieved. CSC-B5 achieves 91.6% removal of gold during the multi-metal adsorption experiment, while CSC-C5 and CSC-A5 achieve 93.6% and 96.6%, respectively.

5.3.2 Mechanism of Gold Adsorption

The mechanism of gold adsorption, as previously mentioned, involves two key processes: 1) the chemisorption process (irreversible process), during which Au(III) species is chemically adsorbed and then reduced mainly to elemental gold Au(0), yielding gold nanoparticles and 2) the traditional physisorption (reversible process). In gold (III) chloride solutions, gold occurs as the aurochlorate $[AuCl_4]^{-1}$ anion complex.[220] The carbonaceous surface of CSCs shows a high affinity for Au(III) due to the high standard electrode reduction potential, E^o ($[AuCl_4]^{-1}$/ Au^0= 1.00V), and the similarly high reduction potential, E^o ($[AuCl_4]^{-1}$/ $[AuCl_2]^{-1}$= 0.93V) for the reduction to Au(I) ion, via this reduction-adsorption mechanism.[28,107,161] This mechanism allows for the creation of vacancies on the surface of the material as the reduced species deposit, which leads to higher uptake of the metal from solution and increased adsorption capacity of the adsorbate surface.[162]

Nonetheless, the system undergoes physisorption as well, which involves weak electrostatic interactions between the species in solution and the surface of the adsorbent material.[163] During physisorption, a thin film of the adsorbate is created on the surface of the material after the species diffuse through the layer and into the pores of the materials.[160] Where physisorption dominates, the film created serves as a monolayer and it prevents irreversible reduction of Au(III) to either Au(I) or elemental gold Au(0). As a result, the formation of the monolayer averts the species from undergoing a chemical reaction with the surface of the material, filling all active adsorption sites and tremendously reducing the creation of new vacancies for chemisorption and subsequent reduction to take place.

Surface chemistry of materials plays a crucial role in the mechanism of adsorption. It is anticipated that owing to the materials oxygen-containing functionalities (carbonyl, carboxyl, hydroxyl groups) present on the carbonaceous surface, supported by XPS and DRIFT data, the system will proceed via chemisorption; reduction of the gold species with simultaneous oxidation of the protonated carbonaceous surface, as observed for Series A CSCs gold adsorption.

Adsorption, though, in the case of Series B CSCs proceeds predominantly via physisorption (Fig.40) suggesting that surface groups are not participating in chemical reactions but interact mainly by weak dispersion forces. It may be assumed that the surface of materials, even though abundant in oxygen-containing groups, can no longer facilitate electron transfers for chemical bonding. The surface of materials, as shown by XPS, contains aromatic carbons, which could attribute to electron-rich regions on the carbon layer of the surface, creating a partial negative charge on it.[221,222] Since, the gold species in solution exists as anion, if the surface is highly electron rich by the presence of resonating electrons of the aromatic rings and π bonds, then it may be assumed that the adsorbent surface and adsorbate anions will repel each other. Repulsion may not be strong enough or permanent, but it could offer an explanation as to why chemisorption is least favoured during the process with Series B materials and why overall adsorption is lower. On that account, physisorption should be hindered too, but as the basic and acidic nature of materials compete during the process, the boundary layer of the adsorbate $[AuCl_4]^{-1}$ species forms allowing for monolayer coverage, dominated by physisorption in this occasion.

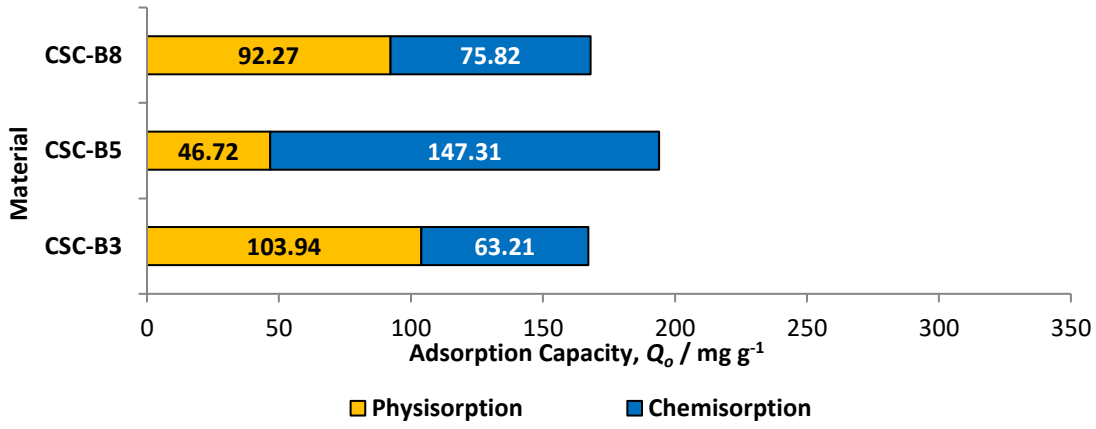

Figure 39 Nature of adsorption for all Series B CSCs

In the case of Series C CSCs, adsorption proceeds via almost equal extents of chemisorption and physisorption (Fig.41). Overall adsorption capacities for the CSCs of this series are higher, in comparison to respective values for the Series B CSCs. Considering the amount of carbonaceous matter in each material of each series (A, B and C), an interesting observation can be made relating to the mechanism/nature of adsorption. Series A materials which have the most carbonaceous matter on their

surface favour chemisorption and reduction, whereas Series B materials which have the least mainly favour physisorption. Series C materials which possess carbonaceous matter in the middle of the range set by Series A and Series B, exhibit rather equal contributions of physisorption and chemisorption throughout the process. These findings can create the hypothesis, that the nature of adsorption can be probed by controlling the amount of carbonaceous matter on the surface of materials. By varying the amount of surface carbon, the number of chemical functionalities is varied as well, and consequently the likelihood of either chemisorption-reduction or physisorption is affected.

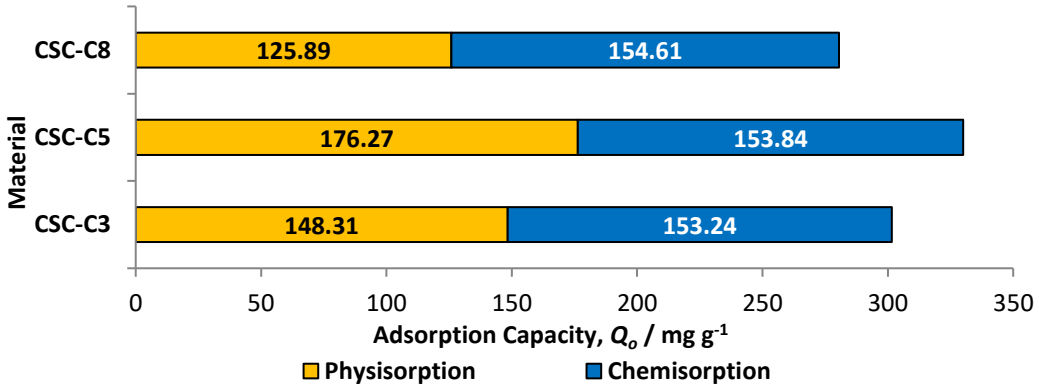

Figure 40 Nature of adsorption for all Series C CSCs

Transmission Electron Microscopy (TEM) images of Series B and Series C CSCs (Fig.43) obtained after adsorption clearly show the formation of gold nanoparticles (AuNPs), and are in good correlation with XPS data, confirming the reduction of Au(III) ions to metallic gold Au(0) after chemisorption has taken place. Spherical, hexagonal and triangular gold nanoparticles of different sizes are observed. The larger nanoparticles seen, may be the result of aggregation of smaller nanoparticles around a core molecule, in this case silica.[165,166]

To further support the formation of AuNPs, physical observations of the adsorption samples show a gradual colour change of the solution from yellow/pale yellow (depending on the concentration of gold (III) chloride) to pale purple/pink (Fig.42). This specific colour change is indicative of the formation of AuNPs in the system.

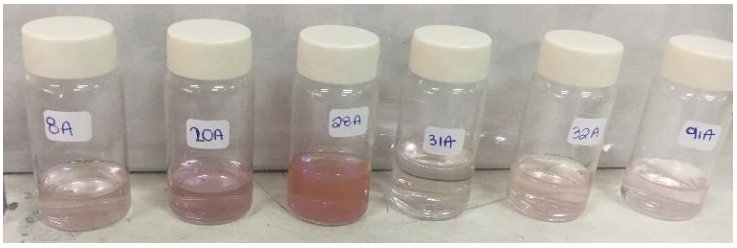

Figure 41 Colour of samples after adsorption

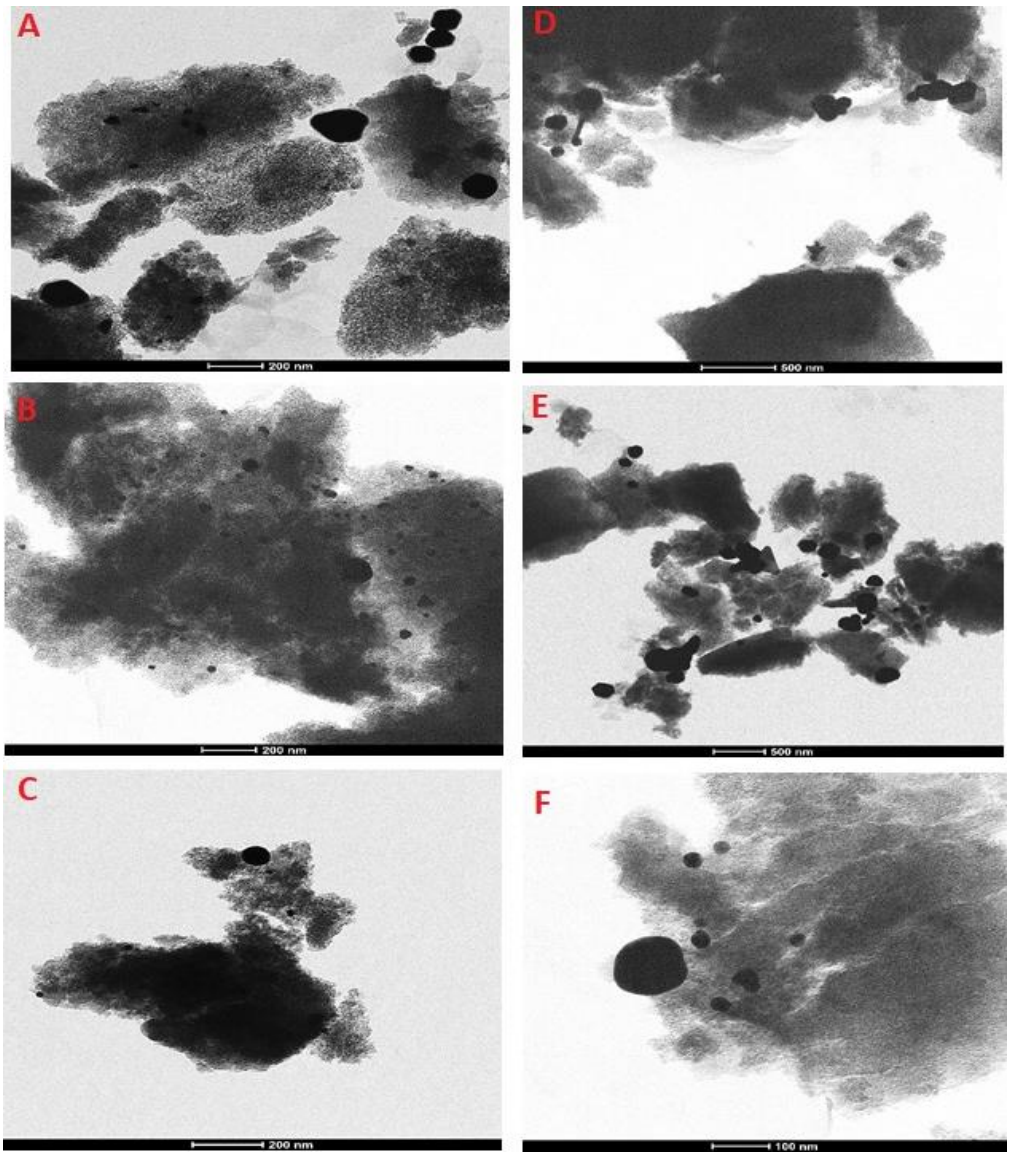

Figure 42 TEM images showing AuNPs formation after adsorption in (A) CSC-B3, (B) CSC-B5, (C) CSC-B8, (D) CSC-C3, (E) CSC-C5, (F) CSC-C8 at 200nm scale

XPS results (Fig.44) clearly showed the presence of gold at the materials' surface. The Au4f spectra can be deconvoluted into three sets of doublets, in which the two peaks within the doublet are 3.7 eV apart with 4:3 relative intensity for the 7/2 and 5/2 orbits, respectively. The main doublet is found at 84.6 eV (7/2) which represents Au(0),

confirming the reduction of $[AuCl_4]^{-1}$. The other two doublets at 86.1 eV and 86.6 eV correspond to the binding energies of Au(I) and Au(III), respectively.

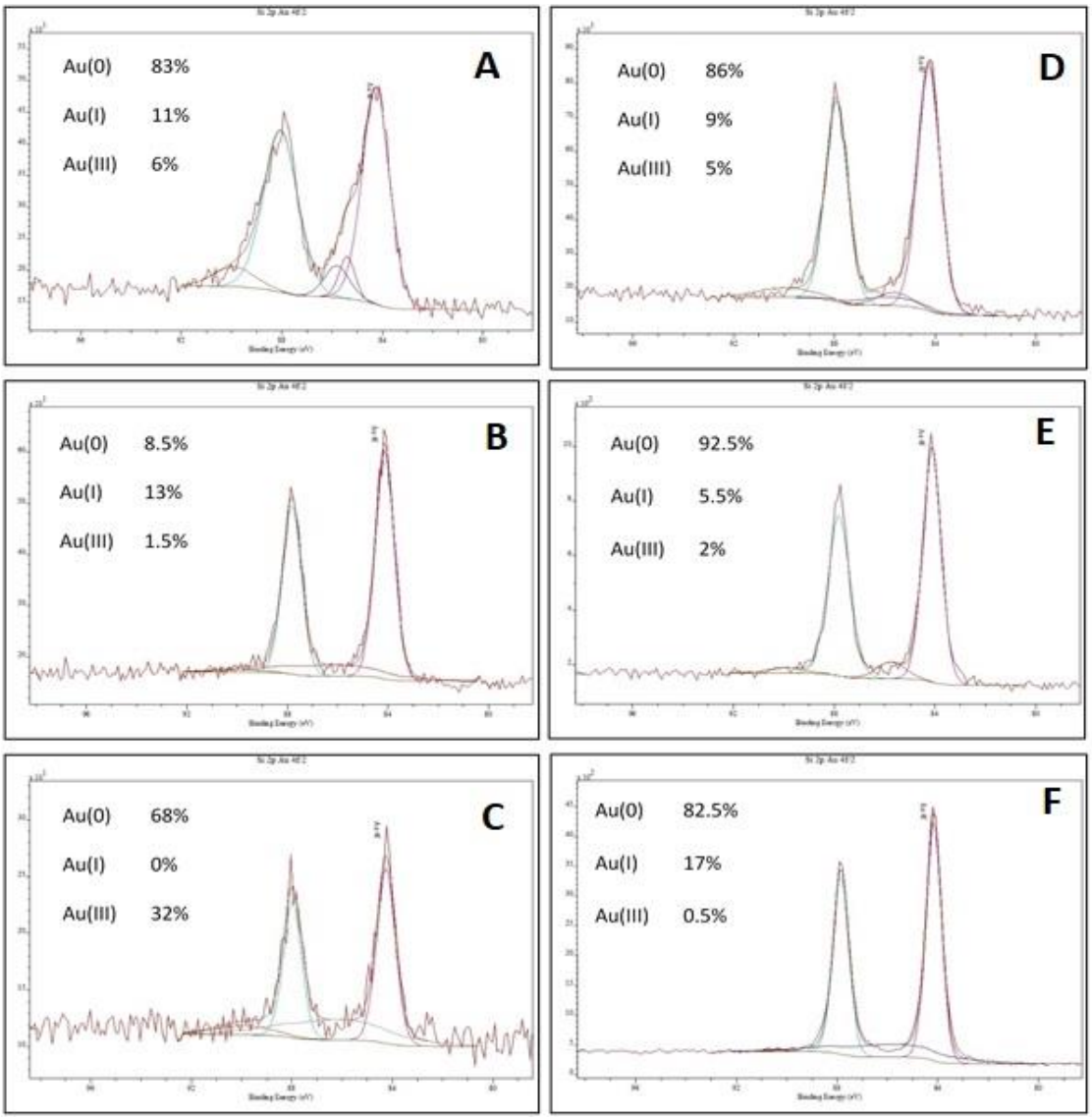

Figure 43 Au4f XPS spectra for (A) CSC-B3, (B) CSC-B5, (C) CSC-B8, (D) CSC-C3, (E) CSC-C5, (F) CSC-C8

Data from the deconvolution of the Au4f XPS spectra (Fig.44) indicate that the gold is almost entirely reduced from Au(III) to Au(0), with a small proportion of it reduced to Au(I). This reduction to Au(0) is well in agreement with the TEM images (Fig.43) of Series B and Series C materials, which illustrate nanoparticle formation due to gold reduction. While Series B materials proceed mainly via physisorption during the adsorption experiments, XPS data support that gold is mostly being reduced. One plausible explanation for this observation is that XPS investigates only the upper layer of the surface (10nm), whereas phase transfer occurs at all accessible layers and pores

of materials that may be well beneath the 10nm depth. As a result, materials can still favour the physisorption mechanism throughout their bulk, with the main interactions on the surface attributed to chemical reaction. A similar hypothesis can apply to Series C materials after adsorption. While the contribution of physisorption and chemisorption are fairly equal during the process, XPS results indicate that the surface undergoes a chemical reaction, leaving the surface with mostly reduced gold Au(0) rather than equal amounts of reduced gold and Au(III).

The reduction of gold ions is without a doubt caused by the oxidation of functionalities on the surface of CSCs. There are several functional groups present on the surface of materials, especially those carbonised at 300 ˚C and 500 ˚C , that can oxidise (i.e. hydroxyl and carbonyl groups) when reacting with the gold species. The following hypotheses can be used to explain the redox mechanism occurring during gold adsorption:

- Oxidation of hydroxyl groups to carbonyl groups: Literature describes that during the process the $[AuCl_4]^{-1}$ is initially adsorbed onto the surface by forming a chelating complex with the oxygen atoms of hydroxyl groups. The hydroxyl groups are then oxidised to ketones, leading to a decrease in the concentration of O-H groups and an increase in the concentration of C=O groups.
- Decomposition of the carbon surface: Oxidation of carboxylic groups to produce CO_2, is accompanied by decomposition of the surface, thus inducing an increase in the C/O ratio after adsorption.

Elemental analysis carried out by XPS shows higher C/O ratios (Table 21) after adsorption for all materials of both Series B and C, suggesting that the surface may be decomposing while at the same time oxidising, thus confirming the chemisorption mechanism.

Table 20 Comparison of CSC C/O ratio before and after adsorption of gold

C/O ratio			
Material	Before adsorption	After adsorption	Variation
CSC-B3	0.2	0.4	+ 0.2
CSC-B5	0.2	0.4	+ 0.2
CSC-B8	0.2	0.3	+ 0.1
CSC-C3	0.4	0.5	+ 0.1
CSC-C5	0.2	0.5	+ 0.3
CSC-C8	0.2	0.7	+ 0.5

Similar to Series A CSCs, it can be suggested that the recovery of gold from solution occurs in three steps: adsorption, reduction and aggregation. During overall adsorption, both reversible physisorption and irreversible chemisorption occur. During physisorption, the $AuCl_4^-$ species is electrostatically attracted and brought to closer to the protonated surface of materials. Then, the $AuCl_4^-$ complex appears to be chemically adsorbed to the surface, at which moment it is possible that one or more of the chloride ligands is replaced by one or more hydroxyl groups on the adsorbent surface. Since, a chemical interaction can be easily assumed to take place, the gold ions are then reduced due to the electron-donor groups on the surface of materials, which oxidise and simultaneously reduce Au(III) to mainly Au(0). Finally, the nanoparticles produced are released from the surface and agglomerate to form clusters of AuNPs (or 'free' gold in solution). The release of AuNPs from the surface of materials, leaves more active sites available for further adsorption in the system. This suggested three-part mechanism is, as previously demonstrated, consistent with data obtained from XPS and TEM.

Even though the chloride ions participate as ligands during the adsorption process, yet again XPS data show no concentration of said ions on the surface of materials. Further investigation needs to be carried out, to clearly determine what happens to the Cl^- ions; this was out of the scope of this work and is discussed in Further Work Chapter 9, Section 9.2.

5.3.3 Gold Adsorption Isotherms

In order to further investigate the mechanism of gold adsorption onto the newly prepared Series B and Series C CSCs, three models are applied; the Langmuir model, the Freundlich model and the Dubinin-Radushkevich (D-R) model. Isotherm parameters are calculated using the linear form of the isotherm equations. All parameters and correlation coefficients (R^2) are summarised in Table 22.

Model fittings are done for the part of adsorption represented by physisorption, where the system was no longer irreversible. Fitting to all three adsorption models shows that the materials had better correlation to the Langmuir type adsorption with R^2 values over 0.98 for all Series B and Series C materials (Table 22). Interestingly, the monolayer adsorption capacities represented by Q_0, are in good agreement with the adsorption capacities calculated experimentally (Table 2).Even though the actual maximum capacities, experimental q_e, for all materials were higher than the calculated Q_o values as per the Langmuir model, difference between them is reasonable and can be accounted for by the different modes of adsorption in the system. As mentioned, adsorption of gold in an aqueous system occurs via both reversible physisorption and irreversible chemisorption. Q_o values calculated from the Langmuir model account for the part of the system progressing via physisorption; the small difference between Q_o and q_e values (Table 22) is indicative of the favourable physisorption during the tests.[172]

Even though all Series B and Series C CSCs have a better fit to the Langmuir model, which assumes monolayer coverage of adsorption sites, some materials illustrate a good fit to the Freundlich and D-R models, too. For instance, CSC-B3 and CSC-B8 show a good fit to the Freundlich model (R^2 values 0.98 and 0.92, respectively) which suggests multi-layer adsorption dependent on the material's surface chemistry.[173] Additionally, Series C CSCs exhibit a good fit to the D-R model, which assumes that adsorption proceeds via pore filling rather than layer-by-layer coverage.[176,177] Materials fit well with other models than the Langmuir as well, as they are proven to have surface heterogeneity which means that adsorption could be multi-layer or accompanied with pore filling, and not limited to monolayer coverage.

Table 21 Isotherm modelling parameters for all Series B and Series C CSCs

Isotherm parameters	CSC-B3	CSC-B5	CSC-B8	CSC-C3	CSC-C5	CSC-C8
q_e (mg g^{-1})	167.15	194.03	168.09	301.55	330.11	280.50
Langmuir						
α_L (L mg^{-1})	0.03	0.08	0.03	0.10	0.09	0.07
K_L (L g^{-1})	6.00	14.92	4.72	29.41	29.59	17.92
Q_o (mg g^{-1})	172.41	196.07	172.41	303.03	333.33	270.27
R^2	0.9982	0.9966	0.9813	0.9991	0.9990	0.9873
Freundlich						
Kf	36.29	79.21	61.33	82.17	79.91	87.04
n	3.96	6.75	6.62	4.29	3.88	5.27
R^2	0.9803	0.7820	0.9249	0.8677	0.8755	0.8475
D-R						
q_m (mol g^{-1})	140.72	176.97	136.46	276.86	300.99	234.96
K' x10^{-6} (mol^2 J^{-2})	1.00	2.00	1.00	2.00	2.00	1.00
E (kJ mol^{-1})	0.70	0.50	0.70	0.50	0.50	0.70
R^2	0.6985	0.9591	0.611	0.9774	0.9729	0.9418

5.3.4 Effect of Gold Concentration on Adsorption Capacity

ICP-OES analysis is used to determine the adsorption capacity and % gold removal for all Series B and Series C CSCs at room temperature. As a general observation, isotherm data indicate over 95% removal of gold (Fig.45 & 46) with decreasing gold concentration in the low concentration regions (50 mg L^{-1} and 100 mg L^{-1}), and a plateau at the higher concentration regions (from 200 mg $L^{-1}$to 500 mg L^{-1}) with values dropping to less than 50% removal.

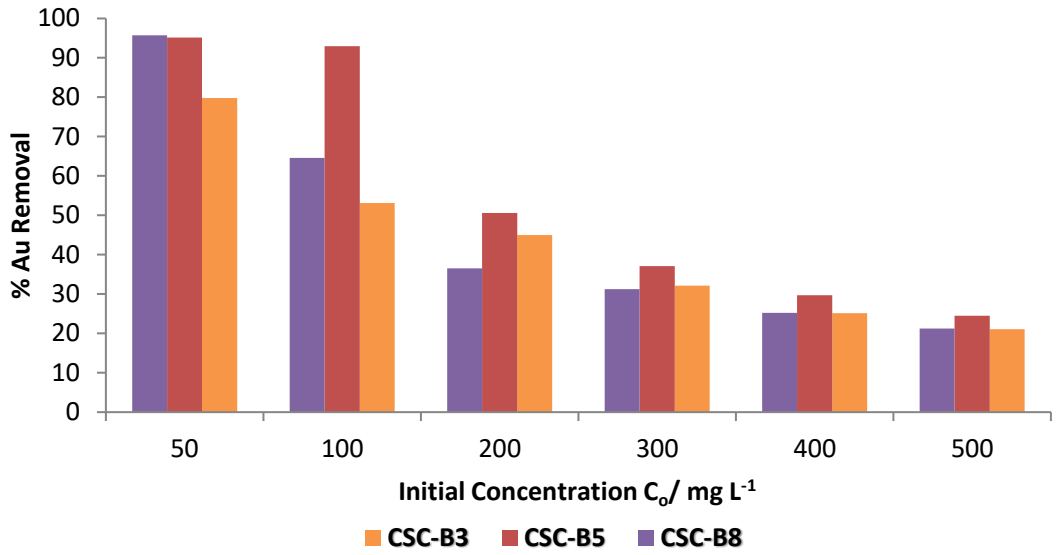

Figure 44 % Gold Removal with Series B CSCs at room temperature

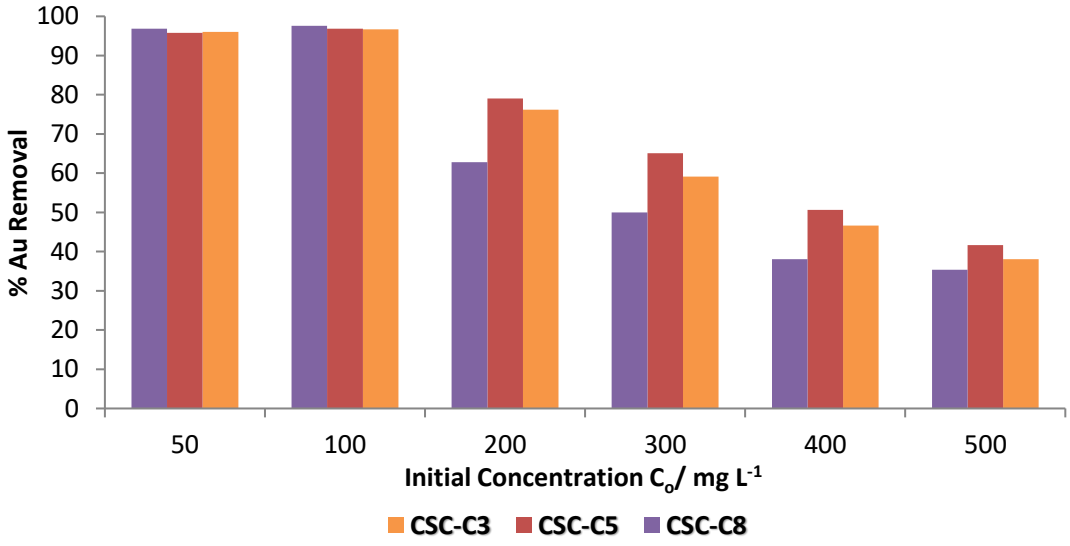

Figure 45 % Gold Removal with Series C CSCs at room temperature

As expected, Series C CSCs have overall higher gold removal than Series B CSCs, with CSC-C3, CSC-C5 and CSC-C8 removing almost identical amounts of gold up to 97% at the low region concentrations (Fig.46). As the solution concentration increases, it becomes evident that CSC-C5 performs the best out of the three materials of Series C, as it shows the highest removal of gold at the range of higher concentrations. As far as Series B is concerned, it is clear (Fig. 45) that at CSC-B5 removes the most gold at the range of concentrations used for the adsorption experiments, with a maximum removal of 96% at the low end of the concentrations used.

These gold removal trends are proof that adsorption is concentration dependent at constant pH. Initially, at the low region concentrations (50 mg L^{-1} and 100 mg L^{-1}), a significant adsorption is observed, resulting in a sharp incline in the adsorption curves. The very high % gold removal observed at those concentrations, along with the XPS data suggest that irreversible chemisorption is taking place as gold is being adsorbed on the active sites of the material via its reduction.[161,178] Adsorption in the higher concentration regions (200 mg L^{-1}, 300 mg L^{-1}, 400 mg L^{-1} and 500 mg L^{-1}) is hence speculated to mainly proceed by reversible physisorption, as the isotherm plots show a less pronounced adsorption and removal of gold from solution. This is in agreement with Au4f XPS spectra for both Series B and Series C CSCs which show the presence of Au(III) ions on the material surface after adsorption (Fig.44).

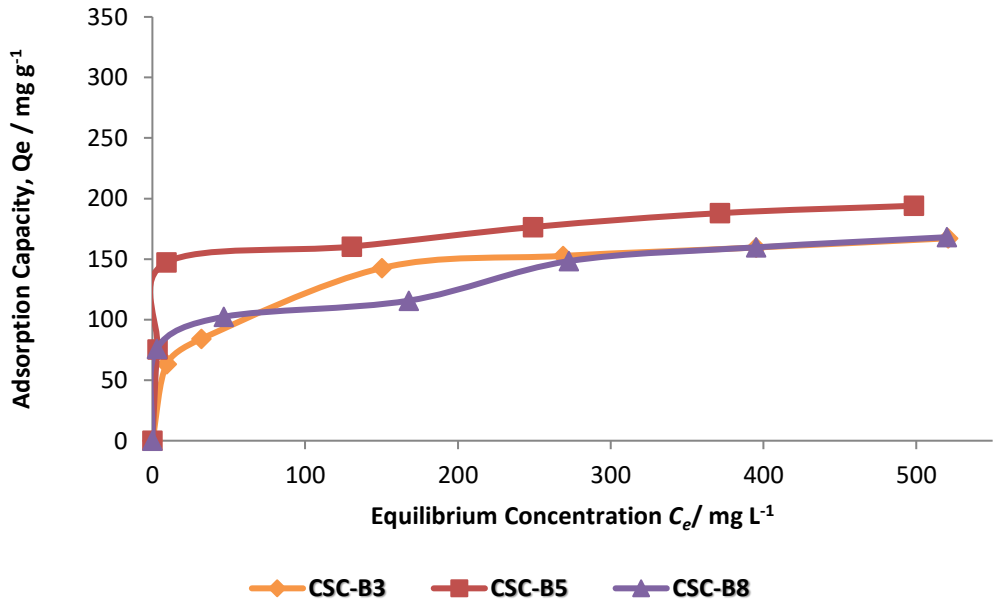

Figure 46 Isotherm plots for Series B CSCs at room temperature

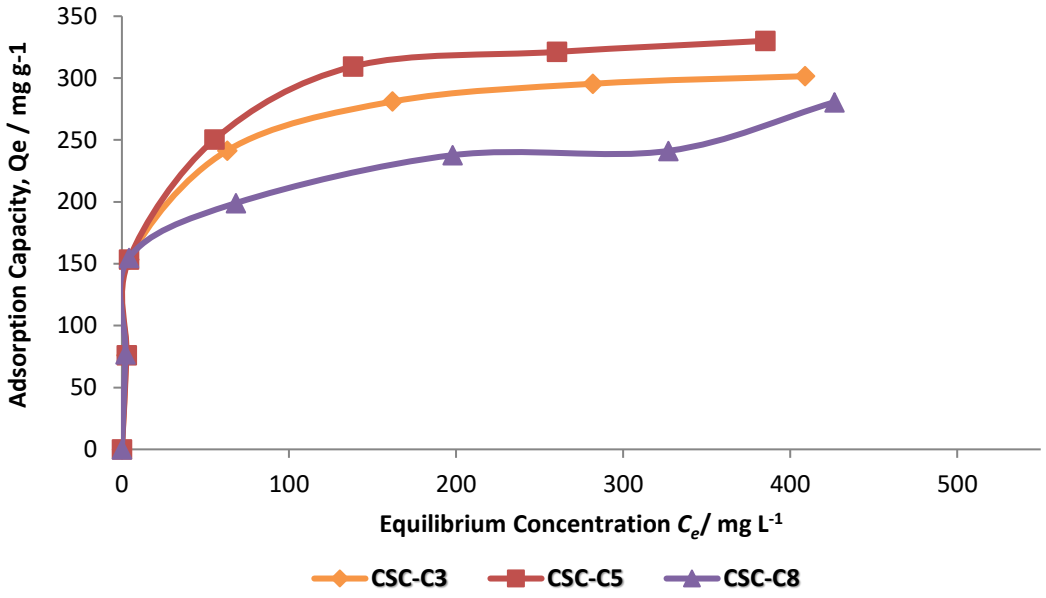

Figure 47 Isotherm plots for Series C CSCs at room temperature

Removal of gold from solution is directly associated with the total adsorption capacity, q_e, of materials. Maximum adsorption capacity values, q_e, (Table 22) demonstrate that the best adsorbent materials of both Series B and Series C are the ones carbonised at 500˚C with adsorption capacities of 194 mg g^{-1} and 330 mg g^{-1} for CSC-B5 and CSC-C5, respectively. The same observation is made for the Series A CSC produced at 500 ˚C which has an adsorption capacity of 320 mg g^{-1}. It appears, that at this temperature the carbon layer has a unique surface structure facilitating a greater extent of adsorption, mainly due to greater reduction ability.[154]

As anticipated, CSC-C5 has a higher loading capacity than CSC-B5 due to the thicker carbon layer on the surface and more oxygenated functionalities available for surface oxidation (deduced from porosimetry and XPS results discussed in Chapter 4). What is surprising though, is that CSC-C5 has a higher capacity than CSC-A5, and in general, that Series C materials perform better than Series A in the sense that they have higher adsorption capacities. The thickness of the carbon layer of Series C CSCs is slightly greater than that of corresponding Series A CSCs, even though carbon content is less. As a result, a greater surface with active sites is available for interactions, either electrostatic or chemical, during the adsorption process, rendering Series C materials with the slightly higher loading capacities than Series A and of course Series B CSCs.

The adsorption capacities of materials can be correlated with the nature of adsorption taking place at the different concentrations. Chemisorption is prominent at the low concentrations of gold, whereas reversible physisorption describes the system better at higher concentrations (in good correlation with the good fits to the Langmuir model). Enhanced chemisorption at the lower concentrations, when physisorption is always observed, allows for increased loading capacities at the range of concentrations tested.[161]

5.4 Conclusion

The two novel series of bio-derived mesoporous carbon/silica composites (Series B and Series C) have been shown to be suitable selective adsorbents for the removal of gold from a range of concentrations of acidic solutions. Mechanistically the process can proceed via 1) irreversible chemisorption, by which the surface of materials oxidises, and the gold species simultaneously reduce and 2) reversible physisorption, by which the aurochlorate anion electrostatically interacts with the surface.

CSC-B5 is the best adsorbent material produced from Series B with an adsorption capacity of 194 mg g^{-1} leading to 96% removal of gold. Series B CSCs perform exceptionally well at the low concentration regions with a greater extent of physisorption, except for CSC-B5 which interacts with the gold solution mostly through chemisorption. Comparing to Series C CSCs, the latter materials perform even better, with an adsorption capacity of 330 mg g^{-1} calculated for CSC-C5 which is the best material. Unlike, Series B CSCs, Series C CSCs undergo similar contributions of physisorption and chemisorption, suggesting that active sites for adsorption are affected by the thickness and functionality of the carbonaceous layer on the surface of materials.

The adsorption data have been successfully modelled using the Langmuir, Freundlich and D-R isotherms, with the Langmuir model giving the best fit for Series B and Series C CSCs materials (R^2 very close to unity). This suggests that monolayer adsorption takes place during the physisorption stage, yet surface heterogeneity and functionality of the six types of CSCs produced may permit multi-layer coverage or interactions that fill the mesopores.

Aside the physical and chemical properties of Series B and Series C CSCs, the concentration of solution affects the amount of gold that can be removed. It has been demonstrated that the CSCs perform better that the lower concentrations with over 90% selectivity and removal of gold, demonstrating that they are ideal for gold recovery from real-life waste (mine tailings) which contains trace amounts of the metal.

PART III

NITROGEN-DOPED CARBON/SILICA COMPOSITES:

SERIES N

Chapter 6.

Nitrogen-Doped Carbon Silica/Composites

Series N: Synthesis and Characterisation

Chapter 6.

Nitrogen-Doped Carbon Silica/Composites Series N: Synthesis and Characterisation

6.1 Introduction

Much attention is paid to the preparation of carbonaceous materials as they serve very well as electrode materials for fuel cells, capacitors and batteries, as catalyst supports, and importantly as adsorbents for separation and recovery processes.[122,128,223,224] Solely focusing on their use adsorbents, it is important that they possess the right physiochemical properties in order to be able to perform with high efficacy to separate and remove any required species, especially during liquid-phase adsorption.

Pore structure and surface chemistry play crucial roles as they can tune the properties of materials and to a large extent affect adsorption properties.[146,152] Many studies have demonstrated the ability of materials to adsorb a range of species, ranging from organic molecules to heavy and precious metals, depending the their porosity.[173,225,226] A great deal of work has been done to design mesoporous carbonaceous materials, as is the focus of this thesis, as mesoporosity remains the ideal pore size for adsorption and mass transfer.[115]

It is becoming increasingly clear though that surface functionality plays an important role as well in the applicability of asborbents.[227,228] Functionalising the surface of materials is mainly achieved by the introduction and incorporation of heteroatoms to the structure.[229] Commonly referred to as doping, the surface design of materials is tailored by chemically inserting heteroatoms which either donate or withdraw free electrons.[230] Advantages of introducing heteroatom-based functionalities into carbonaceous materials include improved metal binding, thermal stability and catalytic activity, thus extending the range of potential applications even further.[146] Examples of heteroatoms include oxygen, sulfur, boron, phosphorous and nitrogen, with nitrogen being the most commonly exploited one.[116,231]

6.1.1 Nitrogen Doping

Nitrogen is by far the most abundantly investigated heteroatom.[139,232] Being a "neighbour" of carbon, nitrogen has a comparable atomic size and its five valence electrons are available to form strong valence bonds and bring the two types of atoms together chemically.[233] The result is a plethora of nitrogen containing carbon based materials that can exhibit variable properties. Nitrogen doping can essentially create intrinsic and extrinsic defects and active sites in carbonaceous materials, thus providing the opportunity for material enhancement.[234]

The acidic character of porous carbonaceous materials, such as the newly synthesised carbon/silica composites for the research purposes of this thesis, is closely related to the oxygen-containing functionalities present on the outer surface of materials. Any basicity of materials is associated with the resonating electrons of aromatic rings present at higher synthesis temperatures. Nitrogen functionalities such as amides, imides, pyrrolic and pyridinic groups, very commonly provide basic properties, which can further improve interactions of the carbon surface.[146,235]

The interest in nitrogen-doped carbonaceous materials has been primarily focused on their use as adsorbents in industry and importantly in environmental protection. [120,127] It has been reported that the incorporation of nitrogen functionalities in the carbonaceous network, can result in porous materials with improved thermal stability, high surface areas and enhanced adsorption capacities of anionic and acidic species. The nitrogenation of porous carbonaceous materials increases the basicity of porous carbon, as previously mentioned, and allows for a co-ordination mechanism to take place during the adsorption of aqueous metal ion species. Such metal ion species include Cr^{3+}, Zn^{2+}, Pb^{2+}, Ag^{+} and Hg^{2+}, which are the cause of water contamination.[236]

Nitrogen doping can be achieved by the reaction with nitrogen-containing agents such as ammonia, nitric acid and amines, or by the activation/carbonisation of nitrogen-abundant precursors such as melamine, chitosan and urea-polymer.[237–239] The current methods utilised for nitrogen doping are divided into: 1) doping directly during the synthesis of materials (in-situ) and 2) post-treatment of already synthesised materials

with a nitrogen-containing precursor.[229,240] This thesis will focus and describe the doping of materials via the in-situ approach.

6.1.2 Urea

Urea, also known as carbamide, is a nitrogenous organic compound containing a carbonyl group attached to two amine groups with the chemical formula $CO(NH_2)_2$.[241] It serves a major role in the metabolism of nitrogen-containing compounds by animals and is the major organic component of mammal urine. It was first discovered and isolated by H.M. Rouelle in 1773 and was then successfully synthesised by F. Wohler in 1828.[242]

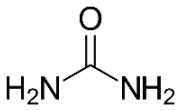

Figure 48 Structure of urea

Urea presents an interesting candidate as a doping agent because of its high nitrogen content, low cost, in addition to being an environmentally friendly raw material [234,239] According to literature reports, urea has been used to produce nitrogen-doped materials that are subsequently used as wood adhesives,[243] electrode materials for supercapacitors and lithium ion batteries,[223,239]adsorbents for CO_2 and NO_2 gases,[244,245] and adsorbents for heavy metals like Cd^{2+} and Ni^{2+}.[246,247]

Being rich in nitrogen content (can result in materials with % N content between 5-8%)[234], urea can be used as doping agent to synthesise nitrogen-containing carbonaceous materials to use as absorbents for precious metals like gold, as proposed in this thesis.

6.2 Aims

The overall objective of this chapter is to provide a qualitative and quantitative analysis the newly developed Series N CSCs, prior to their use in gold removal.

The aims of the work presented herein:

- To investigate the influence of carbonisation temperature on the physiochemical properties of the Series N CSCs.

6.3 Results and Discussion

6.3.1 Preparation of Series N

The bio-oil (BO-C) used for the synthesis of the composite materials is obtained from the microwave-assisted pyrolysis of waste office paper and is the same used for the synthesis of Series C CSCs.

The typical method of preparation consists of four main stages:

1. Milled waste office paper pressed into blocks
2. Microwave-assisted pyrolysis of blocks to collect bio-oil
3. Wet impregnation of bio-oil into silica framework in the presence of urea (ratio 1:1:1)
4. Carbonisation at different temperatures (300˚C, 500˚C, 800˚C) under nitrogen atmosphere.

6.3.2 Physical and Chemical Properties of Series N CSCs

The synthetic conditions and method to produce Series N adsorbents are identical to those followed to produce all previous series of CSCs discussed in this thesis and are fully described in Section 8.1.2.3 (Chapter 8). The three types of nitrogen-doped carbon/silica composites synthesised for this work, are described in Table 23, along with the abbreviated name that will be used throughout this thesis.

Table 22 Material description and abbreviation

Starting Material	Carbonisation Temperature (K and ˚C)	Abbreviation
BO-C, Silica K60 and Urea	573 / 300	CSC-N3
BO-C, Silica K60 and Urea	773 / 500	CSC-N5
BO-C, Silica K60 and Urea	1073 / 800	CSC-N8

Nitrogen adsorption/desorption porosimetry is used to provide quantitative analysis of the textural properties of Series N CSCs. Characterisation of the isotherms obtained from the analysis illustrates type IV isotherm profiles with H2 hysteresis loop classification (Fig.50), as also observed for all other series of materials produced. The type IV isotherm profile indicates that the nitrogen-doped materials are mesoporous, too. The observed H2-type hysteresis loop associated with the gradual capillary condensation is further confirming the mesoporosity of Series N materials and reveals that they have a broader pore size distribution or non-uniform pore structures. The desorption branch is caused by pore-blocking in the necks of the pores, but since a broader pore size distribution is observed for Series N CSCs, the decrease in the desorption branch is gradual as the pore necks vary over a wider range.[216] The open hysteresis loop for observed for CSC-N5 suggests that a proportion of mesopores may be collapsing, while the very steep and incomplete desorption branch observed for CSC-N8 suggests that the necks of pores may be blocked due to evaporation induced by cavitation.

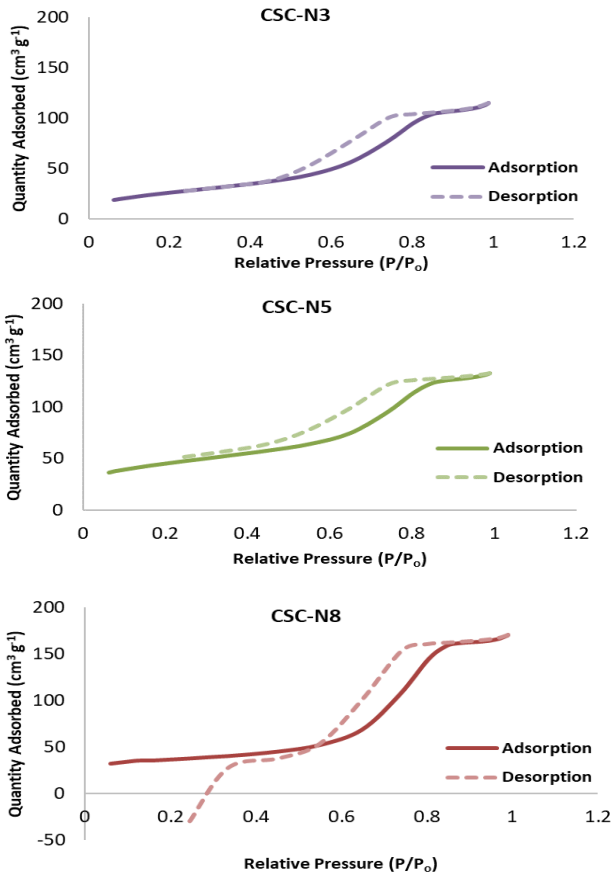

Figure 49 Nitrogen adsorption isotherms for CSC-N3, CSC-N5 and CSC-N8

A summary of material properties is given in Table 24. BET surface area, pore volume and pore diameter of materials produced at 300 ˚C and 500 ˚C are lower than the parent silica due to the introduction of carbon and nitrogen onto the silica surface and within the pores. As adsorption isotherms and hysteresis loops are similar, it can be deduced that that the introduction of organic matter into the silica pores as well as nitrogen doping do not affect mesoporosity significantly.[154,237]

Table 23 Textural properties of Silica K60 and Series N CSCs from porosimetry

Material	BET surface area ($mg^2\ g^{-1}$)	Pore volume ($cm^3\ g^{-1}$)	Pore diameter (nm)	Carbon layer thickness (nm)
Silica K60	467	0.80	6.7	-
CSC-N3	98	0.18	5.6	0.55
CSC-N5	162	0.18	5.3	0.70
CSC-N8	128	0.27	5.4	0.65

At 300 ˚C there is significant reduction in pore volume from 0.80 $cm^3\ g^{-1}$ in Silica K60 to 0.18 $cm^3\ g^{-1}$ in CSC-N3. This reduction demonstrates that the polymerised bio-oil in each case is well distributed within the mesopores, in addition to the presence of urea occupying extra space on the material's surface.[248] As the carbonisation temperature increases to 500 ˚C , there is a slight increase in BET surface area, pore volume and diameter, due to the carbon layer shrinking within the pores.[217] Unlike the other series of CSCs discussed in previous chapters, Series N materials all exhibit considerably lower surface areas and smaller pore volumes as anticipated, due to the presence of the heteroatom flowing through the pores of the materials.[249]

Nonetheless, these increases suggest the loss of some carbon from within the pores and a subsequent formation of a more porous carbon layer on the silica surface. The loss of carbon is associated with the decomposition of bio-oil in each material and is consistent with the rapid release of gases (CO_2, CO and H_2O) that occurs as the carbonisation temperature increases from 500 ˚C to 800 ˚C (Fig.55) This decomposition leads to the formation of aromatic porous carbon on the surface, and as a result surface area increase from 98 $mg^2\ g^{-1}$ to 162 $mg^2\ g^{-1}$ for CSC-N3 and CSC-

N5, respectively (Table 24). On the other hand, CSC-N8 shows a decrease in surface (128 mg^2 g^{-1}) area as carbonisation temperature increases from 500 ˚C to 800 ˚C, suggesting that a portion of the larger and less stable mesopores may be shrinking or collapsing, or very likely being affected by the presence of nitrogen.

Thickness of the carbon layer, as calculated by porosimetry data, is shown to increase for CSC-N5 and then decrease for CSC-N8. Based on findings from previous chapters, it is expected that the thickness of the carbon layer will decrease relative to the carbonisation temperature, but the presence of urea seems to be affecting the surface. It may be that at 500 ˚C, urea interacts in such a way with the bio-oil that allows for more carbon deposition and thus creating a thicker carbonaceous layer.

SEM images and SEM-EDX data are obtained Series N materials to help demonstrate the textural properties of materials upon carbonisation and confirm the presence of nitrogen on the surface.

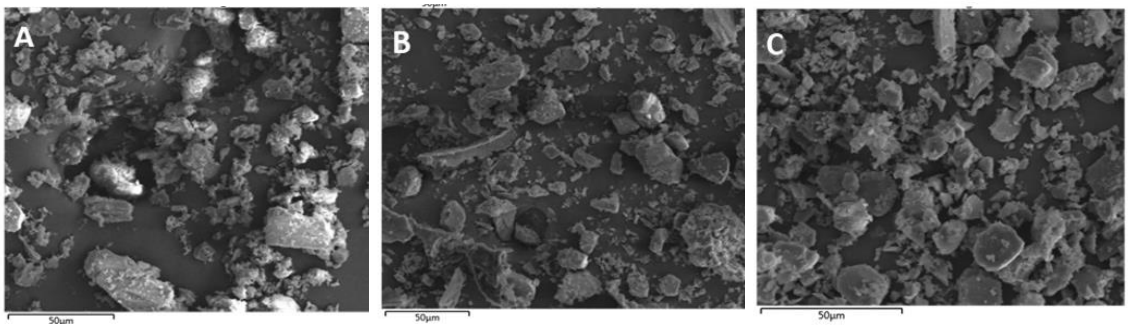

Figure 50 SEM-FIB images of A) CSC-N3, B) CSC-N5 and C) CSC-N8

It is evident in all SEM images (Fig. 51) that the materials have a variation in size and distribution in particles. Series N materials exhibit a similar pattern to Series A and Series C materials; they consist of a combination of smaller and larger particles, with a significant proportion of the smaller particles. As previously proposed, one plausible explanation for these observations may be the mechanical grinding of the CSCs.[154] During the preparation of Series C materials, the abrasive forces induced by the magnetic stirrer bar and the round bottom flask may cause fracturing of some silica and urea particles in the materials leading to the formation of smaller particles. Another possible reason may be the formation of porous char as the carbonisation temperature increases from

300˚C to 800˚C, due to the rapid release of gases upon increasing carbonisation temperature, as suggested by thermal analysis results (Fig.55). The rapid release of gases may be accompanied with the formation of porous carbon particles on the surface, which may appear as the smaller and rougher particles observed in the SEM images of Series N CSCs.

SEM-EDX data (Fig. 52-54) demonstrate that doping of the materials with nitrogen is successful at all carbonisation temperatures, with CSC-N3, CSC-N5 and CSC-N8 possessing 15.0 %, 17.2% and 13.6% nitrogen on their surface. It is also evident from this set of data that there is significant coverage of carbon on the surface of materials, with CSC-N5 having the most carbon detected (Fig. 52E). This is well in agreement with the carbon layer thickness calculated (Table 24), confirming synthesis of the nitrogen-doped CSCs at 500˚C allows for more carbon coverage of the surface. A significant coverage of oxygen is observed as well, which is consistent with XPS and IR data that demonstrate the presence of oxygen containing species, especially for CSC-N3 and CSC-N5. The amount of % Si detected suggests that the silica surface has not been fully coated with the carbon layer and, thus, part of the silica has remained exposed after carbonisation.

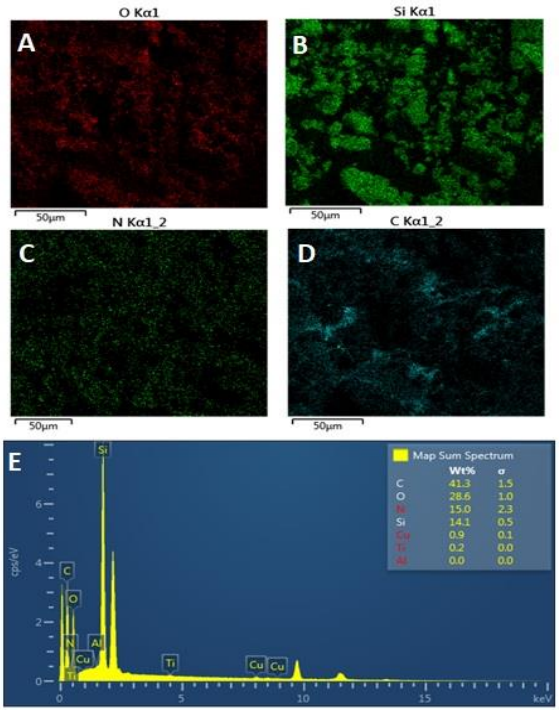

Figure 51 EDX mapping of A) Oxygen, B) Silicon, C) Nitrogen, D) Carbon and E) Chemical composition spectrum of CSC-N3

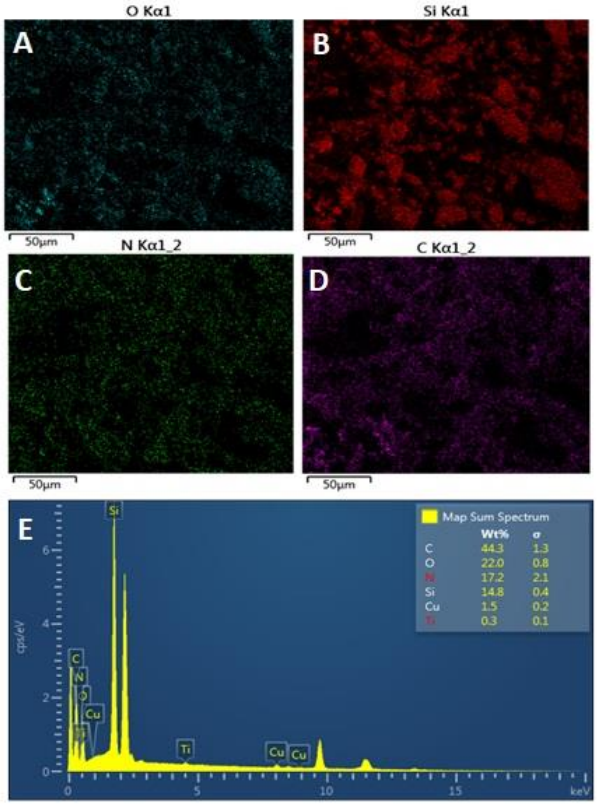

Figure 52 EDX mapping of A) Oxygen, B) Silicon, C) Nitrogen, D) Carbon and E) Chemical composition spectrum of CSC-N5

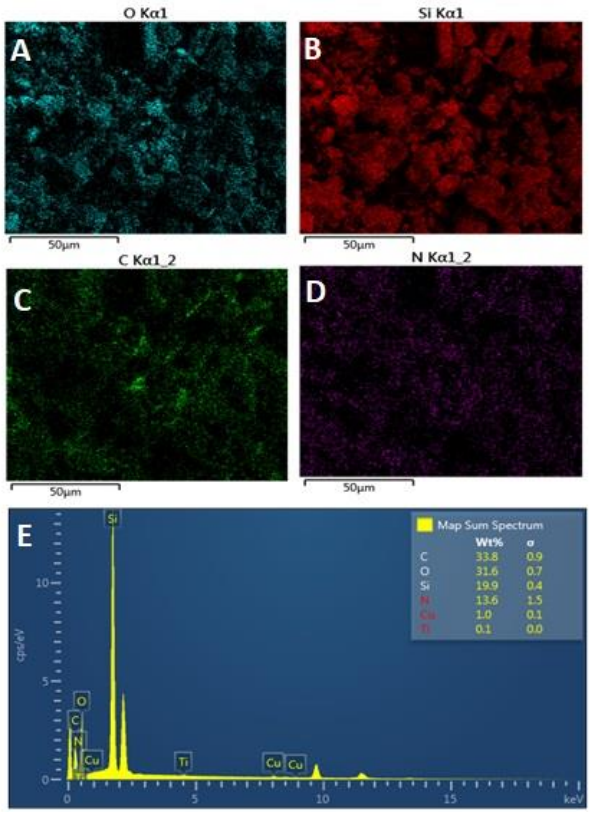

Figure 53 EDX mapping of A) Oxygen, B) Silicon, C) Nitrogen, D) Carbon and E) Chemical composition spectrum of CSC-N8

The TG-IR spectrum of the uncarbonised sample of Series N (Fig.55) is illustrated below.

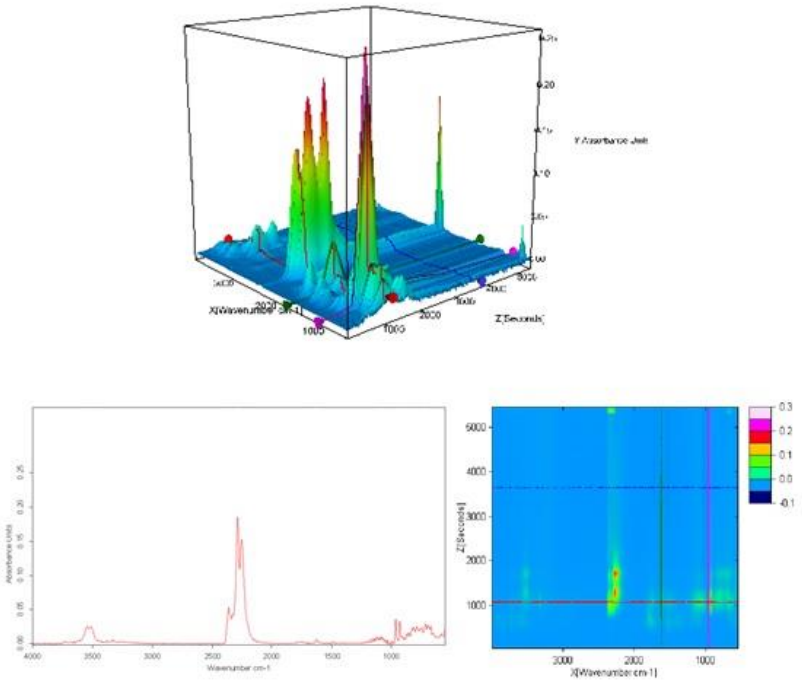

Figure 54 3D TG-IR spectrum of the off-gases from the thermal treatment of the uncarbonised sample used for Series N

The TG-IR spectrum (Fig. 55) of the uncarbonised samples of Series N shows the following peaks:

- Major peak located at 3509 cm^{-1} is mainly attributed N-H vibrations due to the presence of ammonia (ammonia is a decomposition product of urea)[250] and may also be assigned to -CH stretching vibrations, indicating the presence of –CH, $–CH_2$ or $–CH_3$ groups.
- Major peak located at 2388 cm^{-1} is attributed to the vibrations of CO_2, compared to the standard IR spectrum of carbon dioxide. Peaks following at 2264 cm^{-1} and 2251 cm^{-1} can be assigned to $H_2NC{=}N$ and HNCO, respectively, as they are decomposition products of urea.[251]
- Peak at 1811 cm^{-1} may be attributed to the carbonyl group associated with anhydrides, suggesting that these groups were released at this temperature.
- Peak located at 1084 cm^{-1} may be assigned to C-O-C groups, possible due to the decomposition product from saccharides.

- Peaks located at 1058 cm^{-1} and 977 cm^{-1} may be attributed to ammelide and cyanuric acid, respectively, as they are decomposition products of urea.[251]

The spectrum is taken at the maximum decomposition of the uncarbonised material and shows the evolution of gases including CO_2, H_2O and NH_3.[145,154,252] In terms of mass loss relevant to temperature, the following are observed for the uncarbonised sample of Series N:

- Around 100 ˚C, most of the moisture content present from the bio-oil and parent silica is lost.
- Up to 190 ˚C the urea in the mixture undergoes vaporisation and decomposition to produce ammonia and cyanic acid, followed by the reaction of the remainder of urea in the system and the cyanic acid formed to produce biuret (approximately at 160 ˚C).
- Between 180 ˚C and 230 ˚C, the system undergoes elimination reactions and saccharide decomposition, leading to the elimination of volatile acids.
- Between 300 ˚C and 450 ˚C, most of the oxygenated compounds and aliphatic chains undergo decomposition. Additionally, up to 300 ˚C the biuret and cyanic acid present react to produce cyanuric acid and more ammonia.[253] The cyanic acid and urea further react to produce ammelide and water. Within this range, any residual cyanuric acid and ammelide undergo sublimation and decomposition.
- Above 550 ˚C, condensation of the silanol groups of the parent silica begins and the decomposition of aliphatic chains is complete, allowing for aromatisation at higher temperatures. Within this temperature range, CO_2 is given off, too, further establishing the additional porosity of the materials indicated by porosimetry results.

These observations are proof that the nitrogen-doped CSCs produced have tuneable structural and textural properties as the carbonisation temperature during their synthesis increases.

DRIFT spectra of Series N CSCs (Fig. 56) illustrate a similar shift in functional character as expected and observed in all other series of CSCs produced; with increasing carbonisation temperature organic matter decomposes changing the functional

groups present, shifting from an aliphatic and polar oxygenated coated surface to a more aromatic carbon layer. [154] Notably though, IR spectra illustrate the presence of nitrogen-containing functionalities, further confirming the successful incorporation of nitrogen into the materials' matrix.

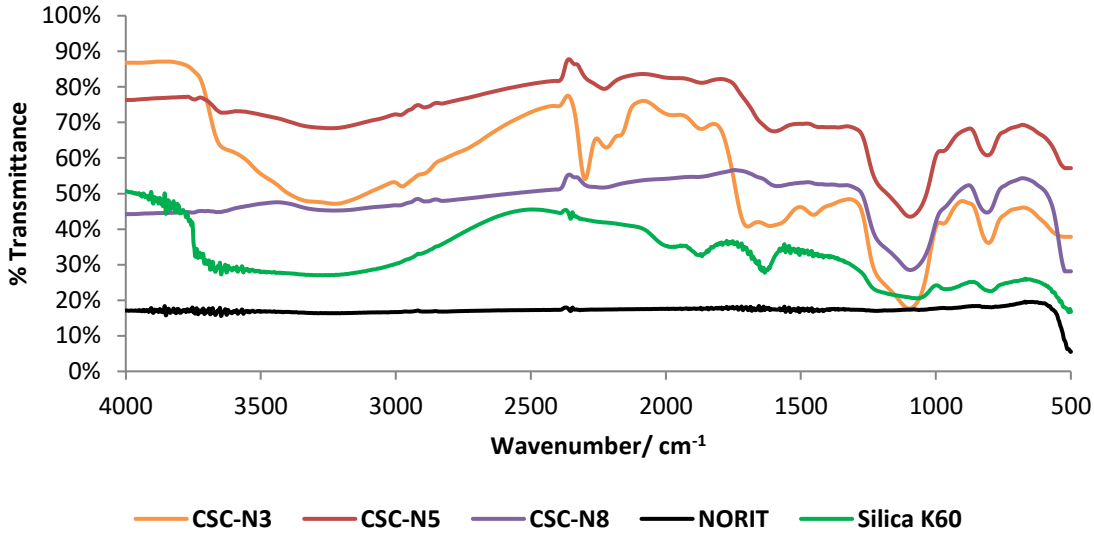

Figure 55 Overlapped DRIFT spectra of CSC-N3, CSC-N5, CSC-N8, NORIT activated carbon and Silica K60

Aliphatic C-H stretching of -CH_2 and -CH_3 observed around 2900 cm^{-1} and C=O stretching at 1633 cm^{-1} are due to the presence of oxygenated compounds like carboxylic acids, ketones, aldehydes and esters, originating from the original components of the bio-oils.[152,153] The peak at around 1690 cm^{-1} may be due C=O stretching and N-H bending motions due to the presence of amides as a result of urea doping.[241,254] These peaks, as well as the O-H stretch at 3364 cm^{-1}, are evident in the spectra of CSC-N3 and CSC-N5 as expected, but weaken and disappear as temperature increases to 500˚C and 800˚C. The hydroxyl group is reduced significantly due to the crosslinking effect of silica. One may also argue that the broad band observed between 3300 cm^{-1} and 3500 cm^{-1} may have contributions of N-H stretching modes.[255] Above 500˚C, bands representing C=O, C-H and O-H bands gradually weaken, being indicative of thermal decomposition taking place and reducing the amount of oxygenated compounds on the surface, leaving a more aromatic surface at 800˚C. The peak observed around 1440 cm^{-1} for CSC-N3 and CSC-N5 may be attributed to bending vibrations of -CH_2-N, resulting from the presence of amine groups as a result of urea

decomposition. The peak situated around 1080 cm^{-1} in all nitrogen-doped CSCs spectra, is indicative of C-O stretching motions of acid functionalities. Spectra for all Series N show stretching bands around 1081 cm^{-1} and 802 cm^{-1} corresponding to Si-O-Si bonds, confirming the presence of the silica substrate in the composite materials and the changes on the carbonaceous part of the structure.[152] The peaks mentioned so far confirm the shift in functionality of the materials from hydroxyl and carbonyl rich surface at 300 ˚C to carbonaceous aromatic surfaces at 800 ˚C .[152,154] Surprsinlgy, two peaks are observed at 2221 cm^{-1} and 2225 cm^{-1} in the CSC-N3 and CSC-N5 spectra respectively, suggesting nitrile formation. A similar observation is made by *J. Attard et al*, who prepared nitrogen-doped Starbons® chitosan and ammonia.[237] The nitrile formed may be a result of either the reaction of amines present with the ammonia produced during the decomposition of urea or the catalytic dehydrogenation of amines to nitriles due to the acidic environment created by the close proximity of hydroxyl groups.

The C, O, Si and N elemental surface content of the Series N CSCs is measured by XPS.

Table 24 % Atomic content deduced from Carbon XPS spectra of C1s for Series N CSCs

	% Atomic Content			
	C	Si	O	N
CSC-N3	27.6	18.4	44.8	6.0
CSC-N5	31.9	18.5	45.1	4.5
CSC-N8	15.9	24.5	58.1	1.5

XPS data show that with increasing carbonisation temperature, the % C content on the surface increases, except for CSC-N8, with an observed increase in % O and % Si, as well (Table 25). Results also confirm the presence of nitrogen on the surface of materials and are in good correlation with results from SEM-EDX mapping discussed earlier.

Based on C1s spectra deconvolution for Series N materials (Fig.57), oxygenated carbon functionalities decompose with increasing temperature, showing an increase in aromatic character and loss of hydrophilic and aliphatic compounds containing oxygen. Oxygen is still substantially present at all temperatures,

along with silicon, confirming the presence the parent silica. The presence of oxygen facilitates the interaction between the polymerised bio-oil and the silanol groups in the parent silica, giving rise to the C-O-Si bond.[154] The presence of silicon and oxygen may further indicate that parts of the material surface are not coated by the carbon film created during carbonisation, as suggested by SEM-EDX mapping spectra of materials, previously discussed. These exposed silica section will very likely affect the adsorption process and overall gold removal discussed in the following chapter, as they will not provide any active sites for adsorption.

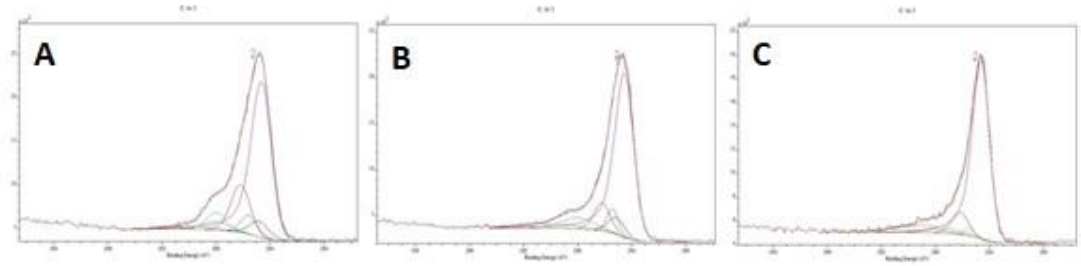

Figure 56 Carbon XPS Spectra of C1s (A) CSC-N3, (B) CSC-N5 and (C) CSC-N8

Every type of bond appears at a specific binding energy which allows for identification of different functional groups through deconvolution of the main peaks. C1s peaks of the spectra are deconvoluted and assigned giving rise to the following contributions: [116,155,156]

- 284.4 eV due to C=C groups (aromatic, sp^2 hybridised),
- 285.6 eV due to C–C groups (aliphatic, sp^3 hybridised),
- Peak overlap at 286.2 eV due to C –O groups (alcohols and ethers) and nitriles,[245]
- 287.9 eV due to C=O groups (ketones and amides),[237]
- 289.2 eV due to C=O groups (anhydrides, esters, ketones).[255,256]

N1s spectra deconvolutions for Series N materials are shown below (Fig.58).

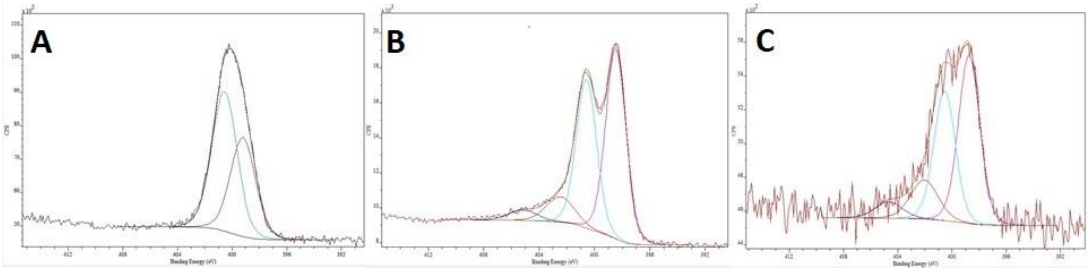

Figure 57 Nitrogen XPS Spectra of N1s (A) CSC-N3, (B) CSC-N5 and (C) CSC-N8

The following contributions can be assigned according to literature:[233,239,257]

- For CSC-N3 the peak at 399.2 eV can be attributed to secondary amines linked to aromatic structures and the peak at 400.2 eV can be assigned to amides and the presence of nitriles.
- For CSC-N5 the peak at 398.5 eV can be attributed to imines and pyridinic nitrogen, the peak at 400.3 eV can be attributed to amides and the presence of nitriles and the peaks at 402.6 eV and 404.8 eV can be assigned to oxidised pyridinic nitrogen.
- For CSC-N8 the peak at 398.7 eV can be attributed to imines and pyridinic nitrogen, the peak at 401.3 eV can be attributed to graphitic and quaternary nitrogen and the peaks at 402.2 eV and 404.6 eV can be assigned to oxidised pyridinic nitrogen.

XPS and DRIFT data are in good correlation, confirming the shift from aliphatic and polar hydroxyl character to aromatic character with increasing carbonisation temperature, in addition to providing further proof of nitrogen-containing functionalities on the surface of the doped materials.

CHN analysis (Table 26), indicates that carbon content slightly decreases with increasing carbonisation temperature, exhibiting that the nitrogen-doped CSCs have similar amounts of carbon throughout their bulk, with carbon concertation significantly differing on the surface of materials. Nitrogen content throughout the bulk of materials appears to be decreasing with carbonisation temperature, which further corroborates the trend observed by XPS results; reduction of bulk nitrogen content affects the relative nitrogen on the surface if materials. Based on CHN analysis, decrease in w/w% O or w/w% Si contents cannot be measured quantitatively, as they are not differentiated and are both accounted for in the rest bulk content value.

Table 25 % Elemental composition of Series N CSCs

	w/w % Elemental composition			
	C	H	N	Rest
CSC-N3	21.5	1.7	6.8	70.0
CSC-N5	20.1	1.2	5.4	73.3
CSC-N8	19.9	0.7	4.1	75.3

6.4 Conclusion

A novel series of nitrogen-doped bio-derived mesoporous carbon/silica composites (Series N) has been successfully prepared from bio-oil, obtained from the microwave-assisted pyrolysis of waste office paper, commercially available Silica K60 gel and urea. This series of materials possesses tuneable surface chemistry and textural properties, which are obtained by varying the carbonisation temperature during their synthesis and the addition of doping agent rich in nitrogen. At low temperatures the materials are rich in oxygen functionalities (CSC-N3), and as the temperature increases the materials begin to lose their aliphatic and polar character becoming more aromatic (CSC-N8); a general trend observed for all Series A, B and C of composite materials.

Interestingly, the incorporation of nitrogen into the matrix of the composite materials enabled the presence of additional functionalities, which in turn affect the porous structure and surface chemistry of materials. BET specific surface areas and pore volumes are lower when compared to composite materials of the other series, suggesting that nitrogen flows through the pores and potentially blocks them along with the polymerised bio-oil. Surface analysis, like IR spectroscopy, SEM-EDX and XPS, beautifully demonstrate the presence of nitrogen functionalities on the surface of materials, with the unexpected formation of nitriles.

Seeing as how, the adsorption behaviour of materials is affected by the surface functionalities and the carbon film, this series of materials produced is expected to present interesting and exciting results. The introduction of nitrogen moieties onto the surface intrinsically modifies the propertied of the carbon film, and as a result the performance of nitrogen-doped materials during adsorption will very likely be affected. The following chapter will test the adsorption ability of Series N carbon/silica composites in order to capture gold from solution.

Chapter 7.

Carbon Silica/Composites Series N: Application in Gold Adsorption

Chapter 7.

Carbon/Silica Composites Series N: Application in Gold Adsorption

7.1 Introduction

The development of Series A, B and C of composite materials and their application in gold adsorption has presented exciting results, creating the need to take the development of materials a step further. Doping of materials with nitrogen is a promising method to allow for the synthesis of materials with enhanced adsorption capacities of anionic species, and thus making them viable candidates for the removal of gold during liquid phase adsorption.

Findings from Chapter 5 show that the production of nitrogen-doped composite materials (Series N), is viable via the use of urea; a precursor rich in nitrogen that enables the formation of more functionalities that may facilitate adsorption. Characterisation of Series N materials exhibits interesting physiochemical properties, and therefore their application in gold adsorption is anticipated to present equally exciting results.

7.2 Aims

The overall objective of this chapter is to provide a full assessment on the performance of the newly synthesised nitrogen-doped Series N composite materials as adsorbents for the removal of gold from acidic solutions.

The aims of the work presented herein:

- To investigate the influence that the physiochemical properties of the Series N composite materials have on adsorption.
- To propose the possible adsorption mechanism on the surface of the N composite materials.

7.3 Results and Discussion

7.3.1 Mechanism of Gold Adsorption

The mechanism for gold adsorption, as previously mentioned, usually involves two processes: 1) the chemisorption process (irreversible process), during which Au(III) species are reduced mainly to elemental gold Au(0), and 2) the traditional physisorption (reversible process). The carbonaceous surface of CSCs has been shown to have a high affinity for Au(III), due to the high standard electrode reduction potential, E^o ($[AuCl_4]^{-1}$/ Au^0= 1.00V), and the similarly high reduction potential, E^o ($[AuCl_4]^{-1}$/ $[AuCl_2]^{-1}$= 0.93V) for the reduction to Au(I) ion, via the reduction-adsorption mechanism.[28,107,161] This mechanism allows for the creation of vacancies on the surface of the material as the reduced species deposit, which leads to higher uptake of the metal from solution and increased adsorption capacity.[162]

Nonetheless, the system undergoes physisorption as well, which involves electrostatic interactions between the adsorbate species in solution and the adsorbent's surface.[163,258] During physisorption, a thin film of the adsorbate is created on the surface of the material, which can facilitate diffusion through the layer and into the pores of the materials.[160] Where physisorption dominates, the film created serves as a monolayer and it prevents the irreversible reduction of Au(III). As a result, the formation of the monolayer hinders the species from undergoing a chemical reaction with the surface of the material, filling up all active adsorption sites and reducing the creation of new vacancies for chemisorption to occur.

Surface chemistry of materials, as demonstrated in previous chapters, plays a vital role in the mechanism of adsorption. It has been shown that owing to the materials oxygen-containing functionalities (carbonyl, carboxyl, hydroxyl groups), originating from the bio-oil, present on the carbonaceous surface, supported by XPS and DRIFT data, the system will proceed via chemisorption; reduction of the gold species with simultaneous oxidation of the protonated carbonaceous surface. Adsorption, though, in the case of Series N CSCs proceeds predominantly via physisorption (Fig.59), suggesting that a smaller proportion of surface groups are participating in chemical reactions. The introduction of nitrogen-containing functionalities into the matrix of

materials, increases basicity of the surface, thus increasing overall negative charge of the surface. Chemisorption is facilitated by the interaction and reaction of the anionic species of gold in solution and reducing surface functionalities; if the nitrogen-doped surface has now a greater net negative charge, then a redox becomes less likely and the extent of irreversible chemisorption is reduced.

The presence of amine functionalities, as indicated by IR and XPS data, can cause protonation of the surface of materials in acidic pH, and as a result this induced positive charge is capable of electrostatically binding the aurochlorate anion. Protonation reduces the ability of materials for a chemical reaction with the gold species, favouring electrostatic interactions and a greater extent of reversible physisorption.[22] Even though Series N CSCs are abundant in oxygen-containing groups, electron transfers for chemical bonding are not so favourable. The surface of materials, as shown by XPS, contains aromatic carbons and nitrogen functionalities, which attribute to electron-rich regions on the carbonaceous layer of the surface, creating a partial negative charge on it.[221,222] Since, the gold species in solution exists as anion, if the surface holds an overall partial negative charge by the resonating electrons of the aromatic rings and π bonds and the nitrogen lone pairs,[155] then it may be assumed that the adsorbent surface and adsorbate will repel each other. Repulsion may not be strong enough or permanent, but it could offer an explanation as to why chemisorption occurs at a lesser degree during the process with Series N materials. On that account, physisorption should be hindered too, but as the basic and acidic nature of materials compete during the process, the boundary layer of the adsorbate $[AuCl_4]^{-1}$ species forms allowing for monolayer coverage, dominated by physisorption in this occasion.

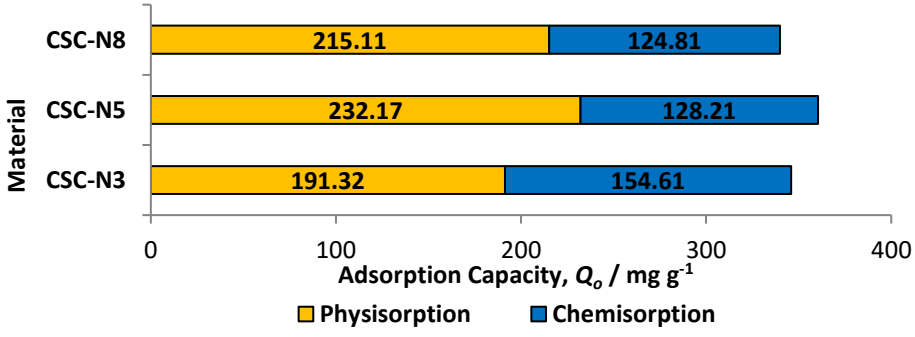

Figure 58 Nature of adsorption for all Series N CSCs

Transmission Electron Microscopy (TEM) images of Series N (Fig.60) obtained after adsorption show the formation of gold nanoparticles (AuNPs), and are in good correlation with XPS data, confirming that Au(III) ions have been reduced to metallic gold Au(0) during the chemisorption step. While the presence of nanoparticles is evident in TEM images of CSC-N5 and CSC-N8 after adsorption (Fig.60B&C), the TEM image for CSC-N3 after adsorption (Fig.60A) does not illustrate distinguishable nanoparticles. XPS data confirm the reduction of Au(III) to Au(0) when CSC-N3 is used, so it can be hypothesised that AuNPs have agglomerated and formed clusters, thus making it difficult to identify separate nanoparticles.

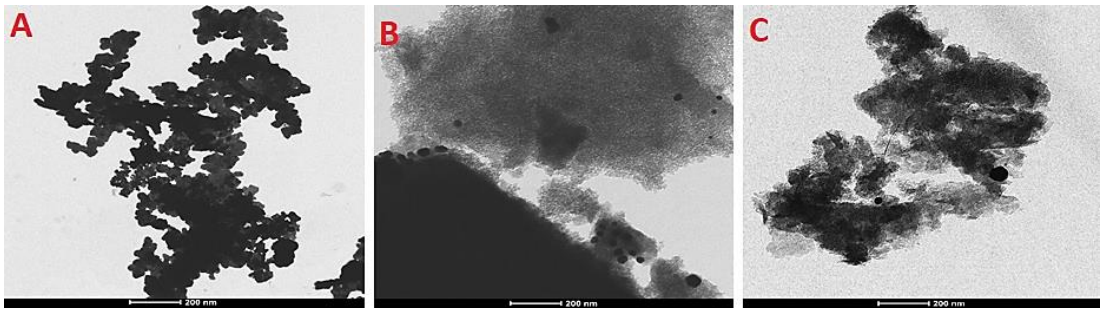

Figure 59 TEM images showing AuNPs formation after adsorption in (A) CSC-N3, (B) CSC-N5, (C) CSC-N8 at 200nm scale

XPS results (Fig.61) clearly showed the presence of gold at the materials' surface. The Au4f spectra can be deconvoluted into three sets of doublets, in which the two peaks within the doublet are 3.7 eV apart with 4:3 relative intensity for the 7/2 and 5/2 orbits, respectively. The main doublet is located at 84.6 eV (7/2) and it represents Au(0), confirming the reduction of $[AuCl_4]^{-1}$. The other two doubles at 86.1 eV and 86.6 eV correspond to the binding energies of Au(I) and Au(III), respectively.

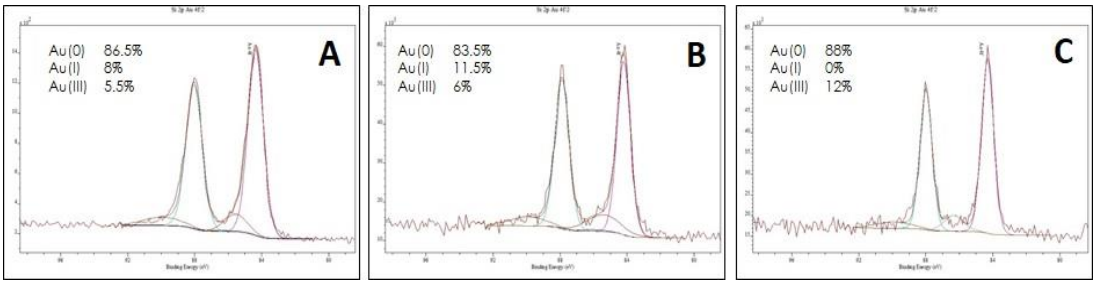

Figure 60 Au4f XPS spectra for (A) CSC-N3, (B) CSC-N5, (C) CSC-N8

Data from the deconvolution of the Au4f XPS spectra (Fig.61) indicate that the gold is greatly reduced from Au(III) to Au(0), with a small proportion of it reduced to Au(I).

This reduction to Au(0) is well in agreement with the TEM images (Fig.60), which illustrate nanoparticle formation due to gold reduction. While Series N materials proceed mainly via physisorption during the adsorption experiments, XPS data support that gold is mostly being reduced. One plausible explanation for this observation may arise from the fact that XPS investigates only the upper layer of the surface (10nm), whereas phase transfer occurs at all accessible layers and pores of materials that may be beneath the 10nm depth. As a result, materials can still favour the physisorption mechanism throughout their bulk, with the main interactions on the surface attributed to an irreversible chemical reaction.

The reduction of gold ions is accompanied by the simultaneous oxidation of the surface of CSCs. There are several functional groups present on the surface of materials, especially those carbonised at 300 ˚C and 500 ˚C, that can oxidise (i.e. hydroxyl and carbonyl groups) when reacting with the gold species. The following hypotheses that apply for all other series of materials produced can be used to explain the redox mechanism occurring in this instance as well:

- Oxidation of hydroxyl groups to carbonyl groups: Literature describes that during the process the $[AuCl_4]^{-1}$ is initially adsorbed onto the surface by forming a chelating complex with the oxygen atoms of hydroxyl groups. The hydroxyl groups are then oxidised to ketones, leading to a decrease in the concentration of O-H groups and an increase in the concentration of C=O groups.
- Decomposition of the carbon surface: Oxidation of carboxylic groups to produce CO_2, is accompanied by decomposition of the surface, thus inducing an increase in the C/O ratio after adsorption.

Elemental analysis carried out by XPS shows higher C/O ratios (Table 27) for Series N materials, suggests that the surface may be decomposing while at the same time oxidising, thus confirming the chemisorption-reduction mechanism.

Table 26 Comparison of CSC C/O ratio before and after adsorption of gold

	C/O ratio		
Material	Before adsorption	After adsorption	Variation
CSC-B3	0.6	0.5	- 0.1
CSC-B5	0.7	0.9	+ 0.2
CSC-B8	0.2	0.5	+ 0.3

7.3.2 Gold Adsorption Isotherms

In order to further investigate the mechanism of gold adsorption onto the new class of nitrogen-doped CSCs, three models are applied; the Langmuir model, the Freundlich model and the Dubinin-Radushkevich (D-R) model. Isotherm parameters are calculated using the linear form of the isotherm equations. All parameters and correlation coefficient (R^2) are summarised in Table 28.

Model fittings are done for the part of adsorption represented by physisorption, where the system is not irreversible. Fitting to all three adsorption models shows that the materials had better correlation to the Langmuir type adsorption with R^2 values over 0.99 for all nitrogen-doped CSCs (Table 28). The monolayer adsorption capacities calculated by Q_0, are in good agreement with the adsorption capacities obtained experimentally. Even though the actual maximum capacities, experimental q_e, for all materials are lower than the calculated Q_o values as per the Langmuir model, the difference between them is reasonable and can be accounted for by the different modes of adsorption in the system. As mentioned, adsorption of gold in an aqueous system occurs via both reversible physisorption and irreversible chemisorption. Q_o values calculated from the Langmuir model account for the part of the system progressing via physisorption; the small difference between Q_o and q_e values (Table 28) is indicative of the favourable physisorption during the tests.[172]

Even though Series N CSCs have a better fit to the Langmuir model, which assumes monolayer coverage of adsorption sites, the materials illustrate a good fit to the Freundlich model, too. For instance, CSC-N5 and CSC-N8 show a good fit to the Freundlich model (R^2 values 0.94 and 0.93, respectively) which suggests multi-layer adsorption dependent on the material's surface chemistry.[173] The nitrogen-doped

materials fit well with this model as well, as they are proven to have surface heterogeneity due to the incorporation of nitrogen and the general functionalisation of the surface during carbonisation, which means that adsorption could be multi-layer or accompanied with pore filling, and not limited to monolayer coverage.

Table 27 Isotherm modelling parameters for Series N CSCs

Isotherm parameters	CSC-N3	CSC-N5	CSC-N8
q_e (mg g^{-1})	345.93	360.38	339.92
Langmuir			
α_L (L mg^{-1})	0.11	0.13	0.12
K_L (L g^{-1})	38.61	43.31	42.74
Q_o (mg g^{-1})	357.14	370.37	344.83
R^2	0.9999	0.9995	0.9977
Freundlich			
Kf	79.18	90.09	8305
n	3.62	3.87	3.82
R^2	0.9007	0.9387	0.9349
D-R			
q_m (mol g^{-1})	285.09	283.72	267.90
K' x10^{-6} (mol^2 J^{-2})	1.00	0.60	0.60
E (kJ mol^{-1})	0.70	0.91	0.91
R^2	0.8456	0.7749	0.7157

7.3.3 Effect of Gold Concentration on Adsorption Capacity

ICP-OES analysis is used to determine the adsorption capacity and % gold removal for all Series N CSCs at room temperature. As a general observation, isotherm data indicate over 97% removal of gold (Fig.62) with decreasing gold concentration in the low concentration regions (50 mg L^{-1} and 100 mg L^{-1}), and a plateau at the higher concentration regions (from 200 mg $L^{-1}$to 500 mg L^{-1}) with values dropping to less than 50% removal.

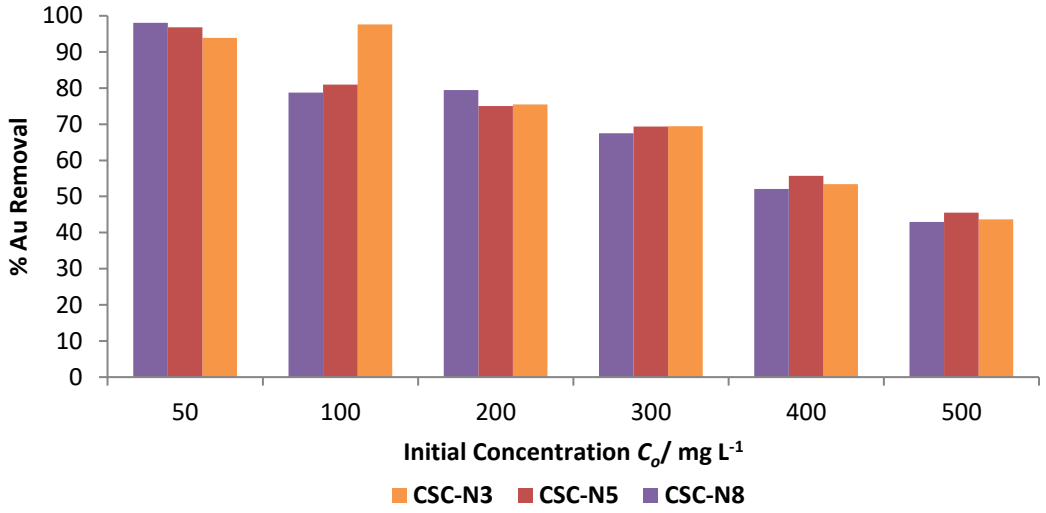

Figure 61 % Gold Removal with Series N CSCs at room temperature

As the solution concentration increases, it is difficult to differentiate between the three materials in terms of performance, as all three have very comparable % removal of gold at the range of concentrations used. This is a trend that has not been observed in the other series of materials produced, as for all Series A, B and C, the best material was the one produced at 500 ˚C; changes in nitrogen functionalities seem to have different effects on the surface.

Nonetheless, the trend in gold removal is proof that adsorption is concentration dependent at constant pH. Initially, at the low region concentrations (50 mg L^{-1} and 100 mg L^{-1}), a significant adsorption is observed, resulting in a sharp incline in the adsorption curves, which may be attributed to fast chemisorption occurring. The very high % gold removal observed at those concentrations, along with the XPS data suggest that irreversible chemisorption takes place, as the anionic gold species is being adsorbed on the active sites of the material via its reduction.[161,178] Adsorption in the higher concentration regions (200 mg L^{-1}, 300 mg L^{-1}, 400 mg L^{-1} and 500 mg L^{-1}), is

hence speculated to mainly proceed by reversible physisorption, which is shown to have the larger effect in the adsorption process, as the isotherm plots show a less pronounced adsorption and removal of gold from solution. This is in agreement with Au4f XPS spectra for Series N CSCs which show the presence of Au(III) ions on the material surface after adsorption.

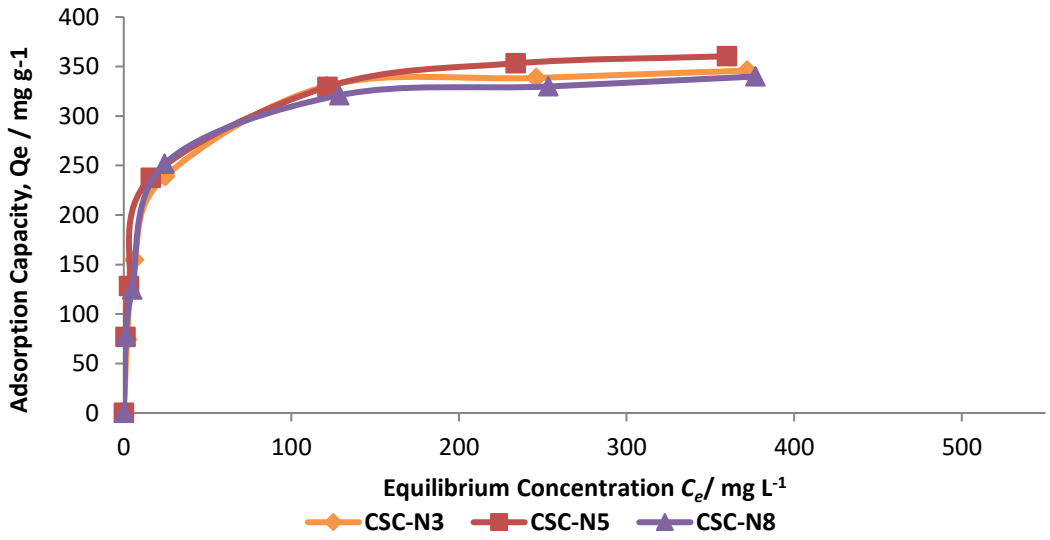

Figure 62 Isotherm plots for Series N CSCs at room temperature

Removal of gold from solution is associated with the total adsorption capacity, q_e, of materials. Maximum adsorption capacity values, q_e, (Table 28) demonstrate that the best adsorbent material is the one carbonised at 500 ˚C with an adsorption capacity of 360 mg g^{-1}. The same observation is made for the Series A, B and C CSCs produced at 500˚C which have the highest adsorption capacities when compared to materials produced at 300 ˚C and 500 ˚C in the same series. It appears, that at this temperature the carbon layer has a unique surface structure facilitating a greater extent of adsorption, mainly due to more electrostatic interactions in the case of Series N CSCs.

As anticipated, CSC-N5 has a higher loading capacity than CSC-N3 and CSC-N8 due to the thicker carbon layer on the surface (0.70nm) and more functionalities available for surface oxidation and electrostatic interactions (deduced from porosimetry and XPS results discussed in Chapter 6).

The adsorption capacities of materials can be correlated with the nature of adsorption taking place at the different concentrations. Chemisorption is prominent at the low concentrations of gold, whereas reversible physisorption describes the system better at higher concentrations (in good correlation with the good fits to the Langmuir model). Enhanced chemisorption at the lower concentrations, when physisorption is always observed, allows for additional surface loading and hence higher loading capacities at the range of concentrations tested.[161]

7.4 Conclusion

The new class of nitrogen-doped materials (Series N CSCs) are proven to be suitable adsorbents for the removal of gold from a range of concentrations of acidic solutions. Mechanistically the process can proceed via 1) irreversible chemisorption, by which the surface of materials oxidises, and the gold species simultaneously reduce and 2) reversible physisorption, by which the aurochlorate anion electrostatically interacts with the surface due to the presence of nitrogen-containing functionalities.

CSC-N5 is the best adsorbent material produced with an adsorption capacity of 360 mg g^{-1} leading to 97% removal of gold. Series N CSCs perform exceptionally well at the low concentration regions with a greater extent of physisorption. The adsorption data have been successfully modelled using the Langmuir, Freundlich and D-R isotherms, with the Langmuir model giving the best fit for Series N (R^2 very close to unity). This suggests that monolayer adsorption takes place during the physisorption stage, yet surface heterogeneity and functionality of the three types of nitrogen-functionalised CSCs produced may permit multi-layer coverage or interactions that affect the mesopores.

Aside the physical and chemical properties of Series N CSCs, the concentration of solution affects the amount of gold that can be removed. It has been demonstrated that the CSCs perform better that the lower concentrations with over 80% removal of gold, demonstrating that are ideal for gold recovery from real-life waste (mine tailings) which contains trace amounts of the metal.

Chapter 8.

Experimental

Chapter 8.

Experimental

8.1 Materials and Methods

8.1.1 Chemicals

Silica K60 and urea were purchased from Sigma Aldrich. Activated carbon NORIT was purchased from Fluka and gold (III) chloride 64.4% min was purchased from Alfa Aesar. Analytical grade solvents including ethanol and acetone, as well as 0.1M HCl, were purchased from Fisher Scientific. All chemicals were used as received. De-ionised water and deuterated acetone were used as supplied by the Chemistry stores, University of York. Milled waste office paper was used as supplied by, University of York.

Materials CSC-A3, CSC-A5 and CSC-A8 were used as prepared by Dr Tengyao Jiang as part of his work and initial testing towards exploitation of carbon/silica synthesis and use.

8.1.2 Methodologies

8.1.2.1 Preparation of Paper Blocks

Milled paper was thoroughly mixed in a container/tray with de-ionised water, until sludge formed. The mixture/sludge was then poured into the paper press equipment to make one big block at a time. After pressing, the blocks were placed in trays, as shown in Figure 64. The trays were then placed in a drying oven set at 50˚C and were left to dry for 48 hours. Once completely dried and hardened, the blocks were cut into smaller pieces (dimensions: 5 cm x 5 cm x 5 cm).

Figure 63 Paper blocks preparation

8.1.2.2 Production of Bio-oil

The 5 cm x 5 cm x 5 cm paper blocks were placed in the microwave reactor of the Milestone RotoSYNTH Rotative Solid Phase Microwave, until half of the available volume of the vessel was occupied (about 150 g of blocks required). The chiller was turned on to get the temperature down to about 4 ^{o}C and the vacuum pump was turned on to ensure pyrolysis occurred under vacuum. Method of pyrolysis was set to start heating at 40 ^{o}C and 800 W for 4 minutes, and then proceed to reach 200 ^{o}C and maximum power of 1200 W for 8 minutes, under vacuum.

The reactor vessel was sealed with a plastic O-ring seal and placed in the microwave chamber. It was attached to a glass tube which then connected to the external set up of glassware. The connecting tube left the microwave chamber and was attached to a condenser that required no water flow, which was then connected to a round bottomed flask. Rubber tubing connected the first round-bottomed flask to a second round bottomed flask, which was fitted with a water condenser. The condenser was fed to the vacuum pump to ensure the whole system was under vacuum. During pyrolysis three products collected: bio-gas, bio-oil and char. Bio-gas was due to the release of water and volatiles from the waste paper blocks, and passed through the first round bottomed flask and rubber tubing to condense in the second round bottomed flask, where it collected as the aqueous fraction. Bio-oil was collected in the firs- round bottomed flask as a brown viscous liquid. Char was the solid residue that remained in the vessel after the process was completed. Illustrated set-up shown in Figures 65 and 66.

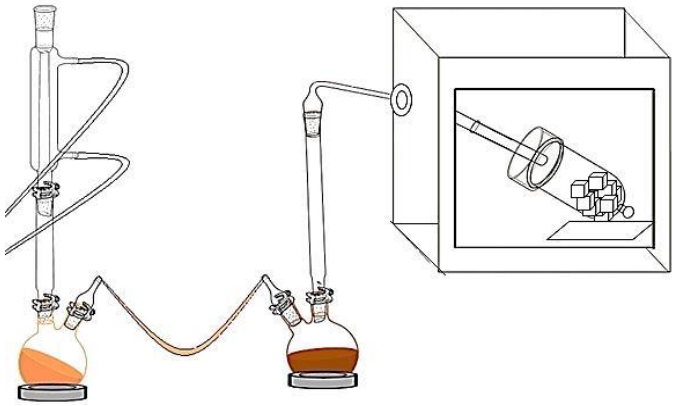

Figure 64 Set-up for microwave pyrolysis of wastepaper blocks

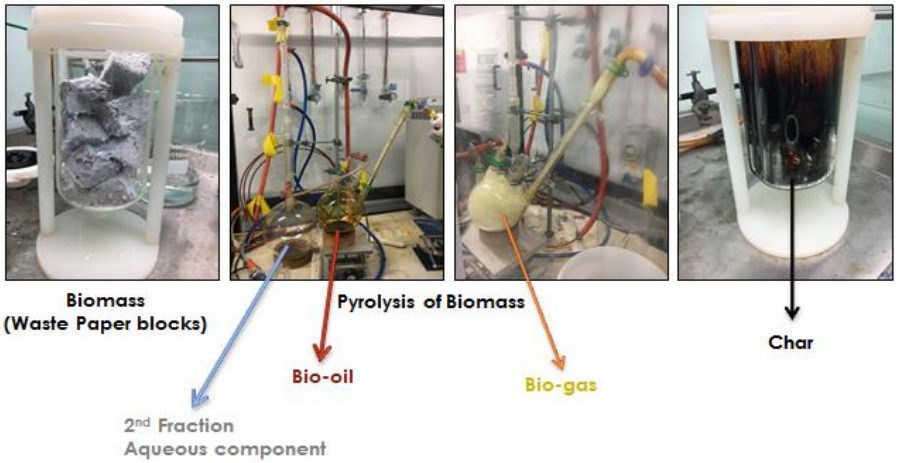

Figure 65 Real-life set-up for microwave pyrolysis of waste office paper blocks and its products

8.1.2.3 Synthesis of Carbon/Silica Composites

8.1.2.3.1 Series A, B and C

The method followed was as described by previous research.[152] The process was a wet impregnation method, involving mixing bio-oil and silica K60 in acetone. 1:1 ratio of bio-oil to silica K60 was used for the mixture (10 g bio-oil & 10 g of silica K60) in a round bottomed flask containing enough acetone to allow stirring. The mixture was left to stir overnight at room temperature. Mixture was then carbonised in the furnace under nitrogen flow (heating rate 5 ^{o}C/ minute, hold time 10 minutes). Acetone was removed during the carbonisation process. The end temperature was set according to the material made (Table 29).

Table 28 Carbonisation temperatures for all series of CSCs made with silica gel K60

Material	Temperature / ˚C
CSC-A3	300˚C
CSC-B3	300˚C
CSC-C3	300˚C
CSC-A5	500˚C
CSC-B5	500˚C
CSC-C5	500˚C
CSC-A8	800˚C
CSC-B8	800˚C
CSC-C8	800˚C

8.1.2.3.2 Nitrogen-Doped CSCs: Series N

The method followed was as described above with the addition of a doping agent.

During the wet impregnation step, bio-oil was mixed with silica K60 and urea in acetone. 1:1:1 ratio of bio-oil to silica K60 to urea was used for the mixture (10 g bio-oil & 10 g of silica K60 & 10 g of urea) in a round bottomed flask containing enough acetone to allow stirring. The mixture was left to stir overnight at room temperature. Mixture was then carbonised in the furnace under nitrogen flow (heating rate 5 ^{o}C/ minute, hold time 10 minutes). Acetone was removed during the carbonisation process. The end temperature was set according to the material made (Table 30).

Table 29 Carbonisation temperatures for Series N CSCs made with silica gel K60 and urea

Material	Temperature / ˚C
CSC-N3	300˚C
CSC-N5	500˚C
CSC-N8	800˚C

8.1.2.4 Adsorption Experiments

8.1.2.4.1 Multi-metal Adsorption

Chloride salts of nickel, copper, zinc, palladium, platinum and gold were dissolved in 0.1 M HCl and de-ionised water to make up a solution of pH 3 (Au: 133.9 mg L^{-1}, Pt: 0.32 mg L^{-1}, Pd: 108.7 mg L^{-1}, Ni: 93.9 mg L^{-1}, Cu: 94.9 mg $L^{-1}$and Zn: 90.6 mg L^{-1}). To a 20 mL vial containing 10 mL of each metal salt, 10 mg of adsorbent material was added and stirred for 24 hours at room temperature. Both the solution and solid were retained for further analysis.

8.1.2.4.2 Gold Adsorption

A stock solution (500 mg L^{-1}) was prepared by dissolving 0.301 g of $AuCl_3$ in 2.5 mL of 0.1 M HCl and 247.5 mL of deionised water to make up a solution of pH 3. Additional concentrations were prepared by diluting the stock solution in separate 10 mL volumetric flasks (400 mg L^{-1}, 300 mg L^{-1}, 200 mg L^{-1}, 150 mg L^{-1}, 100 mg L^{-1}, 50 mg L^{-1}, 25 mg L^{-1}), keeping the solution pH 3.

To a 20 mL vial containing 10 mL of the gold solution 10 mg of adsorbent material was added and stirred for 24 hours at room temperature (Fig.67). Both the solution and solid were retained for further analysis.

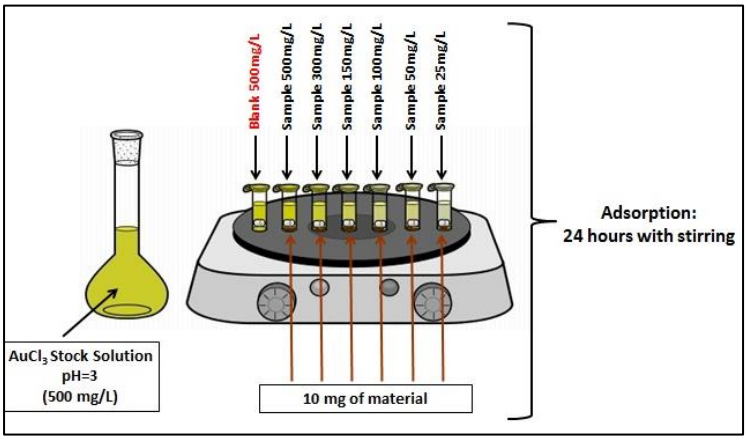

Figure 66 Set-up for gold adsorption experiments

The adsorption capacity q_e of all materials was calculated by:

$$qe = (Co - Ce)\frac{v}{m}$$

Where q_e (mg g^{-1}) is the adsorption capacity, C_o (mg L^{-1}) the initial concentration of the solution, C_e (mg L^{-1}) the concentration of the sample solution at equilibrium after adsorption, v (L) the volume of solution and m (g) the mass of material used.

Four different series of materials were used and tested in gold adsorption:

- Series A: CSC-A3, CSC-A5 and CSC-A8.
- Series B: CSC-B3, CSC-B5 and CSC-B8.
- Series C: CSC-C3, CSC-C5 and CSC-C8.
- Series N: CSC-N3, CSC-N5 and CSC-N8.

8.1.2.5 Kinetics Experiments

Stock solution of $AuCl_3$ (500 mg L^{-1}) was used for this set of experiments. Eight samples were prepared with the same concentration (500 mg L^{-1}), amount of solution (10 mL) and adsorbent (10 mg). At different allocated time intervals 20 µL of solution was transferred from the reaction sample to a vial containing 5 mL of 10% w/w HCl.

Each of the eight samples prepared correspond to the allocated time that the 20 µL from each solution were transferred, the times being 15 minutes, 30 minutes, 1 hour, 3 hours, 6 hours, 12 hours, 18 hours and 24 hours.

The materials used and tested to determine adsorption kinetics were Series A CSC-A3, CSC-A5 and CSC-A8.

8.2 General Analytical and Characterisation Techniques

8.2.1 Electron Microscopy Techniques

All electron microscopy images were obtained with the help of Dr Meg Stark at the Technology Facility in the Department of Biology, University of York, UK.

8.2.1.1 Scanning Electron Microscopy

Samples were immobilised on metallic studs before loading into the instrument. Metallic stubs were labelled on the back side to make identification of each sample easy and were then coated with SEM double- sided tape. A small amount of each solid material was then fixed onto the tape of the corresponding metallic stud (based on sample ID). The specimens were then flashed in vacuum in Argon Plasma to clean the atmposhere and were coated with 7 nm of gold/palladium to make sure all materials were conductive. Starting equipment voltage was set to 1.9- 2 kV, starting plasma current to15 µA and the chamber pressure was increased up to 6 x 10^{-1} mbar Pa^{-1}. As soon as the materials were removed from the pressure chamber (Sputter Coater), they were loaded onto the stage of the SEM instrument.

The materials were observed under various magnifications on a JEOL JSM-6490LV SEM instrument.

8.2.1.2 Transmission Emission Microscopy

Samples were suspended in ethanol in microcentrifuge tubes and were then deposited onto 200 mesh grids with a carbon support film for 20 minutes, to allow for evaporation of the solvent. The dried grid samples were then loaded onto an entry sample holder.

The material were observed under various magnifications on a Tecnai 12 BioTwin at 120 kV instrument.

8.2.1.3 Scanning Electron Microscopy with Energy Dispersive X-Ray Analysis

Samples were immobilised on metallic studs before loading into the instrument. Metallic stubs were labelled on the back side to make identification of each sample easy and were then coated with SEM double- sided tape. A small amount of each solid material was then fixed onto the tape of the corresponding metallic stud (based on sample ID).

Images of the materials were taken using a Heliow Nanolab G3 CX (FEI) – Focused Ion Beam scanning electron microscope.

8.2.2 Infrared spectroscopy

8.2.2.1 Diffuse Reflectance Infrared Fourier Transform

Powdered samples were ground in dried KBr (dilution ratios of a) 1:100 parts/ 10 mg of material: 1 g of KBr & b) 1:20 parts/ 10 mg of material: 200mg of KBr). Samples were then placed on crystal surface with a sapphire anvil clamping. Spectra were taken from 4000 cm^{-1} to 500 cm^{-1}, at 64 scans with a spectral resolution of 4 cm^{-1}, and a blank window for the background.

Spectra were obtained on an Equinox 55 IR FTIR spectrometer.

8.2.2.2 Attenuated Total Reflectance Infrared

Solid and liquid samples were placed on crystal surface with a sapphire anvil clamping. Spectra were taken from 4000 cm^{-1} to 500 cm^{-1}, at 64 scans with a spectral resolution of 4 cm^{-1}, and a blank window for the background.

Spectra were obtained on a Bruker Vertex 70 spectrometer.

8.2.3 Gas Chromatography and Mass Spectral Analysis

GC-MS was used for the qualitative and quantitative analysis of the bio-oils used for material synthesis. A Perkin Elmer Clarus 500 Gas chromatograph with an auto sampler was coupled to a Perkin Elmer Clarus 560s mass spectrometer.

Samples were dissolved in acetone and analysed using a capillary column DB-5HT, 30 m x 0.25 mm I.D. x 0.25 µm film thickness. The oven was held at 60 ^{o}C for 1 minute, then temperature programmed to 300 ^{o}C at 8 ^{o}C min^{-1} and held for 10 minutes. The temperature of the injector was 290 ^{o}C. The mass spectrometer was operated in electron impact mode (EI) at 70 eV. The identification of chromatographic peaks was done by comparison of mass fragmentation patterns with spectra included the NIST library.

8.2.4 Thermal Gravimetric Analysis

TG analysis was carried out using a Netsch 409 STA thermal analyser. Samples were mounted in a 3.5 ml ceramic crucible and heated under a flow of nitrogen (50 ml min^{-1}). Prior to sample analysis, the oven chamber was evacuated and backfilled twice with nitrogen. Samples were heated at 10 K min^{-1} to either 573, 773 or 1073 K. For the TG-IR studies the TG was coupled to a Bruker Equinox 55 Infrared spectrometer via a transfer line. The flow of nitrogen used was 100 mL min^{-1}.

Proximate analysis was carried out the Netsch 409 STA thermal analyser as follows:

Under nitrogen atmosphere (100 mL min^{-1})

- Ramp from 30°C to 105°C at a heating rate of 10°C min^{-1}
- Isothermal at 105°C for 10 min
- Ramp from 105°C to 900°C at a heating rate of 50°C min^{-1}
- Isothermal at 900°C for 1 hour

Under air atmosphere (100 mL min^{-1})

- Ramp from 30°C to 900°C at a heating rate of 50°C min^{-1}
- Isothermal at 900°C for 1 hour

Moisture content was defined by the mass loss in nitrogen atmosphere between 30°C and 105°C. Volatile matter content was defined by the mass loss between 105°C and 900°C under nitrogen atmosphere. Ash content was assigned as the residual mass after heating samples at 900°C for 1h under air. Fixed carbon content was defined at 900°C by the difference in residual mass of the sample between the value obtained

under nitrogen and under air. An illustration of mass loss assignement is presented in Fig. 68.

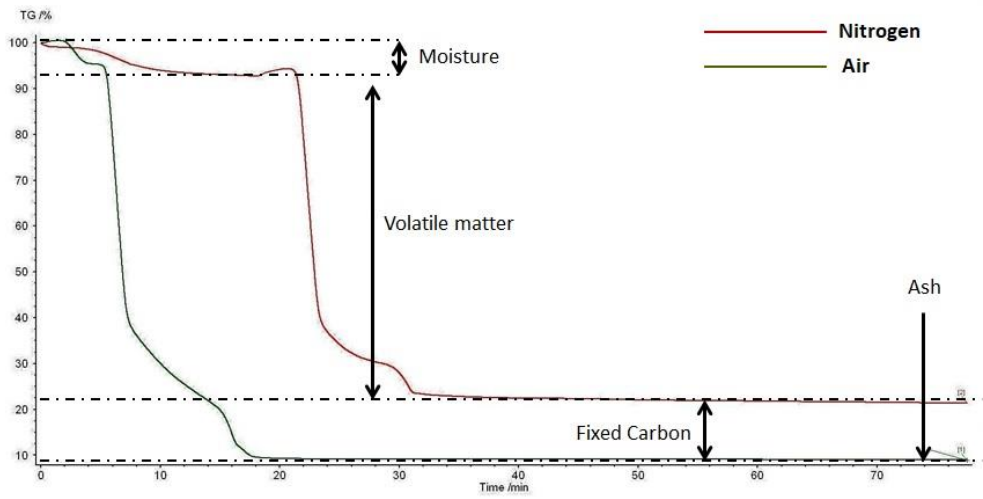

Figure 67 Proximate analysis (moisture content, volatile matter, fixed carbon and ash content)

8.2.5 Porosimetry Analysis

Nitrogen adsorption/desorption isotherms, surface area (BET) and porosimetry measurements (including pore volumes and porous distributions) were obtained by a Micrometrics ASAP 2020 volumetric adsorption analyser at -196 ^{o}C.

Before analysis, samples were degassed at 130°C for 6 hours under nitorgen flow. Specific surface areas were calculated using the Brunauer, Emmett and Teller (BET) method and the total pore volume was determined from the amount of nitrogen adsorbed at P/Po ~0.99. All pore size distribution curves were determined from the desorption branch based on Barrett, Joyner and Halenda (BJH) method.

8.2.6 Inductively Coupled Plasma Spectroscopy

All ICP-OES analysis was carried out by Dr Lorna Eaders at the School of Chemistry, Edinburgh University, Scotland.

Liquid component of samples after adsorption experiments was kept and used for the sample preparation. Concentration of gold in solution had to be 1 ppm to comply with the detection standards of the instrument, therefore three different dilutions were used to prepapre 10 mL samples with stock ICP solution. Stock ICP solution was prepared by dissolving 22.5 mL 0.1M HCl in 477.5 mL of pure deionised water. 1:500

dilution was used for the adsorption samples with initial concentration of 500 mg L^{-1} and 300 mg L^{-1}. 1:200 dilution was used for the adsorption samples with initial concentration of 150 mg $L^{-1}$and 100 mg L^{-1}. 1:100 dilution was used for the adsorption samples with initial concentration of 50 mg $L^{-1}$and 25 mg L^{-1} (Table 31). Samples were prepared in ICP centrifuge tubes and were sealed with paraffin film, before being sent of for analysis.

Data were processed and present as excel tables and plots.

Table 30 Sample preparation for ICP-OES analysis

Initial Concentration / mg L^{-1}	Dilution Factor	$V_{taken\ from\ initial\ sample}$ / µL	V_{total} / µL
500	500	20	10000
300	500	20	10000
150	200	50	10000
100	200	50	10000
50	100	100	10000
25	100	100	10000

8.2.7 X-ray Photoelectron Spectroscopy

All XPS analysis was carried out by the NEXUS team at the School of Mechanical and Systems Engineering, Newcastle Univeristy, UK, as well as by Dr David Morgan at Cardiff Catalysis Institute, School of Chemistry, Cardiff University, Cardiff, UK.

Powdered samples were immobilised on non-conducting tape placed on the clean surface of a microscope slide. They were then wrapped with the shiny side of aluminium foil and labelled on the outside, before being sent off for analysis.

Data were processed and presented using the CasaXPS software.

8.2.8 Elemental Analysis

All elemental analysis (CHN Microanalysis) was conducted by Dr Graeme McAllister at the Department of Chemistry, University of York, UK.

Elemental analysis based on carbon, hydrogen and nitrogen content was carried out using an Exeter analytical CE440 elemental analyser, calibrated against acetanilide with an S-benzyl-thiouronium chloride internal standard.

Chapter 9.

Thesis Conclusions and Future Work

Chapter 9.

Thesis Conclusions and Future Work

9.1 Concluding Remarks

9.1.1 Investigation of Carbon/Silica Composites as Adsorbents

The major aim of this work is to determine the effectiveness of carbon/silica composites produced to selectively remove gold from acidic conditions, mimicking conditions of real-life mining waste.

The work conducted allowed for the preparation of three series of bio-derived CSCs (Series A, B and C) to selectively adsorb significant amounts of gold at various acidic concentrations ranging from 50 mg L^{-1} to 500 mg L^{-1}. The materials possess the combined advantages of easy operation, low-cost waste feedstock, simple maintenance, high selectivity and high adsorption capacities; better than those of reported modified silicas and comparable to those of activated carbons. These virtues coupled with their good mechanical and thermodynamic stability, make them attractive alternatives to existing adsorbents for water decontamination.

Exceptionally high removal of gold at different concentrations has been achieved using CSCs prepared from different bio-oils (BO-A, BO-B and BO-C) obtained from the microwave-assisted pyrolysis of waste office paper and silica K60, after carbonisation at three different temperatures (300 ˚C, 500 ˚C and 800 ˚C). Characterisation of materials produced for Series A, B and C, provides insight to their physiochemical properties, that will in turn affect their adsorption performance. Results have exhibited that as synthesis temperature increases, the materials shift from a polar, oxygen-rich surface with mainly aliphatic components, to an aromatic surface. This proves that the functionality of materials can be tailored, while maintaining their mesoporosity. While this shift in functionality is prominent in all three series of composite materials, produced, the carbon precursor (pyrolysis oil) plays an important role; the bio-oil BO-A with the most carbon content produced materials with significantly thicker carbon layers and richer in chemical functionalities that affect and facilitate adsorption.

Adsorption studies have demonstrated that mesoporous materials prepared at 500 ˚C, regardless of the bio-oil used, are the adsorbents with the best performance with removal rates reaching up to 99% at low concentration spectrum. While % removal of gold is maintained at extremely high levels, the adsorption capacities and nature of adsorption between materials varies.

The mechanism of gold adsorption involves a three-part process: adsorption, reduction and aggregation of the AuNPs formed. The overall adsorption process can be split to two routes: 1) irreversible chemisorption which is followed by the reduction of the gold species in solution from Au(III) to Au(0) and 2) reversible physisorption occurring via weak van der Waals' forces and electrostatic interactions. While all materials adhere to both physical and chemical adsorption during gold recovery, the contribution of each is affected depending on the series of materials used. Series A CSCs proceed predominately via chemisorption-reduction, Series B proceeds with a greater extent of reversible physisorption and Series C has very similar contributions of both . The competition between physisorption and chemisorption-reduction is related to the thickness of the carbon layer on the surface of materials and the quantitative composition of surface functionalities. In the presence of more reducing oxygen-containing functionalities on the surface of materials, a chemical reaction is favoured and thus the system undergoes more chemisorption leading to the formation of AuNPs.

The adsorption capacities between the materials of all three series varied, with the highest observed for CSC-A5, CSC-B5 and CSC-C5 at 320 mg g^{-1}, 194 mg $g^{-1}$and 330 mg g^{-1}, respectively. At this synthesis temperature, the materials have the optimal balance between porosity and surface chemistry, allowing them to perform the best.

Overall, the work presents the great potential that Series A, B and C CSCs have for the selective removal of gold, as they hold the benefit of probing both, physiochemical properties upon carbonisation and the nature of adsorption.

9.1.2 Investigation of Nitrogen-Doped Carbon/Silica Composites as Adsorbents

The major aim of this work is to determine the effectiveness of carbon/silica composites produced to remove gold from acidic conditions, by taking their production a step further; introducing a heteroatom into the carbonaceous matrix to enhance material properties. A new class of carbon/silica composites has been successfully synthesised (Series N), by incorporating nitrogen functionalities via the use of urea as the doping agent. Nitrogen doping has been shown to intrinsically modify properties of carbonaceous materials, especially those used as adsorbents.

The work conducted allowed for the preparation of nitrogen-doped CSCs and their application as adsorbents to recover gold at various acidic concentrations ranging from 50 mg L^{-1} to 500 mg L^{-1}, as done for Series A, B and C CSCs.

Exceptionally high removal of gold at different concentrations has been observed using the nitrogen-doped CSCs prepared from bio-oil BO-C obtained from the microwave-assisted pyrolysis of waste office paper mixed with silica K60 and urea, after carbonisation at three different temperatures (300 ˚C, 500 ˚C and 800 ˚C). Characterisation of Series N materials provides insight to their physiochemical properties, that will in turn affect their adsorption performance, as speculated based on findings from earlier work in this thesis. Results have exhibited that as synthesis temperature increases, the materials shift from a polar, oxygen-rich surface with mainly aliphatic components, to an aromatic surface, accompanied with the presence of nitrogen-containing functionalities. This proves that the functionality of materials can be tailored, while maintaining their mesoporosity.

Adsorption studies have demonstrated that the mesoporous material CSC-N5 prepared at 500˚C, is the adsorbent with the highest adsorption capacity (360 mg g^{-1}), while % removal of gold is very similar for all three nitrogen-doped CSCs at the range of concentrations used, with the highest removal measured at 97%.

The mechanism of gold adsorption as previously mentioned involves two steps: 1) irreversible chemisorption and 2) reversible physisorption. While all materials follow both mechanistic routes during adsorption of gold, the contribution of physisorption is bigger than that of chemisorption for all three materials. The surface of materials still undergoes an oxidation, while simultaneously the gold species is reduced from

Au(III) to Au(0), but adsorption proceeds mainly via electrostatic interactions between the adsorbent surface and the adsorbate in solution as a result of the incorporation of nitrogen on the surface and within the pores of materials.

Overall, the work presents the great potential that Series N CSCs have for the removal gold from solutions, as they have higher adsorption capacities and higher relative % removal throughout the range of concentrations employed than all other CSCs produced for the research purposes of this thesis.

9.1.3 Adsorption and Gold Recovery

A key goal of this work is to further demonstrate the efficiency of adsorption as an emerging green technology for the recovery of precious metals from solution, and in particular gold. A range of practices may be utilised to achieve gold recovery with benefits such as high selectivity, relatively low costs, simplicity and control over the processes, including precipitation, solvent extraction, ion exchange and electrodeposition. Without a doubt extensive work and literature proves how and why these methods work, but the work presented in this thesis concludes and encourages the use of adsorption as opposed to the aforementioned techniques.

While this work, may only provide evidence on a laboratory scale, it presents the following findings:

- No need for the use of auxiliaries or excess reagents to achieve gold recovery.
- No need for harsh conditions to commence or maintain the process until completion.
- Easy operation and handling throughout.
- With the use of the right adsorbent materials, selectivity is achieved leading to easier separation and capture of the metal of interest.
- Upon completion, insignificant amounts of waste left to further treat or dispose of.
- Adsorbent materials achieve gold recovery and hold the potential of regeneration or use as-collected for other industrial processes (i.e. catalysis), leading to closed-loop recycling.

9.2 Further Work

9.2.1 Regeneration of Carbon/Silica Composite Adsorbents

It is important that waste is reduced and that materials are not to be disposed off after their first use. As a result, a method for the regeneration of materials needs to be developed, to allow for the re-use of materials. Suggested methods for the non-destructive regeneration of carbon/silica composites include desorption of gold using a solvent (could be water for the physisorbed species and acid for the chemisorbed species) and electrochemistry (cyclic voltammetry) to strip gold from the surface of materials. If regeneration of the composite materials is successful, testing how many times the materials can be regenerated, re-used and with what efficacy is suggested, as well.

9.2.2 Further investigation into other parameters potentially affecting the adsorption process

While the work carried out investigated the effect of porosity, surface functionality, gold concentration and partially contact time, more parameters need to be looked at to provide a complete mechanistic understanding of the process of gold adsorption. Suggested aspects to look at include the effects of temperature and pH changes, as well as the role of the chloride ions in solution. By investigating these parameters, a deeper understanding and more elaborate explanation can be reached with regards to the mechanism of adsorption (involving both chemisorption and physisorption).

9.2.3 Further investigation into the formation of gold leaves during the adsorption process

During the adsorption process to remove gold from the gold (III) solution at 50mg L^{-1} some very exciting observations have been made; a gold leaf has formed on the layer of solution which deposits after the mixture is filtered and the materials and liquid are retained separately. Series B and Series carbon/silica composites exhibit these interesting observations (illustrated below), but no further extensive study has been

done to investigate the reasons behind gold precipitation and the formation of gold leaves.

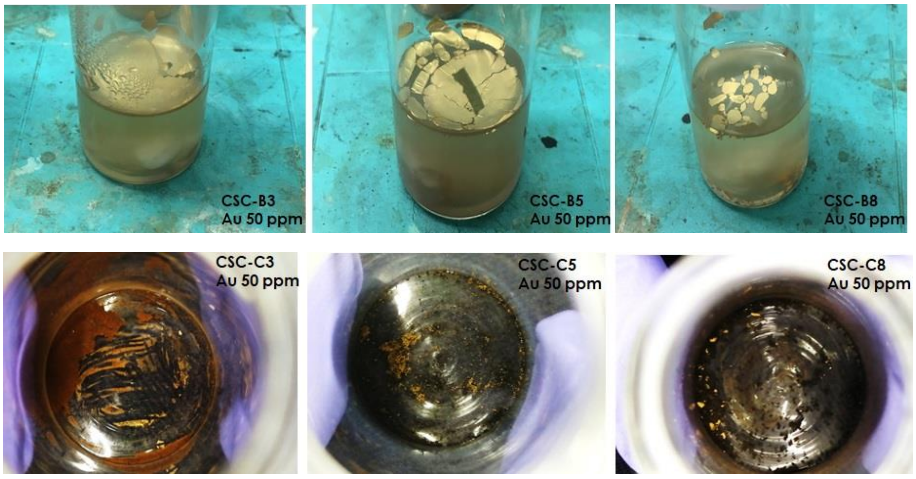

9.2.4 Application of the gold-loaded Carbon/Silica Composites in catalysis

The reduction-adsorption mechanism of gold demonstrated the formation of gold nanoparticles on the surface of materials. As a result, the gold-loaded nanoparticles on materials have the potential to be used in catalysis for reactions like the hydrochlorination of acetylene and the oxidation of CO.

9.2.5 Application of Carbon/Silica Composites in the adsorption of organic pollutants

The carbon/silica composite materials produced for research purposes of this thesis, have been proven suitable adsorbents for the selective removal of gold from multi-metal mixtures, but their potential as adsorbents for organic pollutants is yet to be tested. A range of organic species can be found in wastewaters, including dyes, pigments and phenols. Very commonly used adsorbents for such species are activated carbons, which face diffusion limitations depending on the molecular size of the adsorbate due to their high degree of microporosity. The mesoporosity and surface functionality of materials makes them ideal candidates for the adsorption of organic pollutants, and their potential should be exploited.

9.2.6 Development of 100% bio-derived Carbon/Silica Composites

The composite materials produced for the purposes of this research project are bio-based, as the carbon precursor originates from waste office paper. While the carbon feedstock is obtained by the microwave-assisted pyrolysis of paper, the silica precursor used for material synthesis is not bio-derived. The development of 100% bio-derived composite materials is proposed via the use and pyrolysis of a biomass rich in both carbonaceous matter and SiO_2, such as rice-hull ash (RHA), to provide both precursors necessary for the synthesis of carbon/silica composites.

Appendices

APPENDIX 1. CHN ELEMENTAL ANALYSIS

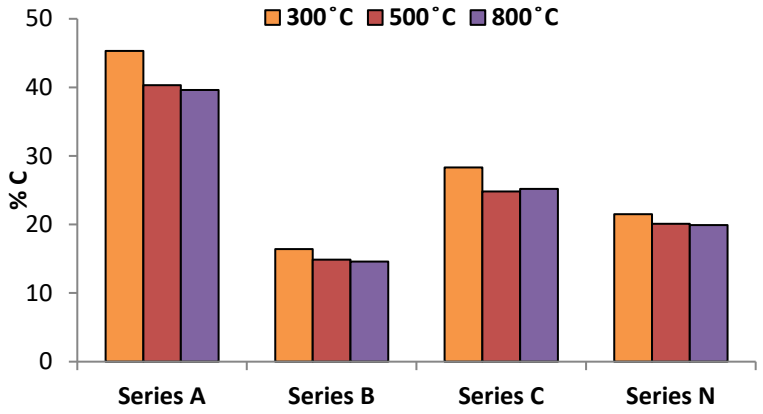

Supplementary Figure 1 % C Elemental composition of all CSCs

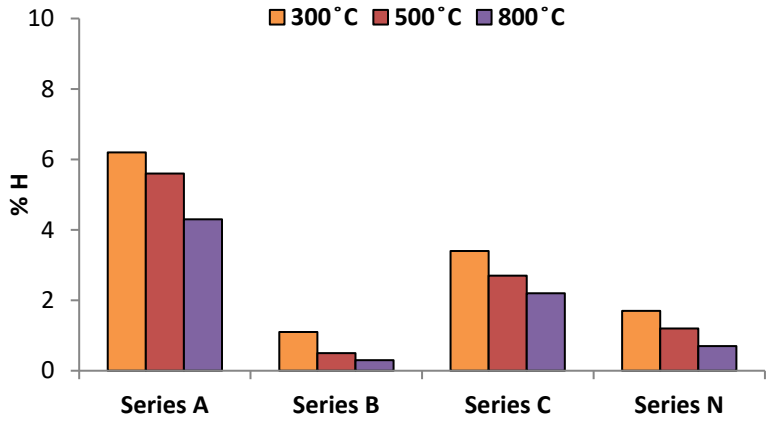

Supplementary Figure 2 % H Elemental composition of all CSCs

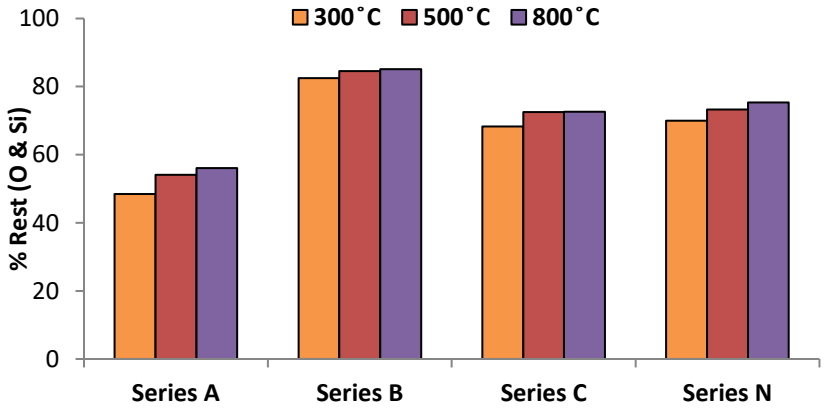

Supplementary Figure 3 %S Rest elemental composition of all CSCs

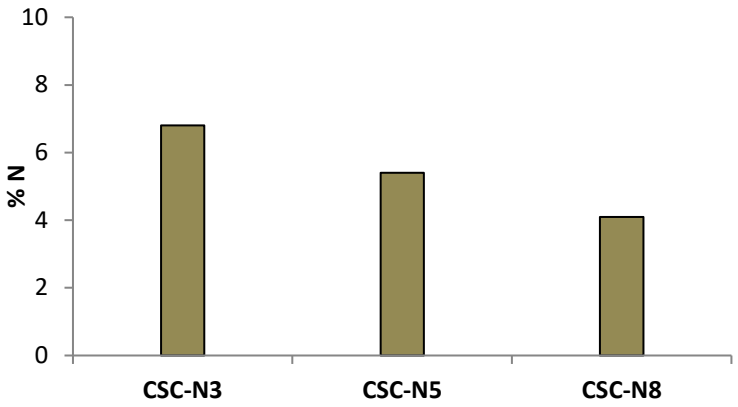

Supplementary Figure 4 % N Elemental composition of Series N CSCs

APPENDIX 2. RATE OF GOLD ADSORPTION

KINETIC MODELS

Pseudo-first Order liner fits

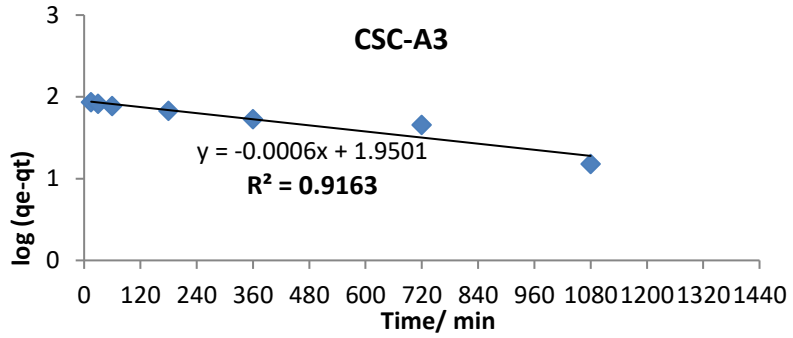

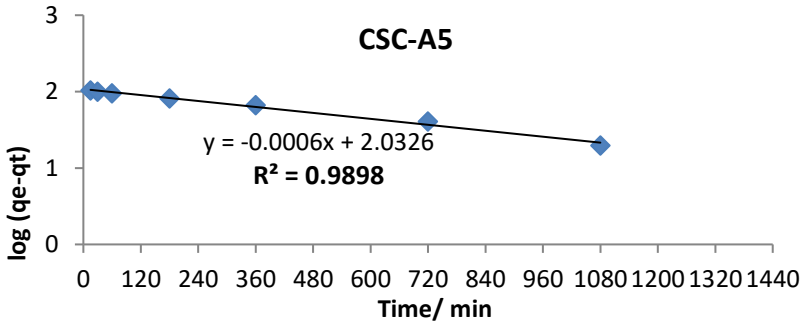

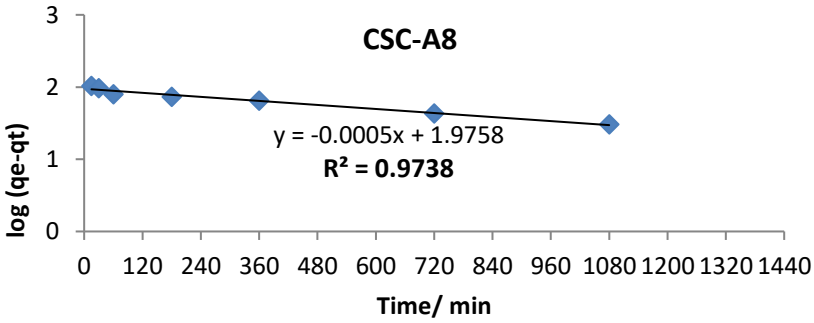

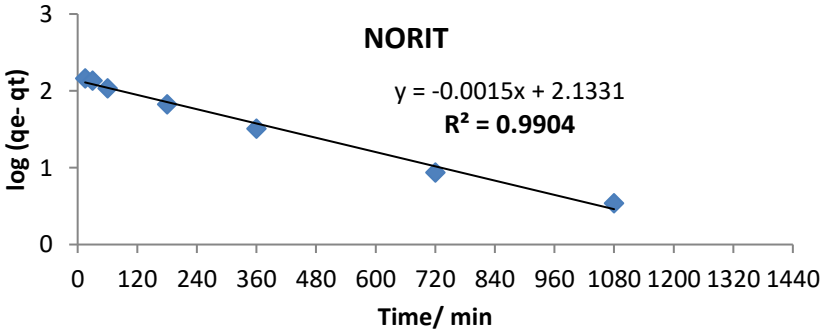

Pseudo-second order linear fits

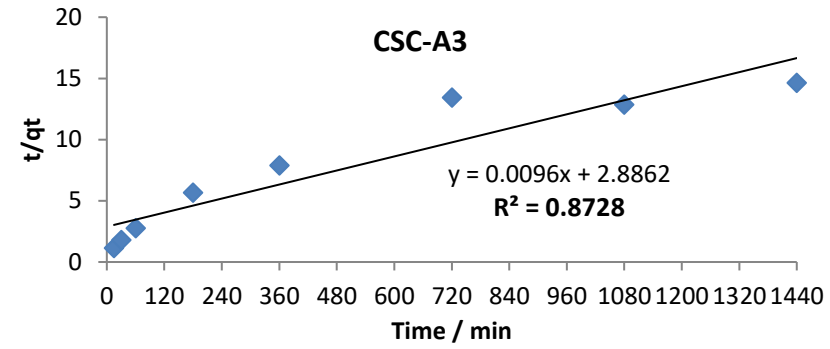

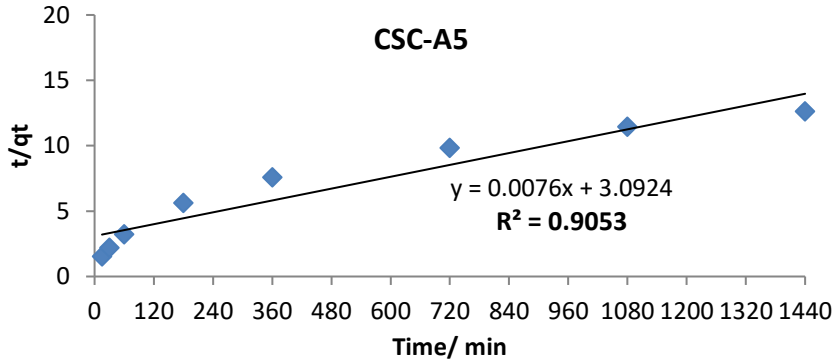

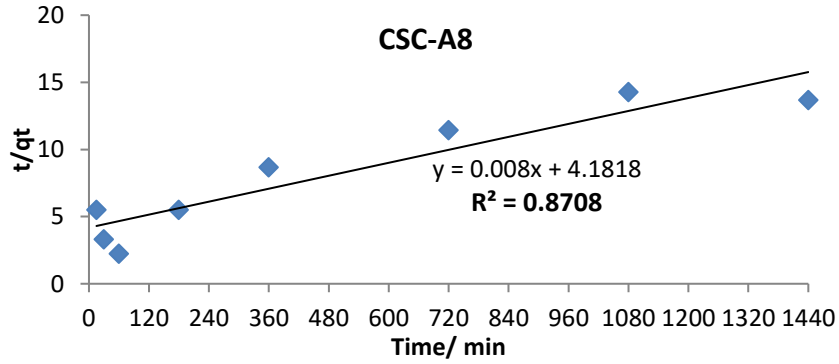

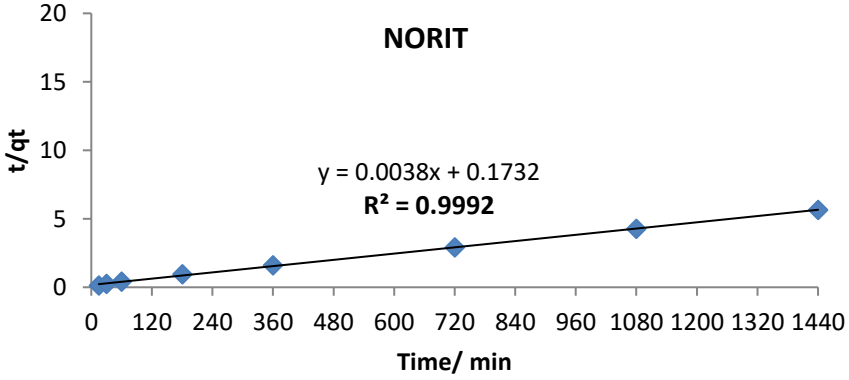

Elovich model linear fits

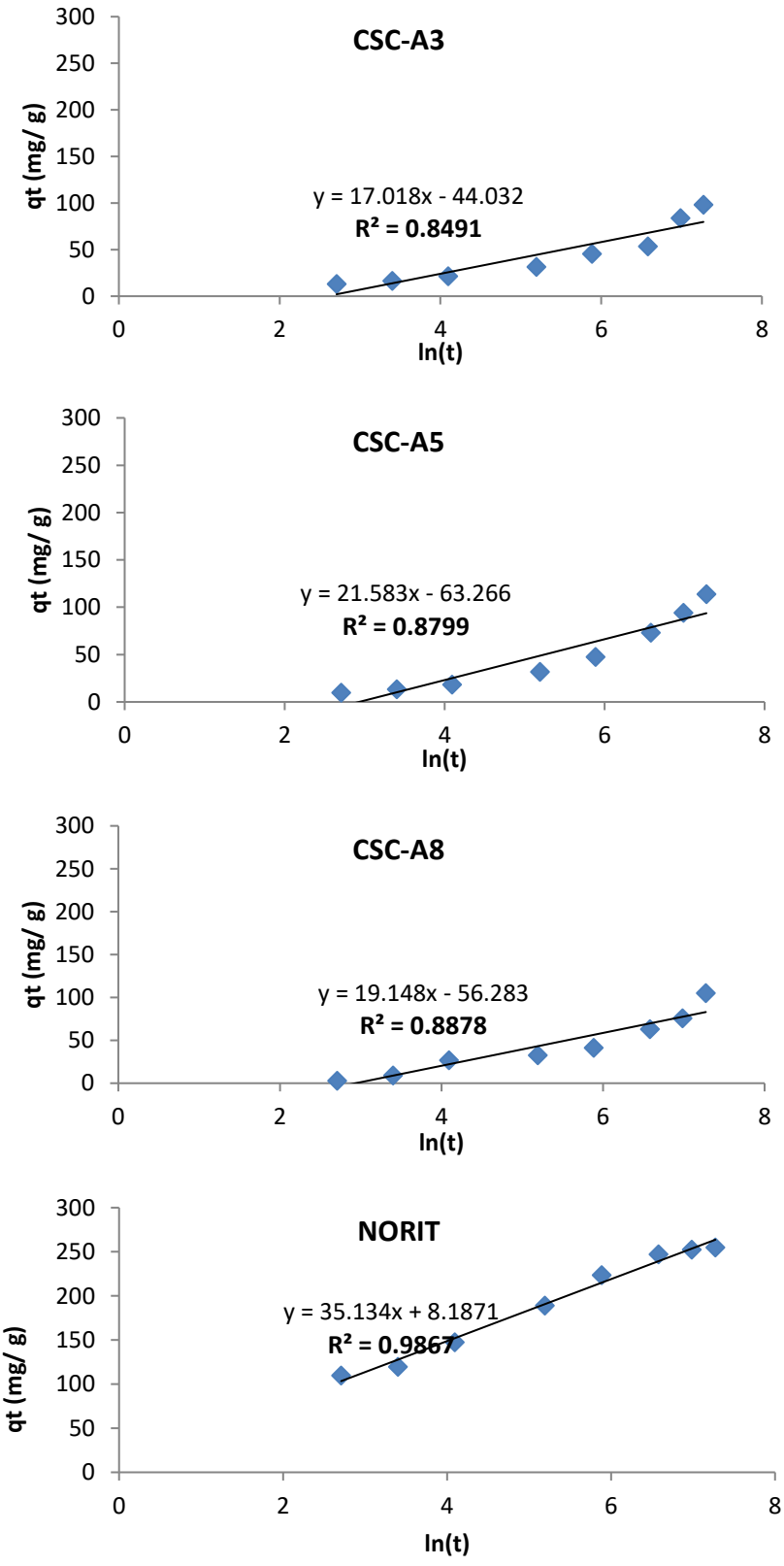

DIFFUSION MODELS

Film-diffusion-transport model linear fits

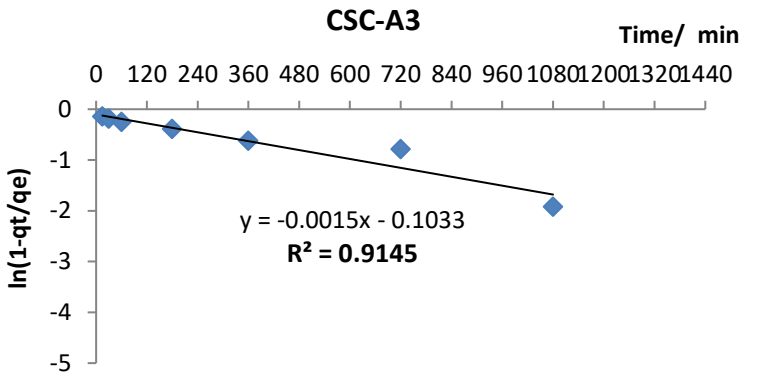

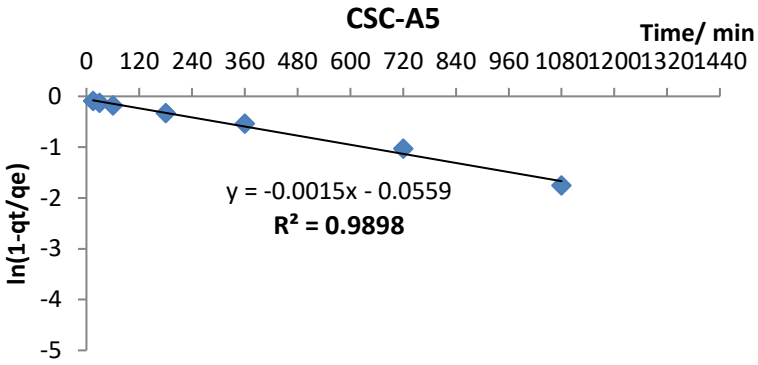

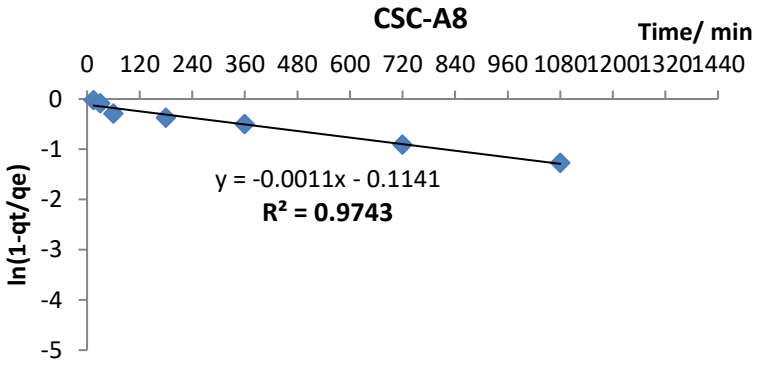

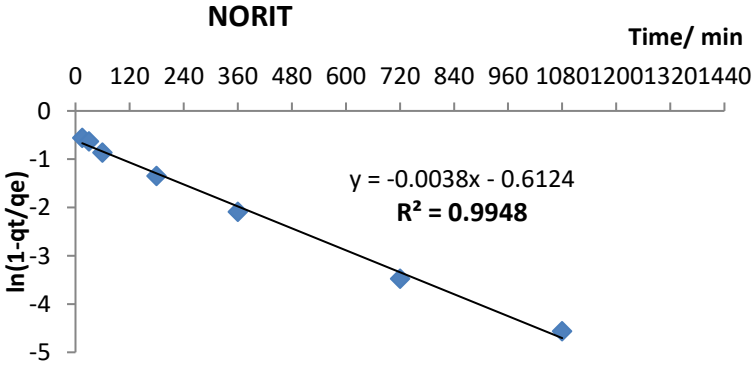

Intraparticle-diffusion-transport model linear fits

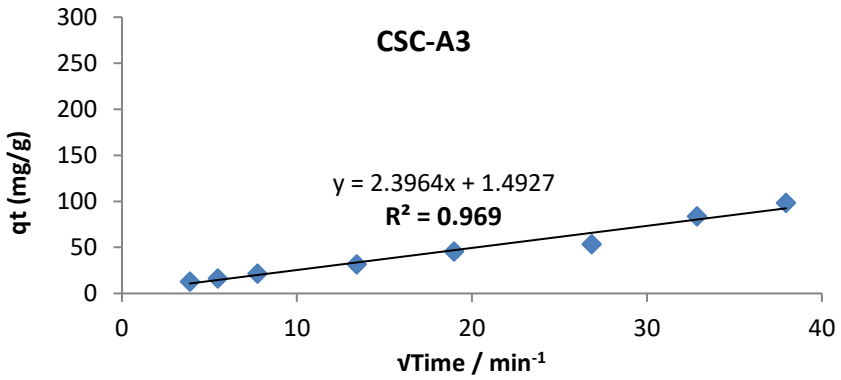

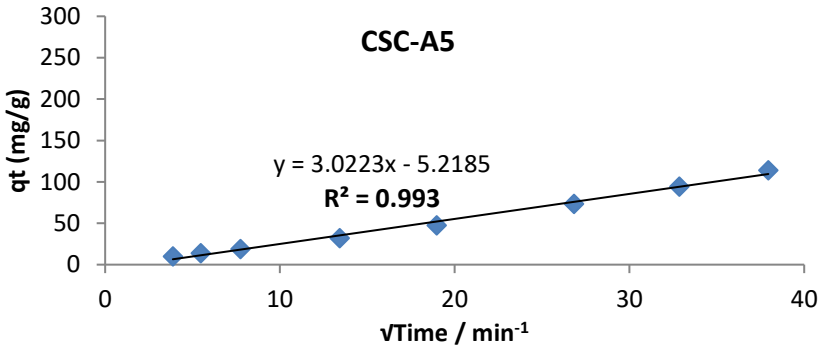

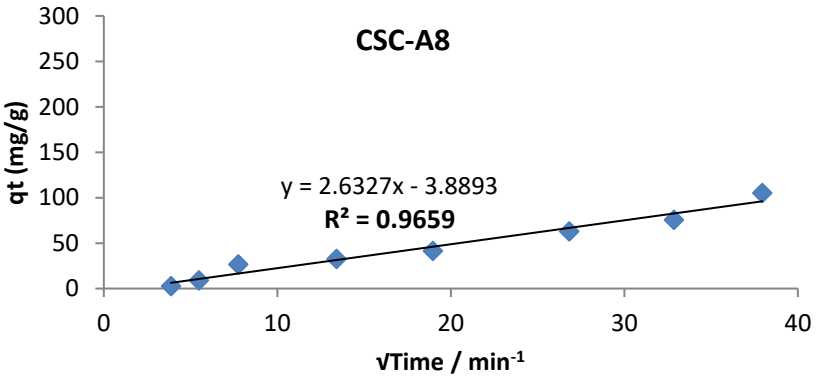

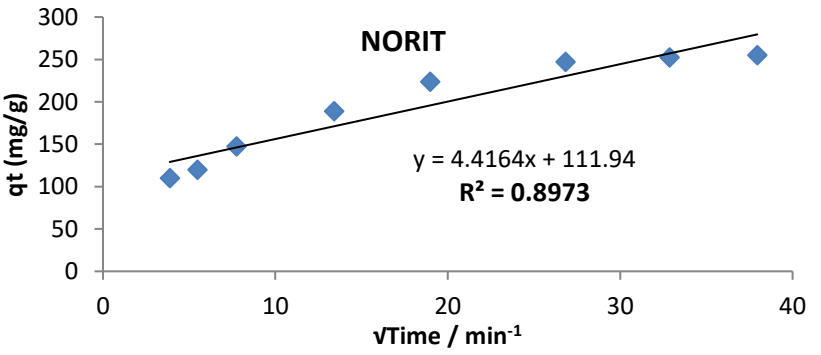

List of Abbreviations

The following abbreviations are included in this thesis in addition to the Mendeleev periodic table symbols:

AC	Alternating current
AFR	sub-Saharan Africa
ATR	Attenuated total reflectance
BE	Binding energy
BET	Brunauer Emmet and Teller
BJH	Barrett Joyner and Halenda
CEPI	Confederation of European Paper Industries
CSC	Carbon/Silica composites
DC	Direct current
DEFRA	Department for Environment, Food and Rural Affairs
D-R	Dubinin- Radushkevich
DRIFT	Diffuse reflectance Infrared Fourier transform
EAP	East Asia and Pacific
ECA	Europe and Central Asia
EEE	Electrical and electronic equipment
EPA	Environmental Protection Agency
EU	European Union
eV	Electron volts
FID	Flame ionisation detector
FT	Fourier transform
FTIR	Fourier transform- Infrared
GC	Gas chromatography
GCCE	Green Chemistry Centre of Excellence

GC-MS	Gas chromatography mass spectrometry
GHG	Greenhouse gases
HMF	5-(hydroxymethyl)-2-furaldehyde
ICP	Inductively coupled plasma
ICP-OES	Inductively coupled plasma- Optical emission spectrometry
ICP-MS	Inductively coupled plasma- Mass spectrometry
IR	Infrared
LAC	Latin America and Caribbean
LCD	Liquid crystal display
MENA	Middle East Asia and North Africa
MS	Mass spectrometry
MSW	Municipal solid waste
NCSC	Nitrogen doped Carbon/Silica composites
NIST	National Institute of Standards and Technology
NMR	Nuclear magnetic resonance
OECD	Organisation for economically developed countries
OES	Optical emission spectrometry
PAH	Polycyclic aromatic hydrocarbons
PCB	Polychlorinated biphenyls
PFO	Pseudo-first-order
PGM	Platinum group metals
ppm	Parts per million
PSO	Pseudo-second-order
R^2	Correlation coefficient
REE	Rare Earth elements
rpm	Revolutions per minute

SAR	South Asia region
S_{BET}	Surface area from BET isotherm
SEM	Scanning electron microscopy
TEM	Transmission electron microscopy
TGA	Thermal gravimetric analysis
TG-IR	Thermal gravimetric infrared analysis
UK	United Kingdom
US	United States
VOC	Volatile organic compounds
WEEE	Waste electrical and electronic equipment
w/w	Weight/ weight
XPS	X-ray photoelectron spectroscopy

References

1 T. J. Collins, *Green, Chemistry, Macmillan Encyclopedia of Chemistry*, Simon adn Schuster Macmillan, New York, 2nd edn., 1997.

2 D. S. Polymers and G. Engineering, 2007, 2169–2173.

3 P. T. Anastas & J. C. Warner, *Green Chemistry: Theory and Practice*, Oxford University Press, New York, 1998.

4 E. N. Anastas P.T., *Chem. Soc. Rev.*, 2010, **39**, 301–312.

5 B. W. C. J. J.B. Manley, P.T. Anastas, *J. Clean. Prod.*, 2008, **16**, 749–750.

6 M. M. Kirchhoff, *Resour. Conserv. Recycl.*, 2005, **44**, 237–243.

7 J. R. Dodson, A. J. Hunt, H. L. Parker, Y. Yang and J. H. Clark, *Chem. Eng. Process. Process Intensif.*, 2012, **51**, 69–78.

8 Y. Yang, R. Boom, B. Irion, D. J. van Heerden, P. Kuiper and H. de Wit, *Chem. Eng. Process. Process Intensif.*, 2012, **51**, 53–68.

9 M.Z. Jacobson; M.A. Delucchi, *Sci. Am.*, 2009, **301**, 58–65.

10 C. Mack, B. Wilhelmi, J. R. Duncan and J. E. Burgess, *Biotechnol. Adv.*, 2007, **25**, 264–271.

11 J. Cui and L. Zhang, *J. Hazard. Mater.*, 2008, **158**, 228–256.

12 N. Das, *Hydrometallurgy*, 2010, **103**, 180–189.

13 J. Wang and C. Chen, *Biotechnol. Adv.*, 2009, **27**, 195–226.

14 A. Tuncuk, V. Stazi, A. Akcil, E. Y. Yazici and H. Deveci, *Miner. Eng.*, 2012, **25**, 28–37.

15 P. L. Gratão, M. N. V. Prasad, P. F. Cardoso, P. J. Lea and R. A. Azevedo, *Brazilian J. Plant Physiol.*, 2005, **17**, 53–64.

16 N. T. Nassar, *Elem. Recover. Sustain.*, 2013, 185–206.

17 H. Wang and Z. J. Ren, *Water Res.*, 2014, **66**, 219–232.

18 Y. C. Lo, C. L. Cheng, Y. L. Han, B. Y. Chen and J. S. Chang, *Bioresour. Technol.*, 2014, **160**, 182–190.

19 J. R. Dodson, H. L. Parker, A. Muñoz García, A. Hicken, K. Asemave, T. J. Farmer, H. He, J. H. Clark and A. J. Hunt, *Green Chem.*, 2015, **17**, 1951–1965.

20 A. J. Hunt, A. S. Matharu, A. H. King and J. H. Clark, *Green Chem. (RSC)*, 2015, **17**, 1949–1950.

21 R. Chand, T. Watari, K. Inoue, H. Kawakita, H. N. Luitel, D. Parajuli, T. Torikai and M. Yada, *Miner. Eng.*, 2009, **22**, 1277–1282.

22 A. Ramesh, H. Hasegawa, W. Sugimoto, T. Maki and K. Ueda, *Bioresour. Technol.*, 2008, **99**, 3801–3809.

23 Y. J. Park and D. J. Fray, *J. Hazard. Mater.*, 2009, **164**, 1152–1158.

24 F. B. Li and X. Z. Li, *Appl. Catal. A Gen.*, 2002, **228**, 15–27.

25 G. C. Bond and D. T. Thompson, *Gold Bull.*, 2000, **33**, 41–50.

26 S. Zhang, Y. Ding, B. Liu and C. chi Chang, *Waste Manag.*, 2017, **65**, 113–127.

27 S. W. Won, P. Kotte, W. Wei, A. Lim and Y. S. Yun, *Bioresour. Technol.*, 2014, **160**, 203–212.

28 F. Wang, J. Zhao, M. Zhu, J. Yu, Y.-S. Hu and H. Liu, *J. Mater. Chem. A*, 2015, **3**, 1666–1674.

29 P. R. Zalupski, R. McDowell and G. Dutech, *Solvent Extr. Ion Exch.*, 2014, **32**, 737–748.

30 S. Syed, *Hydrometallurgy*, 2012, **115**–**116**, 30–51.

31 G. Chen, *Sep. Purif. Technol.*, 2004, **38**, 11–41.

32 M. Graydon, *World Gold Coucil*.

33 M. H. Govett and G. J. S. Govett, *Resour. Policy*, 1982, **8**, 84–96.

34 P. Goodman, *Gold Bull.*, 2002, **35**, 21–26.

35 C. Hagelüken and C. W. Corti, *Gold Bull.*, 2010, **43**, 209–220.

36 G. J. Higby, *Gold Bull.*, 1982, **15**, 130–140.

37 D. A. Giljohann, D. S. Seferos, W. L. Daniel, M. D. Massich, P. C. Patel and C. A. Mirkin, *Angew. Chemie Int. Ed.*, 2010, **49**, 3280–3294.

38 R. Meyer, C. Lemire, S. K. Shaikhutdinov and H.-J. Freund, *Gold Bull.*, 2004, **37**, 72–124.

39 L. Street, .

40 K. F. Lam, C. M. Fong, K. L. Yeung and G. Mckay, *Chem. Eng. J.*, 2008, **145**, 185–195.

41 M. Lekka, I. Masavetas, A. V. Benedetti, A. Moutsatsou and L. Fedrizzi, *Hydrometallurgy*, 2015, **157**, 97–106.

42 R. Asadi-Kesheh, S.-A. Mohtashami, T. Kaghazchi, N. Asasian and M. Soleimani, *Sep. Sci. Technol.*, 2015, **50**, 223–232.

43 J. A. Cox, M. Mulheron, D. Jesson, A. Druckman, M. Smyth and H. Trew, *Proc. Inst. Civ. Eng. Waste Resour. Manag.*, 2015, **168**, 101–114.

44 L. A. Guerrero, G. Maas and W. Hogland, *Waste Manag.*, 2013, **33**, 220–232.

45 D. Hoornweg and P. Bhada-Tata, *Urban Dev. Ser. Knowl. Pap. no.15, World Bank*, 2012, 116.

46 H. L. Parker, .

47 L. Giusti, *Waste Manag.*, 2009, **29**, 2227–2239.

48 J. H. Clark, 1999, 1–8.

49 R. Chandrappa and D. B. Das, , DOI:10.1007/978-3-642-28681-0.

50 A. Pires, G. Martinho and N. Bin Chang, *J. Environ. Manage.*, 2011, **92**, 1033–1050.

51 J. H. Schmidt, P. Holm, A. Merrild and P. Christensen, *Waste Manag.*, 2007, **27**, 1519–1530.

52 H. Cheng and Y. Hu, *Bioresour. Technol.*, 2010, **101**, 3816–3824.

53 U.S. Environmental Protection Agency (EPA), .

54 D. Q. Zhang, S. K. Tan and R. M. Gersberg, *J. Environ. Manage.*, 2010, **91**, 1623–1633.

55 S. E. Vergara and G. Tchobanoglous, *Municipal Solid Waste and the Environment: A Global Perspective*, 2012, vol. 37.

56 M. Sharholy, K. Ahmad, G. Mahmood and R. C. Trivedi, *Waste Manag.*, 2008, **28**, 459–467.

57 G. Jaria, C. Patrícia, C. I. A. Ferreira and M. Otero, 2017, **188**, 203–211.

58 H. Merrild, A. Damgaard and T. H. Christensen, *Resour. Conserv. Recycl.*, 2008, **52**, 1391–1398.

59 T.-N. Ye, W.-J. Feng, B. Zhang, M. Xu, L.-B. Lv, J. Su, X. Wei, K.-X. Wang, X.-H. Li and J.-S. Chen, *J. Mater. Chem. A*, 2015, **3**, 13926–13932.

60 K. Pivnenko, M. E. Olsson, R. Götze, E. Eriksson and T. F. Astrup, *Waste Manag.*, 2016, **51**, 43–54.

61 K. Pivnenko, E. Eriksson and T. F. Astrup, *Waste Manag.*, 2014, **45**, 134–142.

62 A. Villanueva and H. Wenzel, *Waste Manag.*, , DOI:10.1016/j.wasman.2007.02.019.

63 Y. Ikeda, E. Y. Park and N. Okuda, *Bioresour. Technol.*, 2006, **97**, 1030–1035.

64 E. Y. Park, P. N. Anh and N. Okuda, *Bioresour. Technol.*, 2004, **93**, 77–83.

65 W. Charusiri, *Energy Procedia*, 2015, **74**, 933–941.

66 C. R. Adhikari, D. Parajuli, K. Inoue, K. Ohto, H. Kawakita and H. Harada, *New J. Chem.*, 2008, **32**, 1634.

67 P. Shuttleworth, V. Budarin, M. Gronnow, J. H. Clark and R. Luque, *J. Nat. Gas Chem.*, 2012, **21**, 270–274.

68 M. Alcalde, M. Ferrer, F. J. Plou and A. Ballesteros, *Trends Biotechnol.*, 2006, **24**, 281–287.

69 V. L. Budarin, J. H. Clark, B. A. Lanigan, P. Shuttleworth and D. J. Macquarrie, *Bioresour. Technol.*, 2010, **101**, 3776–3779.

70 B. Biswal, S. Kumar and R. K. Singh, *J. Waste Manag.*, 2013, **2013**, 1–7.

71 L. Li, H. Zhang and X. Zhuang, *Energy Sources*, 2005, **27**, 867–873.

72 P. Gramatyka, *J. Achiev. …*, 2007, **20**, 535–538.

73 J. Baxter, K. A. Lyng, C. Askham and O. J. Hanssen, *Waste Manag.*, 2016, **57**, 17–26.

74 J. Li, B. N. Lopez N., L. Liu, N. Zhao, K. Yu and L. Zheng, *Waste Manag.*, 2013, **33**, 923–934.

75 A. S. Matharu, *RSC Green Chem. Ser.*, 2013, **22**, 207–219.

76 F. O. Ongondo, I. D. Williams and T. J. Cherrett, *Waste Manag.*, 2011, **31**, 714–730.

77 B. H. Robinson, *Sci. Total Environ.*, 2009, **408**, 183–191.

78 R. Widmer, H. Oswald-Krapf, D. Sinha-Khetriwal, M. Schnellmann and H. Böni, *Environ. Impact Assess. Rev.*, 2005, **25**, 436–458.

79 S. Salhofer, B. Steuer, R. Ramusch and P. Beigl, *Waste Manag.*, 2016, **57**, 27–35.

80 L. Zhang and Z. Xu, *J. Clean. Prod.*, 2016, **127**, 19–36.

81 P. Schwarzenbach, T. Egli, T. B. Hofstetter, U. Von Gunten and B. Wehrli, ,

DOI:10.1146/annurev-environ-100809-125342.

82 B. Luo, G. H. Huang, Y. Zou and Y. Y. Yin, *J. Environ. Manage.*, 2007, **83**, 181–190.

83 A. A. Rahman, *Glob. Ecol. Conserv.*, 2017, **10**, 9–22.

84 A. Pal, K. Y. Gin, A. Y. Lin and M. Reinhard, *Sci. Total Environ.*, 2010, **408**, 6062–6069.

85 N. K. Niazi, B. Murtaza, I. Bibi, M. Shahid, J. C. White, M. F. Nawaz, S. Bashir, M. B. Shakoor, G. Choppala, G. Murtaza and H. Wang, *Environ. Mater. Waste Resour. Recover. Pollut. Prev.*, 2016, 149–177.

86 D. D. and J. P. M. T. Colburn, *Our stolen future*, New York, 1996.

87 D. Mohan and C. U. Pittman, *J. Hazard. Mater.*, 2007, **142**, 1–53.

88 R. Loos, B. M. Gawlik, G. Locoro, E. Rimaviciute, S. Contini and G. Bidoglio, *Environ. Pollut.*, 2009, **157**, 561–568.

89 S. C. Smith and D. F. Rodrigues, *Carbon N. Y.*, 2015, **91**, 122–143.

90 V. K. Gupta, P. J. M. Carrott, M. M. L. Ribeiro Carrott and Suhas, *Crit. Rev. Environ. Sci. Technol.*, 2009, **39**, 783–842.

91 G. M. Mudd, *Resour. Policy*, 2007, **32**, 42–56.

92 S. H. Oelofse, P. J. Hobbs, J. Rascher and J. E. Cobbing, *CSIR, Nat. Resour. Environ.*, 2004, 617–627.

93 S. R. La Brooy, H. G. I. Linge and G. S. Walker, 1994, **7**, 1213–1241.

94 E. Vences-Alvarez, E. Razo-Flores, I. Lázaro, R. Briones-Gallardo, G. Velasco-Martínez and J. R. Rangel-Mendez, *J. Mol. Liq.*, 2017, **240**, 549–555.

95 R. L. Besagas and R. M. Del Rosario, , DOI:10.24214/jcbps.D.7.3.55964.

96 U. Okereafor, M. Makhatha and L. Mekuto, .

97 I. Anastopoulos, A. Bhatnagar and E. C. Lima, *J. Mol. Liq.*, 2016, **221**, 954–962.

98 M. Fomina and G. M. Gadd, *Bioresour. Technol.*, 2014, **160**, 3–14.

99 M. Karnib, A. Kabbani, H. Holail and Z. Olama, *Energy Procedia*, 2014, **50**, 113–120.

100 A. G. Fane, A. R. Awang, M. Bolko, R. Macoun, R. Schofield, Y. R. Shen and F. Zha, *Water Sci. Technol.*, 1992, **25**, 5–18.

101 D. W. O'Connell, C. Birkinshaw and T. F. O'Dwyer, *Bioresour. Technol.*, 2008, **99**, 6709–6724.

102 E. Worch, *Adsorption Technology in Water Treatment: Fundamentals, Processes, and Modeling*, 2012.

103 A. Zanoletti, I. Vassura, E. Venturini, M. Monai, T. Montini, S. Federici, A. Zacco, L. Treccani and E. Bontempi, *Front. Chem.*, 2018, **6**, 60.

104 M. Soleimani and T. Kaghazchi, *Bioresour. Technol.*, 2008, **99**, 5374–5383.

105 C. Faur-Brasquet, Z. Reddad, K. Kadirvelu and P. Le Cloirec, *Appl. Surf. Sci.*, 2002, **196**, 356–365.

106 H. Qiu, L. Lv, B. Pan, Q. Zhang, W. Zhang and Q. Zhang, *J. Zhejiang Univ. A*, 2009, **10**, 716–724.

107 Y. F. Jia, C. J. Steele, I. P. Hayward and K. M. Thomas, *Carbon N. Y.*, 1998, **36**, 1299–1308.

108 W. K. Buah and P. T. Williams, *Environ. Technol.*, 2010, **31**, 125–137.

109 M. D. Seke, R. F. Sandenbergh and N. M. Vegter, *Miner. Eng.*, 2000, **13**, 527–540.

110 H. J. Zhai, L. L. Pan, B. Dai, B. Kiran, J. Li and L. S. Wang, *J. Phys. Chem. C*, 2008, **112**, 11920–11928.

111 Y. S. Ho and G. McKay, *Process Saf. Environ. Prot.*, 1998, **76**, 332–340.

112 B. H. Bijsterbosch, *J. Colloid Interface Sci.*, 1974, **47**, 186–198.

113 W. H. Cheung, Y. S. Szeto and G. McKay, *Bioresour. Technol.*, 2007, **98**, 2897–2904.

114 H. L. Parker, A. J. Hunt, V. L. Budarin, P. S. Shuttleworth, K. L. Miller and J. H. Clark, *RSC Adv.*, 2012, **2**, 8992.

115 J. Lee, J. Kim and T. Hyeon, *Adv. Mater.*, 2006, **18**, 2073–2094.

116 P. Valle-Vigón, M. Sevilla and A. B. Fuertes, *Mater. Chem. Phys.*, 2013, **139**, 281–289.

117 M. T. Bore, H. N. Pham, E. E. Switzer, T. L. Ward, A. Fukuoka and A. K. Datye, *J. Phys. Chem. B*, 2005, **109**, 2873–2880.

118 I. Langmuir, *J. Am. Chem. Soc.*, 1918, **40**, 1361–1403.

119 V. Zelenak, D. Halamova, L. Gaberova, E. Bloch and P. Llewellyn, *Microporous Mesoporous Mater.*, 2008, **116**, 358–364.

120 L. Zhang, C. Yu, W. Zhao, Z. Hua, H. Chen, L. Li and J. Shi, *J. Non. Cryst. Solids*, 2007, **353**, 4055–4061.

121 D. Mohan and K. P. Singh, *Water Res.*, 2002, **36**, 2304–2318.

122 M. E. Davis, *Nature*, 2002, **417**, 813–821.

123 S. M. L. Dos Santos, K. A. B. Nogueira, M. De Souza Gama, J. D. F. Lima, I. J. Da Silva J??nior and D. C. S. De Azevedo, *Microporous Mesoporous Mater.*, 2013, **180**, 284–292.

124 M. Mureseanu, A. Reiss, I. Stefanescu, E. David, V. Parvulescu, G. Renard and V. Hulea, *Chemosphere*, 2008, **73**, 1499–1504.

125 P. Van Der Voort, P. I. Ravikovitch, A. V. Neimark, M. Benjelloun, E. Van Bavel, K. P. De Jong, B. M. Weckhuysen and E. F. Vansant, 2002, 45–52.

126 E. Demirbas, M. Kobya and M. T. Sulak, *Bioresour. Technol.*, 2008, **99**, 5368–

5373.

127 A. Benhamou, M. Baudu, Z. Derriche and J. P. Basly, *J. Hazard. Mater.*, 2009, **171**, 1001–1008.

128 Z. A. Alothman, 2012, 2874–2902.

129 H. Ebrahimzadeh, N. Tavassoli, M. M. Amini, Y. Fazaeli and H. Abedi, *Talanta*, 2010, **81**, 1183–1188.

130 S. M. L. Dos Santos, K. A. B. Nogueira, M. De Souza Gama, J. D. F. Lima, I. J. Da Silva J??nior and D. C. S. De Azevedo, *Microporous Mesoporous Mater.*, 2013, **180**, 284–292.

131 D. Mohan and C. U. Pittman, *J. Hazard. Mater.*, 2006, **137**, 762–811.

132 J. Dı and A. Jerez, 2001, **188**, 167–175.

133 Y. H. Li, C. W. Lee and B. K. Gullett, *Fuel*, 2003, **82**, 451–457.

134 B. R. Ryoo, S. H. Joo, M. Kruk and M. Jaroniec, *Adv. Mater.*, 2001, **13**, 677–681.

135 T. S. Transformation, , DOI:10.1021/jp991673a.

136 S. De Gisi, G. Lofrano, M. Grassi and M. Notarnicola, *Sustain. Mater. Technol.*, 2016, **9**, 10–40.

137 M. Ahmaruzzaman, *Adv. Colloid Interface Sci.*, 2008, **143**, 48–67.

138 G. Annadurai, R. S. Juang and D. J. Lee, *J. Hazard. Mater.*, 2002, **92**, 263–274.

139 N. Liu, L. Yin, C. Wang, L. Zhang, N. Lun, D. Xiang, Y. Qi and R. Gao, *Carbon N. Y.*, 2010, **48**, 3579–3591.

140 Y. Liu, J. Chen, J. Yao, Y. Lu, L. Zhang and X. Liu, *Chem. Eng. J.*, 2009, **148**, 201–206.

141 P. Valle-Vigón, M. Sevilla and A. B. Fuertes, *Microporous Mesoporous Mater.*, 2010, **134**, 165–174.

142 J. Wang, C. Xiang, Q. Liu, Y. Pan and J. Guo, *Adv. Funct. Mater.*, 2008, **18**, 2995–3002.

143 T. Yokoi, S. Seo, N. Chino, A. Shimojima and T. Okubo, *Microporous Mesoporous Mater.*, 2009, **124**, 123–130.

144 A. M. B. Furtado, Y. Wang and M. D. Levan, *Microporous Mesoporous Mater.*, 2013, **165**, 48–54.

145 I. Janekarn, A. J. Hunt, Y. Ngernyen, S. Youngme and N. Supanchaiyamat, .

146 W. Shen and W. Fan, *J. Mater. Chem. A*, 2013, **1**, 999–1013.

147 F. De Clippel, M. Dusselier, R. Van Rompaey, P. Vanelderen, J. Dijkmans, E. Makshina, L. Giebeler, G. V Baron, J. F. M. Denayer, P. P. Pescarmona, P. A. Jacobs and B. F. Sels, , DOI:10.1021/ja301678w.

148 Y. Fang, G. Zheng, J. Yang, H. Tang, Y. Zhang and B. Kong, , DOI:10.1002/ange.201402002.

149 K. Sotiriou, D. J. Macquarrie and V. L. Budarin, 2015, **1950**, 14156.

150 R. I. W. D.W. Bruce, D. O' Hare, *Porous Materials, Inorganic Materials Series*, 2010.

151 M. Si, D. Feng, L. Qiu, D. Jia, A. A. Elzatahry, G. Zheng and D. Zhao, *J. Mater. Chem. A*, 2013, **1**, 13490.

152 T. Jiang, V. L. Budarin, P. S. Shuttleworth, G. Ellis, C. M. A. Parlett, K. Wilson, D. J. Macquarrie and A. J. Hunt, *J. Mater. Chem. A*, 2015, **3**, 14148–14156.

153 Y. Zhu, H. Li, Q. Zheng, J. Xu and X. Li, *Langmuir*, 2012, **28**, 7843–7850.

154 A. J. Hunt, 2020, 25228–25238.

155 C. Perruchot, M. A. Khan, A. Kamitsi, S. P. Armes, J. F. Watts, T. Von Werne and T. E. Patten, *Eur. Polym. J.*, 2004, **40**, 2129–2141.

156 U. Zielke, K. J. Hüttinger and W. P. Hoffman, *Carbon N. Y.*, 1996, **34**, 983–998.

157 A. Alzate, M. E. López and C. Serna, *Waste Manag.*, 2016, **57**, 113–120.

158 X. Ju, K. Igarashi, S. ichi Miyashita, H. Mitsuhashi, K. Inagaki, S. ichiro Fujii, H. Sawada, T. Kuwabara and A. Minoda, *Bioresour. Technol.*, 2016, **211**, 759–764.

159 M. H. Morcali, B. Zeytuncu, E. Ozlem and S. Aktas, *Mater. Res.*, 2015, **18**, 660–667.

160 S. Lagerge, J. Zajac, S. Partyka, A. J. Groszek and M. Chesneau, *Langmuir*, 1997, **13**, 4683–4692.

161 M. Bystrzejewski and K. Pyrzyńska, *Mater. Chem. Phys.*, 2013, **141**, 454–460.

162 R. J. Davidson, *J. South African Inst. Min. Metall.*, 1974, 67–76.

163 A. H. Berger and A. S. Bhown, *Energy Procedia*, 2011, **4**, 562–567.

164 D. G. Castner, K. Hinds and D. W. Grainger, *Langmuir*, 1996, **12**, 5083–5086.

165 J. Park, M. Atobe and T. Fuchigami, 2006, **13**, 237–241.

166 S. L. Westcott, S. J. Oldenburg, T. R. Lee and N. J. Halas, *Langmuir*, 1998, **14**, 5396–5401.

167 S. J. Allen, G. Mckay and J. F. Porter, *J. Colloid Interface Sci.*, 2004, **280**, 322–333.

168 W. Rudzinski and W. Plazinski, *Langmuir*, 2008, **24**, 5393–5399.

169 M. Arami, N. Y. Limaee and N. M. Mahmoodi, *Chem. Eng. J.*, 2008, **139**, 2–10.

170 K. F. Lam, K. L. Yeung and G. McKay, *J. Phys. Chem. B*, 2006, **110**, 2187–2194.

171 C. Ng, J. N. Losso, W. E. Marshall and R. M. Rao, *Bioresour. Technol.*, 2002, **85**, 131–135.

172 D. A.O, *IOSR J. Appl. Chem.*, 2012, **3**, 38–45.

173 H. L. Parker, V. L. Budarin, J. H. Clark and A. J. Hunt, *ACS Sustain. Chem. Eng.*, 2013, **1**, 1311–1318.

174 S. M. Yakout and E. Elsherif, *Carbon - Sci. Technol.*, 2010, **3**, 144–153.

175 K. Y. Foo and B. H. Hameed, 2010, **156**, 2–10.

176 C. L. Mangun, M. A. Daley, R. D. Braatz and J. Economy, *Carbon N. Y.*, 1998, **36**, 123–129.

177 M. Kilic, E. Apaydin-Varol and A. E. Pütün, *J. Hazard. Mater.*, 2011, **189**, 397–403.

178 E. H. Cho, S. N. Dixon and C. H. Pitt, *Metall. Trans. B*, 1979, **10**, 185–189.

179 F. C. Wu, R. L. Tseng, S. C. Huang and R. S. Juang, *Chem. Eng. J.*, 2009, **151**, 1–9.

180 W. S. W. Ngah and K. H. Liang, *Ind. Eng. Chem. Res.*, 1999, **38**, 1411–1414.

181 G. M. Walker, L. Hansen, J. A. Hanna and S. J. Allen, *Water Res.*, 2003, **37**, 2081–2089.

182 Y. C. Wong, Y. S. Szeto, W. H. Cheung and G. McKay, *J. Appl. Polym. Sci.*, 2004, **92**, 1633–1645.

183 Y. S. Ho and G. McKay, *Process Biochem.*, 1999, **34**, 451–465.

184 Y. S. Ho, *J. Hazard. Mater.*, 2006, **136**, 681–689.

185 F. C. Wu, R. L. Tseng and R. S. Juang, *Chem. Eng. J.*, 2009, **150**, 366–373.

186 Y. S. Ho and G. McKay, *Adsorpt. Sci. Technol.*, 2002, **20**, 797–815.

187 S. Karthikeyan, B. Sivakumar and N. Sivakumar, *E-Journal Chem.*, 2010, **7**, S175–S184.

188 K. K. H. Choy, J. F. Porter and G. M. Kay, 2002, 305–317.

189 F. C. Wu, R. L. Tseng and R. S. Juang, *Chem. Eng. J.*, 2009, **153**, 1–8.

190 K. V. Kumar, *J. Hazard. Mater.*, 2006, **137**, 1538–1544.

191 C. Tien and B. V. Ramarao, *Sep. Sci. Technol.*, 2016, **00**, 1–12.

192 S. S. Lam and H. A. Chase, *Energies*, 2012, **5**, 4209–4232.

193 Y. Wan, P. Chen, B. Zhang, C. Yang, Y. Liu, X. Lin and R. Ruan, *J. Anal. Appl. Pyrolysis*, 2009, **86**, 161–167.

194 A. A. Salema and F. N. Ani, *Bioresour. Technol.*, 2011, **102**, 3388–3395.

195 Y. F. Huang, P. Te Chiueh and S. L. Lo, *Sustain. Environ. Res.*, 2016, **26**, 103–109.

196 R. Hoseinzadeh Hesas, W. M. A. Wan Daud, J. N. Sahu and A. Arami-Niya, *J. Anal. Appl. Pyrolysis*, 2013, **100**, 1–11.

197 D. Mohan, C. U. Pittman and P. H. Steele, *Energy and Fuels*, 2006, **20**, 848–889.

198 C. A. Mullen, A. A. Boateng, N. M. Goldberg, I. M. Lima, D. A. Laird and K. B. Hicks, *Biomass and Bioenergy*, 2010, **34**, 67–74.

199 J. P. Robinson, S. W. Kingman, R. Baranco, C. E. Snape and H. Al-Sayegh, *Ind. Eng. Chem. Res.*, 2010, **49**, 459–463.

200 C. A. Mullen, G. D. Strahan and A. A. Boateng, *Energy and Fuels*, 2009, **23**, 2707–2718.

201 Z. Zhang, D. J. Macquarrie, M. De bruyn, V. L. Budarin, A. J. Hunt, M. J. Gronnow, J. Fan, P. S. Shuttleworth, J. H. Clark and A. S. Matharu, *Green Chem.*, 2015, **17**, 260–270.

202 K. Sipila È, E. Kuoppala, L. S. Fagerna È, A. Oasmaa, K. Sipilä, E. Kuoppala, L. Fagernäs, A. Oasmaa, K. Sipila È, E. Kuoppala, L. S. Fagerna È and A. Oasmaa, *Biomass and Bioenergy*, 1998, **14**, 103–113.

203 W. Nor, R. Wan, M. W. M. Hisham, M. Ambar and T. Y. Hin, *Renew. Sustain. Energy Rev.*, 2012, **16**, 5910–5923.

204 G. C. Galletti, P. Bocchini, M. E. Guadalix, G. Almendros, S. Camarero and A. T. Martínez, *Bioresour. Technol.*, 1997, **60**, 51–58.

205 W. N. R. W. Isahak, M. W. M. Hisham, M. A. Yarmo and T. Y. Yun Hin, *Renew. Sustain. Energy Rev.*, 2012, **16**, 5910–5923.

206 A. J. Ridout, M. Carrier and J. Görgens, *J. Anal. Appl. Pyrolysis*, 2015, **111**, 64–75.

207 A. V. Bridgwater, *Biomass and Bioenergy*, 2012, **38**, 68–94.

208 J. P. Diebold, *Nrel/Sr-570-27613*, 2000, 59.

209 V. L. Budarin, J. H. Clark, B. A. Lanigan, P. Shuttleworth, S. W. Breeden, A. J. Wilson, D. J. Macquarrie, K. Milkowski, J. Jones, T. Bridgeman and A. Ross, *Bioresour. Technol.*, 2009, **100**, 6064–6068.

210 F. Yu, R. Ruan, S. Deng, P. Chen, Y. Liu, Y. Wan, A. Olson and D. Kittelson, , DOI:10.1007/s12010-007-9111-x.

211 B. Pan, B. Xing, B. O. Pan and B. Xing, 2008, **42**, 9005–9013.

212 T. Foyle, L. Jennings and P. Mulcahy, *Bioresour. Technol.*, 2007, **98**, 3026–3036.

213 M. Garcia-Perez, A. Chaala, H. Pakdel, D. Kretschmer and C. Roy, *Biomass and Bioenergy*, 2007, **31**, 222–242.

214 M. Thommes, K. Kaneko, A. V Neimark, J. P. Olivier, F. Rodriguez-reinoso, J. Rouquerol and K. S. W. Sing, 2015, **87**, 1051–1069.

215 C. Sangwichien, G. L. Aranovich and M. D. Donohue, 2002, **206**, 313–320.

216 I. Union, O. F. Pure and A. Chemistry, 1985, **57**, 603–619.

217 L. Téllez, J. Rubio, M. A. Valenzuela, F. Rubio and J. L. Oteo, *Mater. Charact.*, 2008, **60**, 506–512.

218 A. Trunschke, .

219 P. R. Zalupski and R. Mcdowell, .

220 T. M. Sun and W. T. Yen, *Miner. Eng.*, 1993, **6**, 17–29.

221 C. Moreno-Castilla, *Carbon N. Y.*, 2004, **42**, 83–94.

222 C. H. Tessmer, R. D. Vidic and L. I. Uranowski, *Environ. Sci. Technol.*, 1997, **31**, 1872–1878.

223 J. Chen, Z. Mao, L. Zhang, Y. Tang, D. Wang, L. Bie and B. D. Fahlman, *Carbon N. Y.*, 2018, **130**, 41–47.

224 W. Gao, Y. Wan, Y. Dou and D. Zhao, *Adv. Energy Mater.*, 2011, **1**, 115–123.

225 N. Chiron, R. Guilet and E. Deydier, *Water Res.*, 2003, **37**, 3079–3086.

226 H. Hasegawa, S. Barua, T. Wakabayashi, A. Mashio and T. Maki, *Microchem. J.*, 2018, **139**, 174–180.

227 E. F. Mohamed, C. Andriantsiferana, A. M. Wilhelm and H. Delmas, *Environ. Technol.*, 2011, **32**, 1325–1336.

228 W. M. A. W. Daud and A. H. Houshamnd, *J. Nat. Gas Chem.*, 2010, **19**, 267–279.

229 J. P. Paraknowitsch and A. Thomas, *Energy Environ. Sci.*, 2013, **6**, 2839.

230 X. Wang, G. Sun, P. Routh, D. Kim, W. Huang and P. Chen, 2014, 7067–7098.

231 Z. Qiang, Y. Xia, X. Xia and B. D. Vogt, , DOI:10.1021/acs.chemmater.7b04061.

232 X. Li, D. Geng, Y. Zhang, X. Meng, R. Li and X. Sun, *Electrochem. commun.*, 2011, **13**, 822–825.

233 D. Geng, S. Yang, Y. Zhang, J. Yang, J. Liu, R. Li, T. K. Sham, X. Sun, S. Ye and S. Knights, *Appl. Surf. Sci.*, 2011, **257**, 9193–9198.

234 H.-L. Guo, P. Su, X. Kang and S.-K. Ning, *J. Mater. Chem. A*, 2013, **1**, 2248–2255.

235 J. Aguado, J. M. Arsuaga, A. Arencibia, M. Lindo and V. Gascón, *J. Hazard. Mater.*, 2009, **163**, 213–221.

236 M. K. Uddin, *Chem. Eng. J.*, 2017, **308**, 438–462.

237 J. Attard, R. Milescu, V. Budarin, A. S. Matharu and J. H. Clark, *Chem. Commun.*, 2018, **54**, 686–688.

238 D. Long, W. Li, L. Ling, J. Miyawaki, I. Mochida and S. H. Yoon, *Langmuir*, 2010, **26**, 16096–16102.

239 X. Y. Chen, C. Chen, Z. J. Zhang, D. H. Xie and X. Deng, , DOI:10.1021/ie400862h.

240 Y. Shao, J. Sui, G. Yin and Y. Gao, *Appl. Catal. B Environ.*, 2008, **79**, 89–99.

241 R. Keuleers, H. O. Desseyn, B. Rousseau and C. Van Alsenoy, *J. Phys. Chem. A*, 1999, **103**, 4621–4630.

242 F. Kurzer and P. M. Sanderson, , DOI:10.1021/ed033p452.

243 U. W. Adhesives, B. Li, J. Zhang, X. Ren, J. Chang and J. Gou, 2014, **9**, 5125–5133.

244 M. Florent, M. Tocci and T. J. Bandosz, *Carbon N. Y.*, 2013, **63**, 283–293.

245 Z. Liu, Z. Du, H. Song, C. Wang, F. Subhan, W. Xing and Z. Yan, 2014, **416**, 124–132.

246 M. R. M. C. Santos and C. Airoldi, *J. Colloid Interface Sci.*, 1996, **183**, 416–423.

247 B. Sajjadi, J. William, W. Yin, D. L. Mattern, N. O. Egiebor, N. Hammer and C. L. Smith, 2019, **51**, 20–30.

248 Y. Belmabkhout and A. Sayari, 2009, 318–328.

249 J. Song, T. Xu, M. L. Gordin, P. Zhu, D. Lv, Y. B. Jiang, Y. Chen, Y. Duan and D. Wang, *Adv. Funct. Mater.*, 2014, **24**, 1243–1250.

250 S. D. Yim, S. J. Kim, J. H. Baik, I. Nam, Y. S. Mok, J.-H. Lee, B. K. Cho and S. H. Oh, *Ind. Eng. Chem. Res.*, 2004, **43**, 4856–4863.

251 P. M. Schaber, J. Colson, S. Higgins, D. Thielen, B. Anspach and J. Brauer, *Thermochim. Acta*, 2004, **424**, 131–142.

252 M. Koebel and M. Elsener, *J. Chromatogr. A*, 1995, **689**, 164–169.

253 C. L. D. Wang, S. Hui, *Fuel*, 2017, 268–273.

254 C. Nauk, Polska Akademia and Wydzia{\l} III, Polska Akademia Nauk and Matematyczno-Fizycznych, Nauk and i Geologo-Geograficznych, *Org. Chem.*, 1959, **10**, 113–120.

255 P. Burg, P. Fydrych, D. Cagniant, G. Nanse, J. Bimer and A. Jankowska, *Carbon N. Y.*, 2002, **40**, 1521–1531.

256 P.-X. Hou, H. Orikasa, T. Yamazaki, K. Matsuoka, A. Tomita, N. Setoyama, Y. Fukushima and T. Kyotani, *Chem. Mater.*, 2005, **17**, 5187–5193.

257 Y. Liang, L. Cai, L. Chen, X. Lin, R. Fu, M. Zhang and D. Wu, *Nanoscale*, 2015, **7**, 3971–3975.

258 L. Rassaei, M. Sillanpää and F. Marken, *Electrochim. Acta*, 2008, **53**, 5732–5738.